



Doctoral Dissertation

Passive Tip-Injection in Shrouded Low Pressure Turbines

Dipl.-Ing. Pouya Ghaffari

Submitted to the
Faculty of Mechanical and Industrial Engineering
of Technische Universität Wien
for the degree of a doctor of engineering sciences (Dr.techn.)

Supervisor: Ao.Univ.Prof. Dipl.-Ing. Dr.techn. Reinhard Willinger

First Expert: Univ.Prof. Dipl.-Ing. Dr.Ing. Christian Bauer
Institute for Energy Systems and Thermodynamics
Technische Universität Wien
cbauer@mail.tuwien.ac.at

Second Expert: Ass.Prof. Priv.-Doz. Dipl.-Ing. Dr.techn. Emil Göttlich
Institute for Thermal Turbomachinery and Machine Dynamics
Graz University of Technology
emil.goettlich@tugraz.at

Vienna, November 2016

Acknowledgment

As an Employee of the Institute for Energy Systems and Thermodynamics, department for Fluid-Flow Machinery, at Technische Universität Wien I would specially like to thank my doctoral thesis supervisor Ao.Univ.Prof. Dipl.-Ing. Dr.techn. Reinhard Willinger for inspiring me throughout the entire time. He supported me in all aspects and in tough times in spite of his extensive activities as the only professor in the area of turbomachinery.

My special thanks also go to the head of the research area of Fluid-Flow Machinery Univ.Prof. Dipl.-Ing. Dr.Ing. Christian Bauer as a great adviser concerning execution of my doctoral thesis as well as project issues. He was always keen to create an inspiring and pleasant atmosphere placing great emphasis on employees' concerns of any kind.

I would also like to thank Dipl.-Ing. Dr.techn. Albert Benoni for his support in numerical simulations as well as his further advises and being a great colleague during the first period of my employment.

Not to forget Mr. Gerhard Kanzler, who supported me in all activities with his extensive knowledge in the laboratory of turbomachinery offering me more time for my doctoral thesis.

I also thank Dipl.-Ing. Sabine Bauinger, Ass.Prof.i.R. Dipl.-Ing. Dr.techn. Herman-Peter Pirker and Dipl.-Ing. Dr.techn. Andreas Marn for carrying out the measurements for the last part of my thesis and providing me with sufficient data. The long sleepless nights for acquiring the measurement data should not remain unmentioned.

Thanks to my colleagues for our coffee breaks and interesting discussions in the kitchen.

Great thanks to my parents for their presence. Even though they lived in Iran, they supported me throughout my whole life and my carrier in all aspects.

Also thanks to my friends for their presence and the amazing time we had together also in tough times.

The content of this thesis was created based on two projects MICROSHROUD and LPT-Inject. The financial support by the Austrian Aviation Program TAKE OFF of the Austrian Promotion Agency (FFG) is gratefully acknowledged.

I dedicate this thesis to my parents in great gratitude for their endless love and support.

Dearly beloved **Saideh Poosti** and **Reza Ghafari**.

Kurzfassung

Verluste aufgrund des notwendigen Spaltes zwischen den rotierenden und den still stehenden Teilen können zu einem beträchtlichen Teil der Gesamtverluste in einer thermischen Turbomaschine beitragen. Als Beispiel kann der Spalt zwischen den freidrehenden Schaufeln und dem Gehäuse erwähnt werden. Zusätzlich zur geminderten Teilnahme der Spaltströmung an der Arbeitsumsetzung werden stromabwärts Mischungsverluste verursacht, die die Anströmung der nächsten Schaufelreihe negativ beeinflussen können. Verwendung von Winglets, Squealern und Schaufeldeckbändern sowie die Einblasung der Kühlluft in den Spaltbereich in gekühlten Turbinenstufen stellen mögliche Abhilfen gegen die Spaltströmung dar.

Die Entkoppelung der Niederdruckturbinen eines Getriebeturbofans von dem Fan hat höhere Drehzahlen sowie eine bessere Aerodynamik der Niederdruckturbinen zu Folge. Zusätzlich zu einer verjüngten Beschaukelung und einem schmalen Spitzenbereich wird zur weiteren Gewichtssreduktion anstelle eines vollen Deckbandes ein sogenanntes rudimentäres Deckband verwendet, um die mechanischen Spannungen aufgrund der Fliehkräfte im Schaufelfuss zu reduzieren.

Eine Kombination des Schaufeldeckbandes mit der aerodynamischen Dichtung mittels passiver Spalteinblasung in ungekühlten Niederdruckturbinen ist das Thema dieser Dissertation. Der Begriff passiv bedeutet, dass der Einblasemassenstrom aus dem Stufenmassenstrom entnommen wird. Zunächst wird das Durchflussverhalten der passiven Einblasung anhand analytischer und zweidimensionaler numerischer Rechnungen untersucht. Die Ergebnisse zeigen, dass der Einfluss der Einblasung auf den Gesamtspaltmassenstrom stark von der axialen Position der Einblasung über dem Deckband abhängt und eine geführte Einblasung vor der ersten Dichtspitze am wirksamsten ist. In einem weiteren Schritt werden dreidimensionale numerische Berechnungen an einem linearen Gitter mit einem vollen und zwei rudimentären Deckbändern durchgeführt. Es stellt sich heraus, dass eine geführte Einblasung im Fall eines vollen Deckbandes den Gitterwirkungsgrad am stärksten verbessern kann. In weiterer Folge wird der Rotor einer realen Niederdruckturbinen mit voll abgedeckten Schaufeln mit und ohne Einblasung experimentell sowie numerisch untersucht. Die Simulationen werden für eine kompressible Strömung in einem rotierenden System durchgeführt. Zusätzliche analytische Berechnungen behandeln den Einfluss der passiven Einblasung auf das stromabseitige Strömungsfeld sowie das Teillastverhalten. Die analytischen Ergebnisse zeigen, dass der Einfluss der Einblasung auf die spezifische Arbeit von der Neigung der Einblasung gegen die Rotationsrichtung und dem Drall der Zuströmung abhängt und sich unter Umständen negativ auswirken kann. Nichtsdestotrotz weisen die numerischen und experimentellen Ergebnisse eine Verbesserung des abstromseitigen Strömungsfeldes des betrachteten Rotors auf.

Abstract

Tip-leakage losses due to the clearance between the rotational and the stationary parts contribute to a substantial part of the overall losses in turbomachinery. The gap between the blade tip and the casing is addressed as an example. As expected, the flow through the tip clearance, if at all, participates only partially in stage work. The underturned leakage flow further results in mixing losses downstream of the stage affecting the incidence of the following blade row. Structural modifications such as winglets or squealers in case of an unshrouded blade or usage of blade shrouds as well as injection of the cooling air in the tip section acting as a fluidic barrier in cooled stages all aim at reduction of tip-leakage losses.

In the modern technology of geared turbofan (GTF) the low pressure turbine (LPT) is decoupled from the fan operating at higher rotational speed resulting in higher aerodynamic performance. The airfoil of such a high-speed LPT rotor is tapered with a thin tip section. Furthermore a partial shroud is used instead of a full shroud in order to reduce the mechanical stress in the blade root due to centrifugal forces.

The scope of this thesis is to introduce a method combining the sealing effect of blade shrouds with the aerodynamic sealing by means of passive tip-injection in uncooled turbine stages. The term passive means that in contrast to cooled stages the injection mass flow is extracted from the stage mass flow. This method is first investigated based on analytical approaches and 2D numerical calculations taking into account the discharge behavior of the sealing application. The results show that the impact of passive tip-injection on the overall tip-leakage mass flow rate depends strongly on the axial injection position over the shroud and the guided tip-injection upstream of the first sealing fin has the highest effectiveness. The numerical calculations are then extended to 3D calculations in a linear cascade accounting for 3D effects. Two different partial shroud geometries are also investigated for the same cascade geometry. It turns out that the full shroud provided with guided tip-injection is most effective regarding the cascade efficiency. In a further step the calculations are carried out for compressible flow in a rotational frame of reference in a real application. The impact of passive tip-injection is also studied experimentally in this step. Additionally an analytical approach is derived in order to investigate the effect of passive tip-injection on the downstream flow field as well as under off-design conditions. The analytical results demonstrate that the impact of tip-injection on the specific work depends on the inclination angle of the injection against the rotational direction as well as the inflow swirl. The effect of the injection could possibly turn negative and should be considered with caution. Nevertheless the numerical and experimental results exhibit an improvement of the downstream flow field for the given application.

Contents

1. Introduction	1
1.1. Motivation	1
1.2. Low Pressure Turbine	4
1.2.1. Low Pressure Turbine Losses	5
1.2.2. Shrouded Low Pressure Turbine	5
1.3. Scope of the Thesis	6
2. Literature Overview	8
2.1. Shrouded Blades	8
2.1.1. Discharge Characteristics of Labyrinth Seals	9
2.1.2. Interaction of Tip-Leakage Flow and Main Flow	10
2.2. Fluidic Jet Barriers	14
2.2.1. Active Fluidic Sealing	14
2.2.2. Passive Fluidic Sealing in Uncooled Turbines	16
2.3. Computational Fluid Dynamics	17
3. Numerical Calculations	22
3.1. Governing Equations of Fluid Mechanics	22
3.1.1. Relative Velocity Formulation	23
3.1.2. Absolute Velocity Formulation	24
3.2. Turbulence Modeling	24
3.2.1. Treatment of Near-Wall Regions	26
3.2.2. k/ϵ -Model	27
3.2.3. k/ω -Model	28
3.3. Discretization	29
3.4. Solver	30
4. Basic Investigations on Passive Tip-Injection	33
4.1. Analytical Discharge Models	33
4.2. CFD Procedure	34
5. Linear Cascade Investigations	47
5.1. Linear Cascade Geometry	47
5.2. CFD Calculations	48

6. Investigations on a Real Application	62
6.1. LPT Rotor	62
6.2. Application of Passive Tip-Injection	63
6.3. Measurement Instrumentation	64
6.4. CFD Procedure	66
6.5. Mesh Study	93
6.6. Additional Information	95
6.6.1. CFD Contour Plots	95
6.6.1.1. Cavity Flow of the Shrouded Geometry without Injection	95
6.6.1.2. Circumferential Velocity	97
6.6.1.3. Total Temperature	100
6.6.2. Streamlines	102
6.6.3. Contour Plots of Measurement Data in Plane F	104
7. Conclusion and Outlook	108
Bibliography	113
A. Appendix	118
A.1. CFD Results of the LPT Rotor Calculated with the SST k/ω -model	118

Nomenclature

Latin Symbols

A	area	[m ²]
C_D	discharge coefficient (leakage flow only)	[-]
C_D^+	discharge coefficient (leakage flow plus injection)	[-]
C_μ	model constant (k/ϵ -Model)	[-]
e	specific internal energy	[J / kg]
e	error	
f_ω	model constant (k/ω -Model)	[-]
h	specific enthalpy	[J / kg]
h	reference mesh size	[m]
h_i	mesh size	[m]
k	specific turbulent kinetic energy	[m ² / s ²]
Ma	Mach number	[-]
n	normal	
N, S, E, W	north, south, east, west	
n, s, e, w	north, south, east, west	
P	center	
p	pressure	[Pa]
p	discretization procedure order	[-]
S	source term	
T	temperature	[K]
t	time	[s]
T, B	top, bottom	
t, b	top, bottom	
u	velocity	[m / s]
u_τ	shear velocity	[m / s]
V	volume	[m ³]
x, y, z	cartesian coordinates	[m]
y	distance	[m]

Greek Symbols

α	under-relaxation factor	[-]
α	absolute flow angle	[°]
Γ	diffusion coefficient	

δ_{ij}	Kronecker delta	[-]
ϵ	specific turbulent dissipation rate	[m ² / s ³]
λ	thermal conductivity	[W / m K]
μ	dynamic viscosity	[Pa s]
ν	kinematic viscosity	[m ² / s]
ρ	density	[kg / m ³]
σ	contraction coefficient	[-]
τ_w	wall shear stress	[Pa]
Φ	characteristic quantity	
Ψ	scalar transport quantity	
ω	specific dissipation rate	[1 / s]

Vectors and Tensors

I	unit tensor	[-]
\vec{r}	position (vector)	[m]
\vec{v}	velocity	[m / s]
$\bar{\bar{\tau}}$	stress tensor	[Pa]
$\vec{\omega}$	angular velocity	[rad / s]

Superscripts

+	dimensionless
+	measured from the negative circumferential direction
^	dimensionless
T	transposed
'	fluctuation with respect to time averaging
"	fluctuation with respect to Favre averaging
—	time-averaged
=	mass-averaged
~	Favre-averaged

Subscripts

i	direction index
i, j	indices for Einstein notation
k	index for Einstein notation
P	center
r	relative
t	turbulent
t	total
Ψ	scalar transport quantity

2	exit measurement plane
∞	exact solution

Abbreviations

ATM	air traffic management
CAEP	Committee on Aviation Environmental Protection
CFD	computational fluid dynamics
FHP	five-hole probe
FRAPP	fast response aerodynamic pressure probe
GTF	geared turbofan
ICAO	International Civil Aviation Organization
LPC	low pressure compressor
LPT	low pressure turbine
RNG	Renormalization Group
RPK	revenue passenger kilometer
RSM	Reynolds stress model
SST	shear stress transport

1. Introduction

1.1. Motivation

Statistics exhibit strong increase in aviation service. According to Airbus, Global Market Forecast [1] passenger air traffic has doubled every 15 years since the early eighties. Today 47 aviation mega-cities account for 90% of long-haul flights. This number will rise to 91 aviation mega-cities in 2034 ([1]). Total new deliveries (replacement and new aircraft) are thus expected to be close to 32600 aircraft. These facts require a balance between the socio-economic benefits of aviation and the environmental cost which is reflected in more than 30% reduction in fuel burn per revenue passenger kilometer (RPK) in the last 15 years (see also [1]). Since higher aviation demand comes along with higher fuel consumption, CO₂-emission becomes an important issue in the future. Besides CO₂ other components such as NO_x and particles are also included in the aircraft exhaust, which have an impact on environmental conditions. More efficient aircraft are hence needed for new deliveries.

The International Civil Aviation Organization (ICAO) takes action toward global reduction of green house gas emission. The Committee on Aviation Environmental Protection (CAEP) is a technical committee of the ICAO council, which develops proposals to minimize the effects of aviation on the environment. A forecast regarding CO₂-emissions and fuel consumption has been undertaken by CAEP based on the data of 2010. The trends were forecast for 2020, 2030 and 2040 by means of three models and the data were extrapolated to 2050. For more information refer to ICAO [33]. The results are depicted in general in Fig. 1.1 with minor modifications and reduction in presented data compared to [33] for more clarity. Three main factors have been taken into account in this study, which are the contribution of aircraft technology, improved air traffic management (ATM) and infrastructure use. The baseline in this diagram including fleet renewal does not account for any technological and infrastructural improvements. The areas associated with the individual scenarios highlight the distribution regarding low and optimistic improvement. On the right diagram the forecast full-flight CO₂-emission for international aviation is depicted. In this approach it is assumed that 1 kg of jet fuel burn results in 3.16 kg of CO₂. It can clearly be concluded that even at an optimistic technological and advanced operational improvement rate the fuel consumption and the related CO₂-emissions in international aviation increase considerably in the future. According to the environmental report 2013 of ICAO ([33]) 65% of global aviation fuel consumption results from international aviation and is expected to

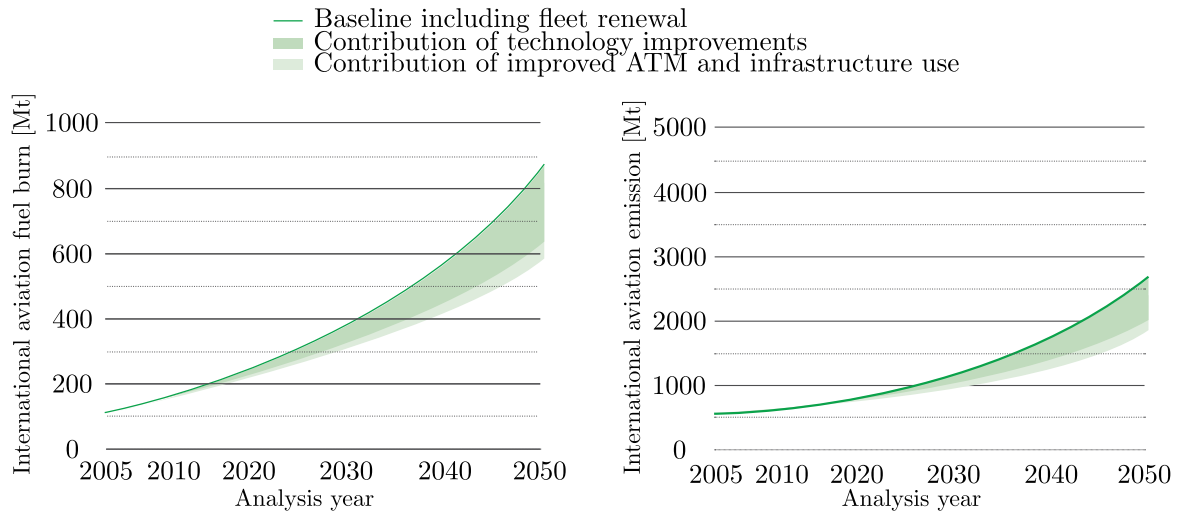


Figure 1.1.: International Aviation Emissions ([33])

grow to nearly 70% by 2050. This fact highlights the importance of enhancement of fuel efficiency in aviation. As expected, there are many factors affecting the fuel consumption. Apart from operational and infrastructural factors, aircraft technology and propulsion technology can make a significant contribution to environmental goals, as it can be seen from Fig. 1.1.

The continuous development in aircraft technology resulted in the priority of jet engines over piston engines as the driving unit, since the engine weight would otherwise rise dramatically for higher airspeed requiring higher power. Besides, a jet engine features higher efficiencies in comparison to a piston engine. Furthermore, the propeller performance deteriorates at higher airspeed due to increased aerodynamic losses. The performance limit of the propeller and the power limit of the piston engines were both overcome by turbojet engines. In spite of the fact that propeller engines feature higher propulsion efficiency at lower Mach numbers, they are perceived as loud, vibration-intensive, and also less safe for passengers (Bräunling [12]).

The combination of the advantages of the propeller engines performing at higher propulsion efficiency at lower flight speeds and the better thermal efficiency of the turbojet engines leads to the so-called Turbofan. It comprises a large-diameter shrouded fan at the front of the engine, which, however, consists of multiple blades in contrast to a conventional propeller. It further consists of a core engine comparable to a turbojet engine, driving the fan and partially contributing to thrust generation.

The thrust generated by a jet engine is determined by the change of the product of mass flow rate and velocity between the inlet and the exit of the engine. Either higher exit velocities or higher mass flow rates result in higher thrust. In a turbojet, the thrust is generated by a single engine (aero gas turbine) consisting of a compressor, combustor, expander, and nozzle. Due to the single-flow concept, the higher velocity at the engine exit provides for the thrust. In a turbofan, however, the generated thrust is only partially contributed by the core engine. The significant fraction of the thrust is attributed to the fan, which is driven by the core engine. Considering

the fact that the thrust is determined by velocity change and mass flow rate, the fan makes advantage of higher mass flow rate due to its large diameter with a small change in the velocity. A variety of definitions of efficiency can be encountered in the literature for aircraft engines. Fuel consumption depends generally on many factors. The drag generated by the fuselage, the wings and the engine itself results in higher thrust. This is, however, attributed to the aerodynamic performance of the airplane. Most importantly the fuel consumption depends on the engine efficiency. The overall engine efficiency is determined by the propulsion efficiency and the thermal efficiency. The propulsion efficiency describes how efficiently the useful power generated by the engine is used to produce thrust. The thermal efficiency describes on the other hand the performance of the thermodynamic process within the engine and how efficiently the thermal energy is converted into useful power. At this point the useful power of an aircraft needs more specification. In contrast to a stationary gas turbine, in which mechanical shaft power is of importance, the useful power of a turbojet is defined by the change of kinetic energy between the engine exit and the engine inlet per time unit (see also [12]). Since a Turbofan is a bypass engine, both air flows need to be accounted for. Taking into consideration the required thrust only, either the exit velocity or the mass flow rate or both can be increased and adjusted. The propulsion efficiency, however, is affected by the choice of these options. According to the definitions of thrust and propulsion efficiency it can be stated that lower engine exit velocities result in higher propulsion efficiency (see [12]). By decreasing the exit velocity toward the inlet velocity of the engine the propulsion efficiency approaches the value of one. This would, however, cause infinitely large fan diameters to provide the required thrust. The goal is hence to increase the fan diameter (higher bypass ratio). This requires a lower fan pressure ratio, which reduces the exit velocity together with the jet noise. This leads to performance-related fan blade adjustment or reduction of fan speed for aerodynamic reasons ([12]). In a conventional turbofan the fan is connected to the low pressure compressor (LPC), which is further linked to the low pressure turbine (LPT) driving both components. Lower fan speed would thus cause lower rotational speed of the LPC and LPT, which results in a higher stage number for a given pressure ratio and hence larger axial length of the engine.

This challenge can be overcome by the modern technology of geared turbofan (GTF), which decouples the low-spinning fan from the LPC and the LPT by means of a gear box allowing them to operate at their optimum speed. With this technology the stage number and thereby the axial engine length can be reduced. This in turn reduces the maintenance costs due to lower parts count. However, the additional weight due to the gearbox, counteracted by a lower stage number though, as well as the additional propulsion efficiency losses associated with the gearbox need to be accounted for.

In this context the GTF family PW1000GT belonging to Pratt & Whitney's next generation PurePower engines can be mentioned as an example (Pratt & Whitney [43]). The PW1100G-JM engine (the second digit denotes the customer) powering the A320neo family has a bypass ratio of 12:1 in comparison to a modern high bypass turbofan with a bypass ratio of 10:1 and features double-digit improvements in fuel efficiency (lower CO₂-emissions and NO_x-emissions)

as well as 50% reduction in noise ([43]). The engine architecture comprises 3 LPC stages and 3 LPT stages. In Fig. 1.2 the PW1100G-JM engine is depicted with the corresponding flow path and the gearbox. For more information regarding differences between conventional and geared turbofans refer to Kurzke [34] and Denos and Paniagua [15].

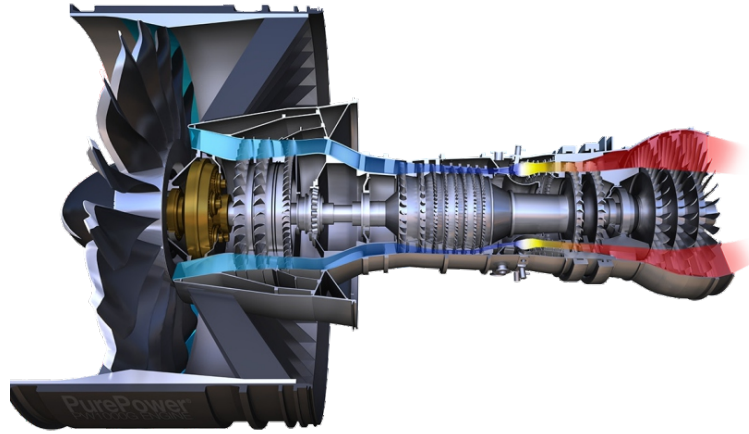


Figure 1.2.: GTF PW1100G-JM (Pratt & Whitney [44])

As described above enhancement of propulsion efficiency can be achieved by higher bypass ratios and the associated restrictions can be overcome by the new technology of GTF. Since, however, the overall efficiency as a product of propulsion efficiency and thermal efficiency affects the fuel consumption, the enhancement of thermal efficiency further improves the overall engine performance. The thermal efficiency is determined by the thermodynamic cycle of the core engine, which depends on thermodynamic parameters such as pressure ratio and turbine inlet temperature as well as component efficiencies. The thermodynamic parameters need to be adjusted for a given operation point. Due to the complexity of the components in an aero engine as in any other thermal turbomachinery it is a difficult task to continuously improve and optimize all components at once. The researchers are hence keen to improve particular components in isolation.

1.2. Low Pressure Turbine

The LPT is the focus of the investigations in this thesis. As mentioned before the operation and design of the LPT depends on the engine architecture. In a GTF the LPT is not linked to the fan and can hence operate close to its optimum rotational speed. According to Dewanji et al. [19] the LPT efficiency therefore increases. This can be explained by considering the Smith diagram, which describes various stage isentropic efficiencies at different flow coefficients and loading coefficients. According to the Smith diagram lower flow coefficients and loading coefficients lead

to higher isentropic efficiencies ([12]). In a GTF the LPT operates in an area of higher efficiency levels due to higher circumferential velocity (see also Malzacher et al. [36] and Kurzke [34]). This advantage, however, comes along with technological challenges. One of the issues is the high stress level in the rotating parts due to increased rotational speed in combination with a high temperature level as noted in [36]. In this case the blade root stress can be reduced by using tapered hollow blades made from low density materials. This is a demanding design regarding efficient work extraction, since the pitch to chord ratios at the root and at the blade tip are quite different ([34]). The tip region of such a blade features a very thin airfoil resulting in very high pitch to chord ratios ([36]), which is, however, in compliance with the principles of aerodynamics of LPTs requiring a higher degree of reaction in the tip section ([12]).

1.2.1. Low Pressure Turbine Losses

The primary aim of every innovative research is to decrease losses and enhance efficiency. This task requires indeed sufficient knowledge about the component being investigated. Since the objective of the current study is associated with uncooled LPTs, adequate knowledge about loss mechanisms in a LPT is of high importance. A large amount of work and publications can be found in the literature regarding losses in LPT stages. According to Denton [17] the loss generation can be broken down into profile loss, endwall loss and leakage loss, although the mechanisms should not be considered independent. It is, however, difficult to understand the interaction and the allocation of individual loss phenomena. It is further stated in [17] that the profile loss is associated with the blade boundary layer well away from the endwalls and can hence be studied based on two-dimensional cascade tests due to its character. It is further argued that the endwall loss is sometimes referred to as secondary loss due to the annulus boundary layer passing through the blade row. It is, however, a combination of many factors and does not directly arise from secondary flow. The leakage loss results from the leakage flow through the tip clearance of the rotor or the hub clearance of stator blades. It is thus clear that the interaction between leakage loss and endwall loss may be considered very strong. Due to the complexity of the individual mechanisms and their interaction the elaboration of all loss phenomena is a difficult task and goes beyond the scope of the current study. The investigations in this thesis are hence devoted to tip-leakage losses in uncooled LPT blades.

1.2.2. Shrouded Low Pressure Turbine

A lot of work has been dedicated to leakage reduction over rotor blade tips in the past. In general the blade tip architecture can be classified in shrouded and unshrouded configurations. According to Arts [6] unshrouded blades are often found in the first stages of a high pressure turbine (HPT). Various geometrical improvements such as winglets and squealers are considerable in order to increase the sealing effect. More information about unshrouded blades and appropriate

sealing can be found in the corresponding literature.

Providing the rotor blades with shrouds brings the advantage of better sealing and complies with structural aspects of the blades. The contiguous arrangement of the shrouds ensures sealing in axial direction over the entire circumference of blade tips. In spite of these advantages using shrouds results in higher stress in the blade root (Halbertschlager [28]) as well as cooling difficulties and higher costs (see also [6]).

Concerning the sealing function a shrouded configuration is comparable with labyrinth seals between rotational and stationary parts and might hence comprise a number of fins over the shroud surface. A variety of geometries have been investigated in the past in order to improve the sealing effectiveness of the shrouds. In Fig. 1.3 a common shroud configuration called stepped labyrinth seal is depicted.

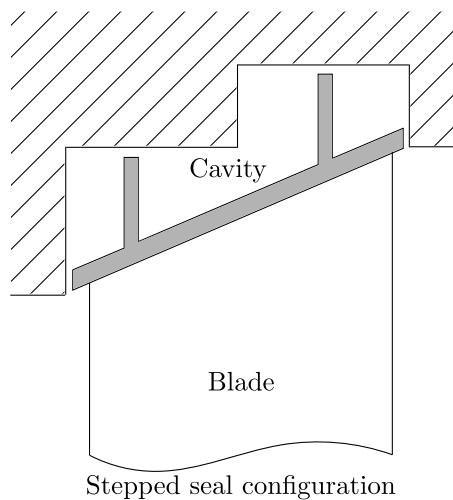


Figure 1.3.: Common Shrouded Blade Configuration

1.3. Scope of the Thesis

As mentioned high rotational speed in combination with higher stage pressure ratio is the characteristic of modern LPTs in GTFs. For mechanical reasons it is necessary to keep the blade mass at outer diameters as low as possible in order to reduce the stress at the blade root due to the centrifugal forces. In Riegler and Bichlmaier [45] it is stated that a careful cut back of the LPT blade shroud is necessary without significant sealing penalty.

It has also been mentioned that higher rotational speed contributes to improvement of the LPT aerodynamics. Higher stage pressure ratios together with a lower axial length and a higher degree of reaction in the blade tip region on the one hand and reduction of the shroud volume on the other hand both result in higher tip-leakage. Improvement of sealing efficiency hence

becomes significant. Furthermore higher sealing should be achieved with no additional weight and low cost in compliance with the requirements of the modern LPT technology.

The objective of the studies in this thesis is the method of passive tip-injection applied to uncooled shrouded rotor blades in LPTs serving as a fluidic jet barrier reducing the tip-leakage losses. This method has already been investigated at the department of Fluid-Flow Machinery of the Institute for Energy Systems and Thermodynamics at Technische Universität Wien on unshrouded blades with satisfactory results. Due to the fact that a shrouded configuration is necessary in some cases for structural reasons, the method of passive tip-injection in combination with blade shrouds is a further step toward application of fluidic jet barriers in LPT stages. Taking into consideration modern LPTs the first stage is cooled due to high turbine inlet temperatures ([36]). The cooling air injected into the tip region can act as a jet barrier in this case. The focus in this work is, however, on uncooled stages and providing them with passive tip-injection. The term passive signifies that the injection mass flow is extracted from the stage mass flow without any external sources. In this spirit it is important that this method is technically feasible and cost-effective.

The impact of passive tip-injection should be considered in terms of reduction of tip-leakage mass flow rate as well as affected downstream flow field. Both issues are of importance and should be taken into account properly. Furthermore the extraction of the injection flow can be undertaken in different ways and various possibilities are given regarding the position of the injection outlet over the shroud with respect to the fins. These aspects affect the effectiveness of the injection and need to be considered taking into account also manufacturing and structural restrictions. In this regard passive tip-injection is a challenging method aiming at reduction of tip-leakage losses with lowest possible aerodynamic penalty due to injection flow extraction and no operational constraints.

As for any sealing application the discharge behavior of passive tip-injection should be studied in the first stage. For this purpose analytical models and simple CFD calculations can help understand the leakage flow and estimate the functionality of the method. However, three-dimensional effects should not be overlooked. In this regard investigations on a linear cascade can be considered as a further step toward understanding the three-dimensional flow physics. Furthermore the influence of passive tip-injection on the leakage flow in case of partially shrouded blades can be studied with reasonable effort. Nevertheless turbomachinery flow is subject to rotation, which in turn affects the injection flow and more importantly the contribution of passive tip-injection to specific work. Finally the impact of a fluidic jet barrier on the downstream flow field should not remain unmentioned, since it affects the incidence of the following blade row and the associated losses.

The issues mentioned above provide the scope of this thesis in order to draw conclusions concerning the effectiveness of passive tip-injection in uncooled shrouded LPT stages.

2. Literature Overview

In this chapter a literature overview is given regarding investigations of leakage flow with special attention being paid to shroud cavity flow and its interaction with the main flow. It should be mentioned that a lot of work has been undertaken in this field, out of which the most relevant ones, in the view of the author, have been taken into consideration in order not to go beyond the scope of the thesis.

2.1. Shrouded Blades

In Yoon et al. [63] the effect of tip clearance on output power and efficiency is studied for shrouded and unshrouded blades at two levels of reaction (24% and 50%) analytically and experimentally. The experiments were undertaken using a single-stage low-speed axial-flow turbine facility. It is noted that there exists a break-even clearance, at which both the shrouded and unshrouded configuration have the same efficiency. At lower clearance the unshrouded turbine is expected to feature higher efficiency than the shrouded turbine. The trend of the measurement data also suggests that at zero clearance the efficiency of the unshrouded configuration is higher. It is argued that this effect is mainly associated with energy dissipation in the upstream and downstream cavities, windage loss over the shroud and changes in the secondary flow loss. An analytical model was also derived in this study applying the Denton loss model ([17]) for estimating the loss coefficient. In contrast to the traditional approach suggesting that the efficiency penalty is determined by the tip-leakage mass flow rate only, this model considers this penalty in terms of dissipated kinetic energy. Furthermore an analytical model was derived regarding the relative change in output power. This model takes mainly into account the corresponding flow angles at the inlet and the outlet of the rotor. There is a good agreement between the analytical approach and the measurements. Both indicate that at a fix flow coefficient the fractional change in output power due to tip clearance is twice the fractional change in efficiency for all configurations.

The investigations in [63] are extended by studying the impact of the work coefficient and the flow coefficient as well as the degree of reaction on the leakage loss across both the stator and the rotor in Yoon [62]. Denton's analytical model [17] is extended to account for the velocity triangle and its associated kinetic energy on each blade row in shrouded and unshrouded configurations. A lower degree of reaction results in lower efficiency loss of the rotor due to tip leakage for a

fixed work coefficient. It, however, increases the efficiency loss in stationary blades. Furthermore it is mentioned that the effect of reduction of the degree of reaction on shrouded blades is more significant than on unshrouded blades. Taking into account the stator as well the dependency of the efficiency loss on the degree of reaction is affected by the number of the seals used in the shroud configuration. At higher seal numbers a reduction in efficiency loss can be achieved by reducing the degree of reaction.

2.1.1. Discharge Characteristics of Labyrinth Seals

There is a variety of investigations regarding the discharge behavior of labyrinth seals in the literature.

In Traupel [55] empirical and theoretical relations concerning the discharge behavior of labyrinth seals are included. Furthermore basic thermodynamics of the flow is discussed. In this spirit engineering relevant correlations are presented.

In Leeb [35] the flow field and pressure distribution in the labyrinth chambers were investigated analytically, experimentally as well as by means of numerical calculations. In the framework of the investigations two common labyrinth seal configurations: staggered labyrinths and straight-through labyrinths were investigated. Furthermore the effects of eccentricity, rotation and swirled flow at the inlet were examined. Besides the flow physics was discussed and analytical approaches were employed. The carry-over effect in the case of straight-through labyrinth seals emerges from the results.

Subsequently Matthias [37] investigated the above mentioned effects in more details by means of three-dimensional numerical calculations. Furthermore analytical as well as empirical relations concerning the thermodynamics of the labyrinth flow and its discharge characteristics were taken into consideration.

In Wittig et al. [61] discharge coefficients have been considered for straight-through and stepped labyrinth seals with various pressure ratios, fin numbers and tip clearances experimentally and numerically (two-dimensional). The results show lower discharge coefficients in the case of stepped labyrinth seal geometry. Furthermore the carry-over effect is present in the results obtained in the case of the straight-through labyrinth seal.

El-Dosoky et al. [21] present in the first part of their work an analytical model for the discharge coefficient of shrouded blades based on conservation of mass, momentum and energy for compressible flow. They state that from three labyrinth fins the effectiveness of the configuration does not change considerably with increasing the fin number due to the inverse relationship of the leakage mass flow rate to the fin number. They further state that higher flow coefficients result in higher leakage mass flow rate. Also the efficiency penalty increases with increasing flow coefficient at constant geometry parameters.

2.1.2. Interaction of Tip-Leakage Flow and Main Flow

In Denton [17] the loss mechanisms in turbomachines including tip-leakage losses for unshrouded as well as shrouded blades are described and examined analytically. The irreversible entropy generation is taken into account as an approach for generated losses. It is stated that the entropy generation due to tip-leakage flow in shrouded blades is primarily associated with the mixing process between the leakage flow and the main flow downstream of the blade row. Furthermore it is stated that the kinetic energy associated with the meridional velocity is mostly dissipated in the labyrinth chamber of the blade shroud. Measurements, however, show that the swirl velocity is not generally changed throughout the shroud clearance and remains the same as in the upstream flow. Mixing losses are generated due to reinjection of the tip-leakage flow with deviating meridional velocity as well as swirl velocity to the main flow, though the difference in the swirl velocity is the most dominant factor. In this spirit an analysis is carried out for incompressible flow with an expansion to compressible flow including simplifications verified by measurements. This theory further predicts that any loss of swirl velocity of the leakage flow before mixing with the main flow reduces the overall loss. It also confirms that the entropy rise per percent of leakage flow is determined almost entirely by the mixing process downstream of the blade row, while the processes over the shroud mainly affect the leakage mass flow rate.

In the second part of the work by El-Dosoky et al. [21] the losses due to mixing of the tip-leakage flow with the main flow are considered analytically. In this spirit the entropy generation due to the mixing as well as deviating turning and temperature differences of the leakage flow in comparison to the main flow are investigated by means of analytical considerations. They further show that the injection angle at which the leakage flow enters the main flow can considerably affect the entropy generation downstream of the rotor.

In Pfau et al. [42] labyrinth cavity flow and its interaction with the main flow has been investigated experimentally by means of traversed pneumatic probes as well as pressure tapings on the shroud and cavity endwalls. The results are acquired in a stationary test rig without rotation. In this spirit the labyrinth flow is taken into account in an isolated manner. In the framework of the investigations three important characteristics have been examined. These are periodic trailing edge pressure field, passage vortex and interaction between the leakage flow with high angular momentum and low axial velocity and the main flow. The flow has a highly three-dimensional feature in the vicinity of the tip gap outlet and in the interface between the main flow and the leakage flow. At the tip gap outlet the main flow enters the cavity on the pressure side of the passage and leaves it on the suction side resulting in a periodic flow field.

Wallis et al. [57] investigated the enhancement of extraction and reinjection of the tip-leakage flow into the main flow. Based on the analytical considerations in [17] these investigations aim at reducing a portion of the generated losses by reintroducing the tip-leakage flow into the main flow with the same value of tangential velocity as in the downstream flow, which also reduces the

deviation of the mixed out flow angle from its design value. In the framework of the investigations a four-stage low aspect ratio air turbine was used. The shroud configuration of the third stage was modified by positioning a turning device consisting of a row of tiny bladelets positioned immediately downstream of the radial sealing fin onto the shroud. Four configurations resulted on the whole, while the first one was the datum configuration. The time-mean flow field was measured by means of a three-hole probe in the shroud cavity and by means of a four-hole probe over the full span downstream of the rotor. It could be noticed that the absolute angular momentum did not vary significantly through the shroud cavity of the datum configuration. The combination of relatively high absolute tangential velocity with low axial velocity increases the incidence angle onto the next blade row over -30° in the outer region of the blade. Concerning the flow field in the exit cavity it could be found that there was an ingress of the main flow close to the pressure surface of the blade. The flow reenters into the main flow close to the suction side resulting in a circumferentially varying flow field in the casing region at the outlet. The last configuration using baffles downstream of the sealing fins on the casing made it possible to align the leakage flow to the main flow direction before leaving the cavity. However, none of the configurations could improve the efficiency. It is therefore concluded that understanding the unsteady three-dimensional flow phenomenon in the shroud cavity is of high importance regarding developing methods aiming at any kind of improvement.

The investigations in [57] are followed by Rosic and Denton [46]. They present experimental results in a low-speed three-stage model turbine with low aspect ratio blading representative of steam turbine industrial practice. Prior to the investigations five numerical calculations were carried out regarding various parameters separately. These include the inlet shroud cavity, the exit shroud cavity, combined influence of both cavities, windage loss caused by the shroud rotation and finally the combined impact of the mentioned parameters with leakage flow. The fact that the unturned leakage flow maintains its swirl velocity almost entirely over the shroud is emphasized. This makes the improvement of reentering conditions of the leakage flow into the main flow necessary. Furthermore it is stated in [46] that in shrouded low aspect ratio turbines the flow is dominated by the leakage flow and the secondary casing flow migrates radially toward the midspan. Reduction in the leakage flow reduces this migration in the downstream flow field. In order to analyze the effect of turning the leakage flow into the axial direction experimentally, three turning vane configurations consisting of two, four and eight turning vanes per rotor blade pitch respectively were investigated. In contrast to [57] the turning vanes were mounted into the downstream shroud exit cavity of all three rotor rows. Additionally experiments with open shroud cavities as well as closed cavities (leakage mass flow rate of 0.7% of the main flow) were carried out for the sake of comparability. It could be shown that the distribution of the absolute exit yaw angle was increasingly improved with increasing the vane number in the vicinity of the casing but also toward the midspan. The presence of eight turning vanes could almost completely eliminate the high swirl of the leakage flow resulting in an absolute yaw angle distribution similar to that measured with closed cavities. The difference in tangential velocities at the tip gap outlet

creates a highly skewed boundary layer at the inlet of the downstream stator. This results in increased secondary flow and radial migration of the low momentum endwall fluid. Furthermore the configuration with eight turning vanes resulted in an efficiency improvement of 0.4% at the design point, which agrees with the predicted offset loss associated with the mixing losses of the reentering leakage flow and the losses in the downstream stator blade row.

The model turbine in [46] was further taken into consideration for investigations regarding the effect of various geometries of the cavity and the shroud on the leakage mass flow and turbine efficiency in Rosic et al. [47] and Rosic et al. [48]. In [47] the second rotor of the model turbine was simulated numerically with different cavity lengths at the inlet and at the outlet (by varying the axial cavity endwall positions and the shroud overhang separately) and shroud thicknesses. Furthermore different shroud cavity depths and fin clearances were considered numerically. The mixing plane approach was used in order to isolate the shrouded rotor from the influence of the upstream and downstream stator. It is stated for the model turbine that the rotor blade pressure field dominates the flow field in the exit cavity, while the downstream stator potential field causes the circumferential variation of the reentry of the leakage jet. Without going into more details, it could be shown that the flow field in the inlet cavity and in the outlet cavity as well as the main flow ingress into both cavities and its mixing were affected by the mentioned parameters in different ways and at different levels of intensities. It could be found that reduction of the length of both cavities (by rearranging the axial casing endwall position and expansion of the shroud overhang in the inlet cavity) is beneficial regarding the leakage mass flow rate and the turbine efficiency. Reduced shroud thickness for a fixed cavity size also resulted in reduced leakage mass flow rate. The dominant effect of the leakage flow and shroud geometry parameters on the mainstream aerodynamics could hence be confirmed.

In the second part of the investigations ([48]) numerous cavity modifications (chamfered and contoured cavities, different types of axial deflectors, radial deflectors, etc.) were investigated experimentally as well as numerically for the same model turbine configuration. It could be found that the interaction between the mainstream flow and the cavity flow can affect the efficiency mostly. The improvement of this interaction can hence improve the efficiency rather than the reduction in tip-leakage fraction only. Furthermore the reentry of the leakage flow causing a separation on the casing thickens the boundary layer, which in turn increases the secondary losses of the following stator row. It could be concluded that higher effectiveness of the optimized geometry (efficiency improvement of 0.75% compared to the datum geometry) could be achieved at higher tip clearance.

Anker and Mayer [2] and Giboni et al. [27] investigated the interaction of labyrinth seal flow and main flow in a 1.5-stage axial turbine consisting of two stator rows and a rotor. In [2] two different labyrinth clearance heights of 0.6% and 1.8% of the blade height were studied numerically and experimentally. The results show that higher clearance results in a negative incidence of greater magnitude in the vicinity of the casing. This effect leads to pressure side separation of the following stator row and higher losses. In [27] measurements using pneumatic five-hole probes

and three-dimensional hot-wire probes were carried out. Furthermore the measurements were compared to numerical results calculated for incompressible flow and with the k/ϵ turbulence model and sliding mesh method for rotor-stator interaction. An increase in the strength of the leakage jet could be observed toward the suction side, where it enters the main flow with high radial components separating at the casing edge and forming a large zone of recirculation. Further in circumferential direction the flow features higher axial components and the recirculation zone changes its axis into the rotor axis. The circumferential flow unsteadiness due to the leakage flow affects the stator incidence angle as well as the size and position of its casing sided passage vortex.

Pfau et al. [41] and Pfau et al. [40] investigated the flow field in the shroud cavity in a two-stage turbine rig by means of time averaged five-hole probe measurements as well as time-resolved virtual four-sensor probe measurements. In [41] the flow field in the inlet cavity of the second rotor is investigated in various measurement planes in axial direction. The pressure fields of the rotor and the stator as well as the complex and three-dimensional vortex structure in the inlet cavity of the rotor have been examined precisely. They argue that besides mixing losses and vortex stretching the cavity flow affects the rotor through the low total pressure flow spilled into the main flow in the vicinity of the tip gap inlet resulting in a negative incidence in this region. In [40] the cavity flow field in different rotor cavities and stator cavities has been examined. Furthermore the velocity triangles of the main flow and the leakage flow are considered and an analytical mixing approach has been derived. It is further concluded that the influence of the cavity depends on its position and the circumferential momentum of the incoming flow. Further flow features such as boundary layer thickening and secondary flow strengthening due to the cavity flow and leakage flow are also discussed. Based on the results design changes are proposed.

In Bohn et al. [11] the near-shroud cavity flow field is investigated numerically in a two-stage axial turbine with three configurations: without cavities, without radial gaps and with cavities and radial gaps. The presence of cavities at both the leading edge and the trailing edge causes periodic main flow ingestion into the cavity. Furthermore other flow patterns including horseshoe vortex and secondary flow displacement due to the increased boundary layer have been discussed.

Szymanski et al. [54] investigated the impact of pressure ratio, rotational speed and roughness on the mass flow rate in labyrinth seals by means of CFD calculations. They could observe that at higher pressure ratios the effect of rotation is merely limited. Furthermore they could show that the wall roughness increases the influence of the rotational speed on the leakage mass flow rate.

2.2. Fluidic Jet Barriers

Implementation of fluidic barriers requires a high pressure supply in order to ensure sufficient injection mass flow rate acting as a blockage. At this point it can be differentiated between active and passive methods. Active fluidic jet barriers take advantage of an external high pressure fluid supply, commonly the compressor, in order to provide the proper injection mass flow rate. This case is comparable to cooled turbine blades, where the injection of cooling air in the tip section of the rotor acts as an active fluidic sealing against the tip-leakage flow. In this case further flow parameters regarding heat transfer behavior of the tip section of the blades are of great importance. Due to this fact the impact of the cooling air on tip-leakage flow can not be considered in an isolated manner. Since passive tip-injection is the objective of the current study, the effects of cooling applications on leakage flow would go beyond the scope of the investigations and are therefore not considered in this work. In the method of passive injection the mass flow is extracted from the stage flow itself. The position of extraction is therefore essential, since it should be ideally chosen in a way that high total pressure is available with lowest amount of penalty regarding flow aerodynamics. Furthermore the injection position should be chosen taking into account the flow conditions in the leakage region. Lastly the implementation of the injection channel connecting the extraction slot to the injection slot should be feasible from the manufacturing point of view. In the following some active and passive methods in uncooled turbine applications are presented briefly.

2.2.1. Active Fluidic Sealing

In Curtis et al. [14] the Impact of active injection on leakage flow as well as turbine efficiency is investigated analytically, numerically as well as experimentally. A single-stage low-speed intermediate pressure air turbine was used for the investigations. The injection was realized by means of a continuous circumferential nozzle in the casing supplied by a plenum mounted circumferentially in the casing as well. The jet was inclined by 45° against the leakage flow direction. The analytical considerations were undertaken in two ways in terms of momentum conservation and injection jet curvature respectively. It is stated that the compressibility could be neglected in the case under investigation. The results show that the overall tip-leakage mass flow rate at the tip gap outlet as well as the overall turbine efficiency taking into account also the injection jet both depend considerably on the injection mass flow rate. It could also be shown that the highest efficiency increase of 0.4% could be achieved at an injection ratio of 1.2% of the main flow. Perfect sealing (no mass flow leaking out of the mainstream ahead of the rotor) could be achieved at an injection ratio of 3.5% of the main flow. This case, however, resulted in a decrease in efficiency of 0.6%.

Hogg and Ruiz [31] investigated the influence of active fluid injection on the leakage flow numerically. In the first part of their investigations a straight channel was considered with no labyrinth

seals. Taking into account the overall mass flow rate at it is concluded that a perpendicular injection would increase the overall leakage flow at the channel outlet. Considering the injection mass flow rate extracted at high pressure, this reduces the amount of working flow. They could also show that an inclined jet (against the leakage flow direction) reduces the overall mass flow rate. This was explained by the fact that the injection flow being turned and accelerated into the direction of the leakage flow results in a higher pressure drop in axial direction. Nevertheless they concluded that a simple air curtain sealing application has only limited potential regarding leakage flow reduction. In the second part of the investigations a straight-through labyrinth seal was taken into calculation. The configuration consists of three sealing fins with the central fin inclined by 45° against the oncoming leakage flow. The active injection is carried out along the upstream surface of the central fin in a way that the jet flow is supported by the fin. In this case a significantly greater potential exists for improving the sealing performance. It is further stated that the leakage reduction potential under low pressure conditions is even greater than under high pressure conditions. In addition to the active injection, some applications of passive fluidic sealing systems using the swirl kinetic energy of the upstream flow as a driving force for the injection jet are proposed and discussed without going into further details.

Auyer [8] patented an active sealing arrangement by means of fluid jet over blade tips. In this configuration the blade shroud is uncommonly attached to the casing without any sealing fins providing proper clearance to the tip section. There exists an annular space between the shroud and the casing supplied by external compressed air (from compressor). The compressed air is injected to the blade tip section by means of a circumferentially arranged and toward blade leading edge inclined slot. The slot is positioned in a distance of 25% axial chord length upstream of the blade trailing edge. This position is stated as advantageous regarding the profile pressure distribution of the blade considered in the patent. The fluidic jet acts as a barrier and is capable of redirecting the leakage flow into the main flow over the tip section before leaving the tip gap at the blade trailing edge without participating in stage work, as stated in the patent.

Auld et al. [7] studied the impact of active fluidic jet barriers in a high-speed single-stage axial turbine numerically. The overall mass flow rate at the outlet of the shroud cavity has been taken as a measure for sealing effectiveness. Different jet widths and inclination angles were investigated at different pressure ratios driving the injection. They reason that the jet induces higher static pressure upstream of the injection resulting in lower pressure gradients driving the leakage flow. The higher static pressure is due to the direction of the fluidic jet opposing the leakage flow. They further take into account the shear forces in the cavity region of the shroud resulting in reduction of the inlet swirl of the leakage flow and contributing to the stage work. They further argue that the injection flow gains swirl momentum by the rotor having a negative effect on the stage work. It is mentioned that this negative effect can be eliminated by positioning the jet close to the downstream edge of the shroud. They further state that this has a positive effect regarding mixing losses downstream of the rotor. They could also show that higher inclination of the jet toward the leakage flow direction increases the sealing effectiveness.

2.2.2. Passive Fluidic Sealing in Uncooled Turbines

In Turnquist et al. [56] a variety of fluidic sealing arrangements is presented. Some of these arrangements comprise a circumferential fluidic diode with its inlet and outlet at two different axial positions along the flow path through the labyrinth seal. The inlet and especially the outlet of the diode can be disposed in a way that the fluidic jet is guided by the sealing fin. Other configurations such as disposing the inlet and the outlet of the fluidic diode between adjacent fins are also presented in this patent. In a further configuration the injection channel inlet is placed at the upstream face of the labyrinth seal arrangement outside of the clearance between the rotor and the stator. In contrast to the cases, in which the fluidic barrier acts passively, an active method is presented as well. In this case the fluidic jet is supplied by higher pressure and injected between two adjacent fins. Furthermore in the majority of the arrangements the sealing fins are inclined against the leakage flow direction in order to achieve higher sealing effectiveness. This inclination could also be applied to the fluidic channel to improve the functionality.

The method of passive tip-injection, as it was named for the investigations regarding improvement of leakage behavior in uncooled and unshrouded LPT blades, was presented at Technische Universität Wien. The extraction slot is positioned at the blade leading edge with a proper distance to the tip due to the casing boundary layer. It is further reasoned that high total pressure and low losses are encountered in this region. The injection position over the blade tip is chosen on the basis of profile pressure distribution in the tip region.

The first investigations on passive tip-injection were carried out by Hamik [30] for unshrouded blades in an analytical way as well as by means of simple 2D CFD. The analytical considerations take into account the tip-leakage mass flow rate at the tip gap inlet and the impact of the injection flow is incorporated in the calculation of the stage efficiency. In this spirit a discharge coefficient is defined accounting for the leaking mass flow rate over the blade tip in a 2D configuration only. These considerations were extended and an injection arrangement consisting of an injection channel perpendicular to the leakage flow direction was implemented in a linear cascade test rig. The experimental results were followed by Hamik [29] and could show improvements compared to the unshrouded case without injection. The analytical considerations in [30] were extended by the second part of the work by Ghaffari [23] in a way that the injection mass flow rate was also taken into account in the formulation of the discharge coefficient. The 2D simulations in [30] were further adapted in a way that the flow extraction was also simulated, however, with restrictions. The results could show a decrease in leakage mass flow rate at the tip gap inlet. The overall mass flow rate, however, increased due to passive tip-injection. In the next step the investigations in [29] were extended by inclination of the injection direction by 45° toward the leakage flow direction. This case was studied experimentally and by means of numerical simulations. The results are presented in Benoni [9]. The linear cascade used for the measurements and the numerical calculations was the same as in [29]. The CFD calculations were carried out for incompressible flow. The injection channel was, however, not modeled by CFD,

since it resulted in unexpected low injection mass flow rates. The measurements showed a high dependence of the results on small changes in geometry and operational conditions attributed to the test rig. It could, however, be stated that inclined passive tip-injection has a potential of reducing the tip-leakage losses in unshrouded blades especially for small tip gap heights.

2.3. Computational Fluid Dynamics

Numerical calculations contribute to a substantial part of investigations. Great improvements have been undertaken over the years in the area of meshing complex geometries and resolving complex flow features. Commercial and in-house CFD codes allow for more physical insight into the flow regions, which are still challenging for experimental techniques. The numerical results should, however, be taken into consideration with caution, since commercial and feasible CFD still faces limitations and modeling needs. In this spirit the turbulence and its modeling still remain a sophisticated task and the numerical calculations are limited due to the computational resources. In this regard the direct numerical simulation (DNS) should not be left unmentioned. With DNS the three-dimensional unsteady Navier-Stokes equations are calculated for a turbulent flow. It is the most precise numerical method, since a wide range of time scales and length scales in a turbulent flow is resolved. It requires, however, extremely fine and high-quality meshes as well as high computational performance. DNS is therefore not feasible for commercial and general purpose.

In Denton and Dawes [18] a review of main CFD methods together with their limitations are presented. In this work the application of CFD is discussed without describing the numerical methods or turbulence modeling. Since this paper belongs to the year of 1999, it is helpful regarding the improvements in CFD. In this spirit it is stated that all modeling limitations except turbulence are overcome if the unsteady 3D flow can be calculated in multiple blade rows (in the foreseeable future). It is further mentioned that as the flow primary path becomes more and more predictable, the secondary flow paths such as tip-leakage flow and cavity flow and their interaction with the primary flow become increasingly important and can have a surprising impact on the overall aerodynamic performance. Calculating secondary flows requires precise knowledge about the shape and the thickness of the inlet boundary layer, which are unknown in most practical applications. This is a severe limitation regarding the ability of single blade row calculations to predict the secondary flow in a real machine. It is further argued that the tip-leakage flow itself is primarily inviscid and only its mixing depends on turbulence modeling. Furthermore the authors state that the accuracy of the calculations of unsteady 3D flow through a whole machine will be limited by turbulence and transition modeling and these restrictions might never be overcome.

In Denton [16] the limitations of CFD are discussed. It is stated that errors can arise from following sources:

- Numerical errors due to finite difference approximation
- Modeling errors due to unknown or complex flow physics - e.g. turbulence modeling
- Unknown boundary conditions
- Unknown geometry such as tip clearance or leading edge shape
- Assumption of steady flow

In comparison to the past, when CFD was restricted by limited number of grid points, turbulence and transition modeling remain a major source of error especially for separated and transitional flows, since they have improved little over the years. As an example the use of any turbulence model is found dubious for a gridded tip gap, since the accelerating flow into the gap damps any turbulence and the Reynolds number based on the tip clearance is low. It is hence arguable that the flow in the gap is transitional and possibly laminar up to the throat of the leakage jet followed by a turbulent reattachment. Further modeling errors can arise from the mixing plane approach. Whereas the mixing process should conserve mass, energy and momentum, the entropy will increase at the mixing plane, observable as a jump in lost efficiency. The numerical errors are addressed as proportional to the square of the grid spacing times the second derivative of the flow property concerned in the case of a linear approximation. It is further stated that a fine grid around a thick trailing edge would cause less accurate results due to the unsteady behavior associated with vortex shedding. If a fine grid is used around a thick trailing edge the flow does not separate early enough at the junction between the pressure surface and the trailing edge circle resulting in extremely high streamline curvature and subsequently a low pressure on the rear of the pressure surface. Furthermore in most applications the unknown boundary conditions are likely to be the main sources of errors as well. It is common to specify the pressure at one point at the pressure outlet and to apply radial equilibrium to obtain the spanwise pressure profile. It is stated that if the radial equilibrium is applied well downstream of the last blade row, it does not have much effect on the predicted performance. However, the inlet boundary conditions, which are almost never known, can have a significant impact. Further examples are also provided in this work addressing limitations of CFD. The author concludes that it seems unlikely that an universal model for turbulence or transition will be developed until DNS calculations become a design tool. It is also stated that CFD must be used on a comparative basis rather than as an absolute predictor of performance.

Walters and Lylek [58] investigated the aerodynamic impact of film cooling on a linear turbine airfoil cascade experimentally and numerically. In the first part of the investigations four turbulence models were verified based on solid blade calculations without cooling injection and the results were compared to experiments. Since this part is important regarding the choice of the turbulence model in the current study, it is discussed briefly. The turbulence models investigated are the standard k/ϵ -model and its two variations RNG k/ϵ -model and realizable

k/ϵ -model as well as the Reynolds stress model (RSM). It should be mentioned that all k/ϵ -models are two-equation turbulence models suffering from inherent isotropic turbulent viscosity and lack of history effects on the individual Reynolds stresses and inability to represent turbulence at multiple scales. In contrast all Reynolds stresses are modeled in the RSM model. In comparison to the standard k/ϵ -model the RNG model contains an extra source term in the transport equation for the dissipation rate ϵ resulting in increased turbulent dissipation in regions with high rates of strain. The transport equation for ϵ in the realizable k/ϵ -model is similar to the standard k/ϵ -model with small differences in the generation and destruction terms. It meets the realizability constraints while using the Boussinesq relationship for the Reynolds stresses. The realizability condition as well as the Boussinesq relationship are discussed briefly later in this thesis. The investigation on the solid blade showed that both the standard k/ϵ -model and the RNG k/ϵ -model overpredict the downstream wake spreading and feature local regions of negative loss. The realizable k/ϵ -model and the RSM model, however, showed good qualitative agreement with the experiments with an excellent prediction of the area-averaged loss coefficient. Taking into consideration the contours of turbulent kinetic energy normalized by the average exit velocity, it was evident that both the standard k/ϵ -model and the RNG k/ϵ -model featured high turbulence levels near the suction surface of the airfoil. This excess turbulence is responsible for overpredicting the growth of the suction side boundary layer and thus overpredicting the downstream loss coefficient. The reason for this turbulence production can be traced back to the fact that the realizability condition can be violated by both models. Finally the realizable k/ϵ -model was chosen for the numerical calculations, since the RSM model has high computational requirements.

Dhakal and Walters [20] present curvature and rotation sensitive variants of the well-known SST k/ω -model based on a curvature and rotation sensitive linear eddy viscosity formulation. They used the commercial CFD solver Fluent 6.2.16 for implementing the new variants of the SST k/ω -model. They tested the two variants on fully developed and rotating channel flow as well as the flow in a U-bend. In the case of the rotating channel the deviations between the SST k/ω -model and its variants increase with increasing rotation. Both variants of the k/ω -model are able to capture the asymmetric velocity distribution indicated by the DNS results. On the suction side of the rotating channel both variants overpredict the suppression of turbulence. On the pressure side both variants show an augmentation of turbulence level following the DNS results. The degree of augmentation is, however, underpredicted. The SST k/ω -model does not show any response to rotation, since it is not intended to be sensitized to effects of curvature or rotation. In the case of the U-bend both variants predict turbulence augmentation near the concave wall and turbulence suppression near the convex wall. The SST k/ω -model, however, shows less sensitivity toward the effects of streamline curvature.

Smirnov and Menter [52] suggest a modification of the well-known SST k/ω -model based on an adaption with respect to rotation-curvature correction. The modified model is called SST-CC and was tested for a wide range of both wall-bounded and free shear flows with system rotation

and/or streamline curvature in the framework of the investigations. The cases presented in this work are fully developed, turbulent 1D flow in a plane rotating channel and in a curved channel, 2D flow in a channel with U-turn, 3D flow in a hydro cyclone, 3D flow in a centrifugal compressor and 3D flow past the NACA 0012 airfoil with a round tip. The results are compared to experimental data and DNS as well as to the results obtained with the original SST model. Better agreement of the SST-CC results with the experimental data or DNS is observable for the 1D cases. Furthermore the SST-CC turned out to have a better behavior in comparison to the baseline version of the Reynolds stress model (RSM) predicting the velocity profile in the middle of the U-section in the case of the U-turn channel. Taking into consideration the calculations of the hydro cyclone the standard SST model fails in capturing the correct vortex profile, while the SST-CC model is in good agreement with the experimental data. More specifically the SST model fails to represent the Rankine vortex consisting of a free vortex at the peripheral part and a forced vortex close to the axis of the cyclone. The SST-CC model also resulted in a considerably better agreement with the experiment than the original SST model calculating most of the operating points of the centrifugal compressor. Finally the results of the NACA 0012 tip vortex showed that the original SST tangibly overestimates the rate of decay of the axial velocity, whereas the SST-CC model shows better agreement with the experiments. However, even the SST-CC model does not accurately represent the axial velocity downstream of the wing.

Spataro et al. [53] investigated various numerical setups regarding interaction of rotor and stator in a two-stage two-spool test rig. These variations consist of well-known numerical methods of mixing plane, frozen rotor and sliding mesh at increasing level of unsteadiness taking into account the rotor-stator interaction. These methods were combined in five different ways with respect to four rotor-stator interfaces. The SST k/ω -model was applied for turbulence modeling. The numerical results were finally compared to the measurements. The test rig comprises a transonic HPT followed by a counter rotating LPT. The LPT rotor of this test rig was also investigated in the current thesis. The total and static pressure coefficients and the yaw angle were evaluated in the proceeding of the studies. The last steady case in this work is relevant for this work. In this case all interfaces except the interface between the LPT outlet and the exit duct were modeled by the mixing plane approach. The latter was modeled within a single rotating frame of reference with corresponding velocities for stationary walls. Comparing the circumferentially averaged yaw angles of the time-averaged transient results and the last steady case with the measurements downstream of the LPT no remarkable differences are apparent between the transient and the steady calculations. Small deviations can, however, be observed between individual cases, although the tendency is similar for all simulations and differs from the measurements in some regions. Taking into consideration the circumferentially averaged static pressure coefficient almost no difference can be observed in the CFD results. Nevertheless an offset exists between the CFD and the measurements. The circumferentially averaged total

2. Literature Overview

pressure coefficients calculated by the last steady case, however, feature an offset against other CFD cases as well as the measurements but all have a similar tendency with small deviations.

3. Numerical Calculations

Numerical calculations have been carried out throughout all investigations in this thesis. Due to this reason the fundamentals of fluid mechanics and numerical simulations are presented briefly. First the governing equations of fluid mechanics such as continuity, Navier-Stokes equations and energy conservation are illustrated in this chapter. Since most types of problems in turbomachinery are related to a rotational frame of reference the governing equations as well as their transformation with respect to the absolute or relative frame are summarized briefly. In the next step turbulence modeling and its integration into the governing equations and the numerical calculations are discussed as well.

3.1. Governing Equations of Fluid Mechanics

For the scalar transport quantity $\Psi(x, y, z, t)$ the transport equation can generally be written as

$$\frac{\partial \rho \Psi}{\partial t} + \underbrace{\nabla \cdot (\rho \vec{v} \Psi)}_{\text{Convection}} = \underbrace{\nabla \cdot (\Gamma \nabla \Psi)}_{\text{Diffusion}} + \underbrace{S_{\Psi}}_{\text{Source}}. \quad (3.1)$$

The mass conservation equation also called the continuity equation is

$$\frac{\partial \rho}{\partial t} + \nabla \cdot (\rho \vec{v}) = 0. \quad (3.2)$$

Taking into consideration the flow velocity field with $\vec{v}(x, y, z, t)$ the momentum conservation equation disregarding the gravitational force and external body forces can be expressed as follows in vector form taking into account each velocity component:

$$\frac{\partial}{\partial t} (\rho \vec{v}) + \nabla \cdot (\rho \vec{v} \vec{v}) = -\nabla p + \nabla \cdot (\bar{\bar{\tau}}). \quad (3.3)$$

This equation is further known as the Navier-Stokes equation and the stress tensor $\bar{\bar{\tau}}$ is defined as follows:

$$\bar{\bar{\tau}} = \mu \left[(\nabla \vec{v} + \nabla \vec{v}^T) - \frac{2}{3} \nabla \cdot \vec{v} I \right], \quad (3.4)$$

where μ is the molecular viscosity and I is the unit tensor.

In many situations regarding turbomachinery a rotational frame of reference is of interest. Although the flow field is unsteady when viewed from a stationary frame, it can be modeled as a steady-state problem with respect to the moving frame. In this case the momentum equation

has to be modified in a way that additional acceleration terms are incorporated due to the transformation from the stationary to the moving reference frame. Since the majority of the cases in turbomachinery do not feature a translational motion of the domain, this velocity is not further taken account of. Considering an arbitrary point in the domain the relative velocity of this point can be written as follows:

$$\vec{v}_r = \vec{v} - (\vec{\omega} \times \vec{r}), \quad (3.5)$$

with $\vec{\omega}$ as the angular velocity and \vec{r} the position vector to the corresponding point. In this regard the governing equations can be expressed in two different ways taking into account the relative or absolute velocities as dependent variables (ANSYS Fluent 15.0 [4]). For reasons of simplicity the angular acceleration of the rotational frame is neglected. Furthermore it is assumed that no external body forces affect the flow.

3.1.1. Relative Velocity Formulation

In this formulation the mass conservation equation can be written as

$$\frac{\partial \rho}{\partial t} + \nabla \cdot (\rho \vec{v}_r) = 0. \quad (3.6)$$

The momentum conservation equation will transform to

$$\frac{\partial}{\partial t} (\rho \vec{v}_r) + \nabla \cdot (\rho \vec{v}_r \vec{v}_r) + \rho \left(\underbrace{(2\vec{\omega} \times \vec{v}_r)}_{\text{Coriolis acceleration}} + \underbrace{(\vec{\omega} \times \vec{\omega} \times \vec{r})}_{\text{Centripetal acceleration}} \right) = -\nabla p + \nabla \cdot (\bar{\bar{\tau}}_r). \quad (3.7)$$

The viscous stress tensor $\bar{\bar{\tau}}_r$ has the same form as in Eqn. 3.4 except that relative velocity derivatives are used. In order to calculate compressible flow the energy conservation equation is needed. With h as the specific static enthalpy one obtains for the relative specific internal energy e_r and the relative specific rothalpy h_r by definition

$$e_r = h - \frac{p}{\rho} + \frac{1}{2} \left(\vec{v}_r^2 - (\vec{\omega} \times \vec{r})^2 \right), \quad (3.8)$$

$$h_r = e_r + \frac{p}{\rho}. \quad (3.9)$$

The energy conservation equation taking into account relative velocities and without source terms can hence be expressed as

$$\frac{\partial}{\partial t} (\rho e_r) + \nabla \cdot (\rho \vec{v}_r h_r) = \nabla \cdot (\lambda \nabla T + \bar{\bar{\tau}}_r \cdot \vec{v}_r). \quad (3.10)$$

3.1.2. Absolute Velocity Formulation

Using the absolute velocity formulation the governing equations can be written as

$$\frac{\partial \rho}{\partial t} + \nabla \cdot (\rho \vec{v}_r) = 0, \quad (3.11)$$

$$\frac{\partial}{\partial t} (\rho \vec{v}) + \nabla \cdot (\rho \vec{v}_r \vec{v}) + \rho (\vec{\omega} \times \vec{v}) = -\nabla p + \nabla \cdot (\bar{\tau}), \quad (3.12)$$

$$\frac{\partial}{\partial t} (\rho e) + \nabla \cdot (\rho \vec{v}_r h + p (\vec{\omega} \times \vec{r}^\wedge)) = \nabla \cdot (\lambda \nabla T + \bar{\tau} \cdot \vec{v}). \quad (3.13)$$

In these equations e and h are the absolute specific energy and enthalpy respectively. As one can clearly see the explicit formulation of both the Coriolis acceleration and the centripetal acceleration is implicitly expressed by the convection and the subsequent term. It is obvious that the different ways of formulation can affect the discretization of the velocity components.

3.2. Turbulence Modeling

The majority of the flow situations in engineering applications are turbulent, characterized by inherent, three-dimensional and time-dependent nature. This makes an appropriate modeling necessary introducing the minimum amount of complexity while capturing the essence of the relevant physics (Wilcox [59]). Due to the fact that engineering problems involve inhomogeneous turbulence, time averaging turns out to be the most appropriate approach. In this spirit all flow quantities are expressed as a sum of a mean and a fluctuating part. Taking into consideration Eqn. 3.1 one obtains

$$\Psi(\mathbf{x}, t) = \bar{\Psi}(\mathbf{x}, t) + \Psi'(\mathbf{x}, t), \quad (3.14)$$

$$\bar{\Psi}(\mathbf{x}, t) = \frac{1}{\Delta t} \int_t^{t+\Delta t} \Psi(\mathbf{x}, t) dt, \quad (3.15)$$

$$\mathbf{x} = x, y, z. \quad (3.16)$$

It has to be mentioned that Eqn. 3.14 refers to an unsteady flow in general. The time averaging in Eqn. 3.15, which is further called Reynolds averaging, is only valid if the turbulent time scale differs from the time scale belonging to the average unsteady flow by several orders of magnitude. For relevant engineering problems with no distinct boundary between the imposed unsteadiness and the turbulent fluctuations other averaging methods are applied. For further information in this regard refer to [59]. For compressible flow it is useful to define an additional averaging procedure resulted by mass averaging also called as Favre averaging.

$$\bar{\rho} \tilde{\Psi} = \overline{\rho \Psi}, \quad (3.17)$$

$$\Psi = \tilde{\Psi} + \Psi''. \quad (3.18)$$

It is clear that in case of incompressible flow $\tilde{\Psi} = \bar{\Psi}$ and $\Psi'' = \Psi'$. In the first step all conservation equations are Favre (or Reynolds) averaged.

$$\frac{\partial \bar{\rho}}{\partial t} + \frac{\partial}{\partial x_i} (\bar{\rho} \tilde{u}_i) = 0, \quad (3.19)$$

$$\frac{\partial}{\partial t} (\bar{\rho} \tilde{u}_i) + \frac{\partial}{\partial x_j} (\bar{\rho} \tilde{u}_j \tilde{u}_i) = - \frac{\partial \bar{p}}{\partial x_i} \left[\bar{\tau}_{ij} - \overline{\rho u_j'' u_i''} \right]. \quad (3.20)$$

The energy conservation equation can be obtained in a similar way, which is omitted here for reasons of preserving a clear overview. Equations 3.19 and 3.20 differ from Eqn. 3.2 and 3.3 only by the appearance of the Favre-averaged Reynolds stress tensor as a result of non-linearity of the convection term in the Navier-Stokes equations. The Reynolds stress tensor is defined as

$$\tau_{t,ij} = - \overline{\rho u_i'' u_j''}. \quad (3.21)$$

Due to the new unknown Reynolds stresses a closure problem results from averaging the conservation equations. The objective is hence to develop an appropriate closure approximation contrary to the direct solution of the unsteady turbulent flow field (DNS). The compressibility of the flow makes it even more difficult to develop an approximation suitable for a wide range of applications ([59]). Without going into further details two quantities used in most of the turbulence models called as specific turbulent kinetic energy k and specific turbulent dissipation rate ϵ are introduced for compressible flow

$$\bar{\rho} k = \frac{1}{2} \overline{\rho u_i'' u_i''}, \quad (3.22)$$

$$\bar{\rho} \epsilon = \overline{\tau_{ji} \frac{\partial u_i''}{\partial x_j}}. \quad (3.23)$$

For incompressible cases these two equations are simplified to

$$k = \frac{1}{2} \overline{\rho u_i' u_i'}, \quad (3.24)$$

$$\epsilon = \nu \overline{\frac{\partial u_i'}{\partial x_k} \frac{\partial u_i'}{\partial x_k}}. \quad (3.25)$$

The different turbulence models differ in the number of differential equations used for the closure problem. Nearly all common zero-, one- and two-equation models use the Boussinesq approximation with a suitable generalization for compressible flows. In this approximation the effect of the Reynolds stresses is described by increased viscosity. Consequently the closure problem is reduced to determination of the eddy viscosity μ_t calculated as follows:

$$\tau_{t,ij} = - \overline{\rho u_i'' u_j''} = 2\mu_t \left[\frac{1}{2} \left(\frac{\partial \tilde{u}_i}{\partial x_j} + \frac{\partial \tilde{u}_j}{\partial x_i} \right) - \frac{1}{3} \frac{\partial \tilde{u}_k}{\partial x_k} \delta_{ij} \right] - \frac{2}{3} \bar{\rho} k \delta_{ij}. \quad (3.26)$$

In this spirit the momentum conservation equation is extended by the Reynolds stresses calculated by means of the turbulent viscosity, which first has to be modeled. The simplest possibility is calculating the turbulent viscosity using an algebraic equation ensuring the equilibrium of production and dissipation of turbulent quantities. This approach is called zero-equation turbulence model. Higher modeling levels are achieved by adding transport equations for turbulence quantities. The two-equation turbulence models are the most common for engineering applications with moderate calculation time and cost. For more information about the two-equation turbulence models in compressible flow refer to [59]. Different two-equation models incorporate transport equations for k and either ϵ or ω (specific dissipation rate) which can be defined as

$$\omega = \frac{\epsilon}{k}. \quad (3.27)$$

The two-equation models differ regarding production and dissipation terms in the transport equations of k , ϵ and ω as well as their ability to expand into and solve the viscous sublayer. It is also possible not to reduce the closure problem to determining a turbulent viscosity but to model the components of the Reynolds stress tensor each. This kind of modeling is called Reynolds stress modeling (RSM). In this case six additional transport equations are taken into calculation regarding the components of the Reynolds stress tensor, which is a symmetrical tensor with respect to its diagonal.

3.2.1. Treatment of Near-Wall Regions

Taking into consideration the turbulent boundary layer, it can basically be differentiated between the viscous sublayer and the fully turbulent region. In Fig. 3.1 the universal turbulent velocity profile in near-wall regions is depicted. The turbulent boundary layer is described by means of two dimensionless quantities y^+ and u^+ .

$$y^+ = \frac{yu_\tau}{\nu} \quad \text{and} \quad u^+ = \frac{u}{u_\tau}, \quad (3.28)$$

$$u_\tau = \sqrt{\frac{\tau_w}{\rho}}. \quad (3.29)$$

τ_w is the wall shear stress in this equation. In the viscous sublayer laminar shear stress dominates the flow. Dimensional analysis of this region results in a linear relationship between the dimensionless velocity u^+ and the dimensionless wall distance y^+ . In the fully turbulent boundary layer a logarithmic relationship between u^+ and y^+ can be derived. This region is hence called logarithmic region. Using turbulence modeling one has to take into consideration that it is only valid in the fully turbulent region. Some turbulence models are, however, able to be applied throughout the viscous sublayer as well using damping functions calculating the turbulence parameters, whereas other models are only applicable in the turbulent region. The viscous sublayer is modeled by wall functions in this case. Since the various regions in the turbulent

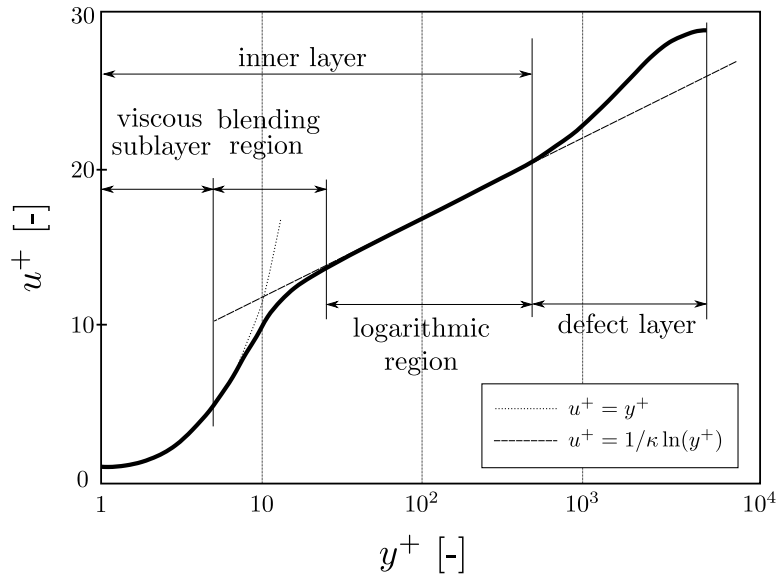


Figure 3.1.: Universal Turbulent Velocity Profile

boundary layer are characterized by y^+ , this value is taken into consideration regarding applicability of corresponding turbulence models. In this spirit it is important that following condition is satisfied for the sake of correct modeling in case of using wall functions:

$$30 \leq y^+ \leq 300. \quad (3.30)$$

Due to the formulation of y^+ these turbulence models are called high Reynolds number models.

3.2.2. k/ϵ -Model

The k/ϵ turbulence model belongs to the two-equation models involving two additional transport equations for k and ϵ . The k/ϵ -model is available as standard, realizable and RNG k/ϵ -model. The standard k/ϵ -model is a high Reynolds number model using following equation for calculating the turbulent viscosity:

$$\mu_t = \bar{\rho} C_\mu \frac{k^2}{\epsilon}. \quad (3.31)$$

C_μ is a model constant, which is set to 0.09 by default. The RNG k/ϵ -model involves additional terms enhancing the accuracy for swirling flow. Furthermore the RNG theory provides an analytically derived differential formula for the turbulent viscosity, which with appropriate wall treatment accounts for low Reynolds number effects. In high Reynolds number limit it yields Eqn. 3.31.

The realizable k/ϵ -model contains an alternative formulation for the turbulent viscosity and incorporates a modified transport equation for the dissipation rate ϵ . The term realizable means

that the model satisfies certain mathematical constraints on the Reynolds stresses, consistent with the physics of turbulent flows. Neither the standard k/ϵ -model nor the RNG k/ϵ -model is realizable (ANSYS Fluent 15.0 [3]). Taking into consideration Eqn. 3.26 for an one-dimensional incompressible flow one obtains for the Reynolds normal stress

$$\overline{u'^2} = \frac{2}{3}k - 2\nu_t \frac{\partial \bar{u}}{\partial x}. \quad (3.32)$$

Using Eqn. 3.31 yields for negative Reynolds normal stress

$$\frac{k}{\epsilon} \frac{\partial \bar{u}}{\partial x} \geq \frac{1}{3C_\mu}. \quad (3.33)$$

As one can clearly see the Reynolds normal stress $\overline{u'^2}$ can become negative, when the strain is large enough (non-realizable). The most straightforward way to ensure realizability is to make C_μ variable with respect to the main flow and the turbulence.

The realizable k/ϵ -model shows substantial improvements, where the flow features strong streamline curvature, vortices and rotation. The initial studies have shown that this model provides the best performance of all the k/ϵ -model versions for several validations of separated flows and flows with complex secondary flow features. Furthermore the realizable k/ϵ -model includes the effects of mean rotation in the definition of the turbulent viscosity (variable C_μ), which has been tested on single moving reference frames and should be taken into calculation with caution for multiple reference frames (ANSYS Fluent 15.0 [3]).

3.2.3. k/ω -Model

Two common versions of the k/ω -model are the standard k/ω -model and the shear stress transport (SST) k/ω -model, which are both low Reynolds number turbulence models. As one can expect an additional transport equation has to be solved for the specific dissipation rate ω aside from k . The SST k/ω -model is a combination of the transformed k/ϵ -model and the standard k/ω -model. It differs from the standard k/ω -model in the gradual change from the inner region to the outer part of the boundary layer as well as modified turbulent viscosity formulation to account for the transport effects of turbulent shear stress. In general the SST k/ω -model makes advantages of the independence of the k/ϵ -model in the far field in order to compensate the sensitivity of the solution to the values of k and ω outside the shear layer (freestream sensitivity). The turbulent viscosity is calculated as follows with different formulations of f_ω depending on the model version chosen:

$$\mu_t = \bar{\rho} f_\omega \frac{k}{\omega}. \quad (3.34)$$

3.3. Discretization

The conservation equations for mass, momentum and energy are derived in a continuum. For numerical calculations the transport equations are discretized in order to obtain a system of algebraic equations. Integrating Eqn. 3.1 and applying the Gaussian method of integration yield

$$\int_V \frac{\partial \rho \Psi}{\partial t} dV + \oint_A \rho \Psi \vec{v} \cdot d\vec{A} = \oint_A \Gamma \nabla \Psi \cdot d\vec{A} + \int_V S dV. \quad (3.35)$$

In order to obtain the flow variables at discrete points, the entire calculation domain is divided into smaller control volumes (cells). This procedure is called pre-processing carried out by a variety of commercial and in-house codes. For discretization of the cases investigated in this thesis the commercial software ANSYS ICEM CFD 13.0 was used. Applying Eqn. 3.35 to each cell yields in discretized form (see Fig. 3.2)

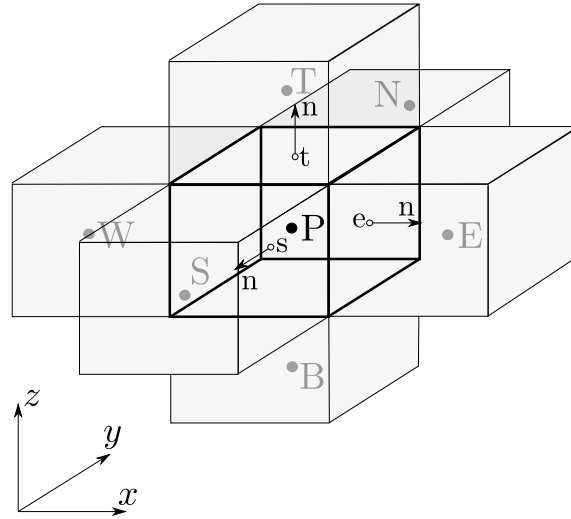


Figure 3.2.: Finite Volume with Corresponding Directions

$$\frac{\partial (\rho \Psi)_P}{\partial t} V_P + \sum_i \rho_i \vec{v}_i \Psi_i \cdot \vec{A}_i = \sum_i \Gamma_i \nabla \Psi_i \cdot \vec{A}_i + S_P V_P, \quad (3.36)$$

$$i = n, s, e, w, b, t.$$

In this notation the capitals characterize the center points of each cell and the lower-case letters the corresponding centers of the boundary surfaces related. As one can see the algebraic equations are non-linear. The first term in this equation refers to temporal alternation and needs time step discretization. Furthermore one can see that flow variables are needed at the center points of the boundary surfaces. The quantities are, however, calculated at the center points of the cells, which makes an appropriate interpolation necessary. In the following some of the common interpolation schemes are presented briefly.

3.4. Solver

The commercial CFD solver ANSYS Fluent 13.0 (used for the CFD calculations in this thesis) allows for application of a wide range of different interpolation schemes such as first order upwind, second order upwind, power law and QUICK, which generally differ in the order of the discretization and thus their accuracy. Furthermore it has to be mentioned that the diffusion terms in Eqn. 3.36 are central differences and always second order accurate.

First Order Upwind

In this scheme the face value of the transport quantity is set equal to the value at the cell center in the upstream cell. It is hence assumed that the cell center value of a transport quantity represents an average value throughout the entire cell. This scheme can be applied, when the flow is mainly dominated by convection terms at pure diffusion.

Power Law

The power law scheme interpolates the face values using the exact solution of an 1D convection-diffusion equation. Whereas the upwind scheme can be applied to flow situations with dominating convection, the power law can be used for flow fields with convection and diffusion of similar orders.

Second Order Upwind

When second order accuracy is desired, the quantities at the cell faces are computed using a multi-dimensional, linear reconstruction approach. Higher order accuracy is achieved through a Taylor series expansion of the solution at the cell center. In this case the face value is computed as follows:

$$\Psi_i = \Psi_P + \nabla \Psi \cdot \vec{r}. \quad (3.37)$$

In this equation Ψ and $\nabla \Psi$ are the cell centered value and its gradient in the upstream cell and \vec{r} is the displacement vector to the face center.

It has to be mentioned that for all these quantities the 1D convection-diffusion equation was taken into consideration for evaluating the accuracy of the discretization scheme. Since the transport quantities and their equations (especially the turbulence quantities) feature source terms, the evaluation of the discretization scheme applied to the solution has to be considered with more caution.

It should also be mentioned that there are different interpolation methods for the pressure in ANSYS Fluent 13.0, which are standard, linear, PRESTO, second order and body-force-weighted. For most cases the standard scheme is applicable. For mixture or multiphase models as well as for the flows with high swirl numbers or flows in strongly curved domains the PRESTO scheme and for problems involving large body forces the body-force-weighted scheme are recommended. The linear scheme computes the face pressure as the average of the pressure values in the ad-

jacent cells. The second order scheme reconstructs the face pressure values in the same way as for the second order interpolation of the convection terms described above. In spite of some improvements over the standard and linear schemes the second order scheme may, however, cause some trouble for poor meshes or if it is used at the start of a calculation. The standard scheme interpolates the pressure values at the faces using momentum equation coefficients. For further information about this approach refer to [3]. This procedure works well as long as the pressure variation between cell centers is smooth. In case of high pressure gradients at the cell faces using this scheme may cause overshoots or undershoots of cell velocity. In such cases it is necessary to pack the mesh in regions of high gradient.

In addition to the explicit values of the transport quantities, their gradients appear in the discretized equations as well. Among the applicable discretization methods the least squares cell based method permits sufficient accuracy and was also chosen for the CFD calculations carried out for this thesis. In this method the solution is assumed to vary linearly. The cell gradient is then determined by solving the minimization problem in a least squares sense. For more information about this method as well as other discretization methods refer to [3].

In ANSYS Fluent two solver technologies called as pressure-based and density-based solvers are available. In both methods the velocity field is obtained from the momentum equations. In the density-based solver approach the continuity equation is used to obtain the density field, while the pressure field is determined from the equation of state. On the other hand, in the pressure-based approach the pressure field is extracted by solving a pressure correction equation, which is obtained by manipulating the continuity equation and the momentum equations. Each method, however, solves the governing integral equations for conservation of mass, momentum, energy and turbulence quantities described above ([3]).

According to [4] both solvers are applicable to incompressible as well as highly compressible flows. Due to the subsonic character of the flow throughout all numerical calculations in this thesis, the pressure-based solver was chosen for all numerical simulations, which showed satisfactory results.

Furthermore two algorithms exist under the pressure-based solver in ANSYS Fluent 13.0, which are named as segregated and coupled algorithms. The segregated algorithm solves the governing equations sequentially, while in the coupled algorithm the momentum equations and the pressure-based continuity equation are solved in a coupled manner ([4]). Due to the higher memory requirement of the coupled algorithm a segregated algorithm was chosen for the calculations in this thesis.

ANSYS Fluent 13.0 further provides different segregated algorithm types such as SIMPLE, SIM- PLEC and PISO. Generally steady-state calculations use SIMPLE or SIM- PLEC, while PISO is recommended for transient calculations. For more information concerning the procedure of pressure correction and mass conservation applied in each algorithm refer to [3], since a detailed explanation would go beyond the scope of the thesis. Generally it is stated that the SIM- PLEC algorithm can speed up the convergence for relatively uncomplicated problems (laminar flows with no additional models) due to higher pressure correction under-relaxation factor. Since all

calculations in the framework of this thesis were carried out for turbulent flow the SIMPLE algorithm was applied for all CFD simulations in this work.

The pressure-based solver uses under-relaxation of equations (implicit relaxation) to control the update of computed variables at each iteration and to stabilize the convergence ([3, 4]). Taking into consideration the under-relaxation of a transport variable Ψ with a change of $\Delta\Psi$ during an arbitrary iteration step with respect to the value Ψ_{old} of its preceding iteration step, the new value for the next iteration step can be written as

$$\Psi = \Psi_{\text{old}} + \alpha\Delta\Psi, \quad (3.38)$$

with α as the under-relaxation factor ($0 \leq \alpha \leq 1$). The under-relaxation reduces the change of Ψ during each iteration and provides for more stability during the calculation. An under-relaxation factor of zero signifies no change in the calculated value for the next step, whereas an under-relaxation factor of one incorporates the new calculated value entirely for the next iteration step. For information concerning under-relaxation of equations also known as implicit relaxation used in the pressure-based solver refer to [3].

The under-relaxation factors need to be chosen with caution depending on the problem and the complexity of the case as well as turbulence modeling. In some cases it is suitable to reduce the under-relaxation at the beginning of a simulation in order to achieve a stable-running calculation. They can then be increased in order to speed up the convergence. This procedure was used for the majority of the CFD calculations carried out in this work.

4. Basic Investigations on Passive Tip-Injection

Before applying costly experiments and CFD, basic investigations on the performance of passive tip-injection are of importance. In this regard analytical considerations and simple CFD calculations offer a good opportunity.

In this chapter the impact of passive tip-injection on the discharge behavior of shrouded blades is analyzed by means of 1D analytical models and 2D CFD calculations. The results are presented later in paper 1.

4.1. Analytical Discharge Models

An analytical 1D discharge model has already been presented in Willinger and Haselbacher [60] for unshrouded blades and incompressible flow in a cross-section perpendicular to the blade chord. In [30] this model was modified in a way that it takes account of passive tip-injection for unshrouded blades. These considerations were further followed by [23].

Whereas the above mentioned discharge models yield in a single position referring to the maximum profile pressure difference in the case of an unshrouded blade, many possibilities are given regarding positioning of passive tip-injection in the case of a shrouded blade. In this spirit a simple shroud geometry with two sealing fins was taken into consideration for the analytical model. Three different injection positions were further studied with respect to the shroud cavity and the fins together with the corresponding 1D analytical approaches in the framework of the investigations. In contrast to the previous models for unshrouded blades, the injection mass flow rate was calculated analytically for the individual positions. In this spirit two discharge coefficients C_D and C_D^+ were evaluated, which account for the ratio of the real tip-leakage mass flow rate at the tip gap inlet and at the tip gap outlet respectively to the ideal tip-leakage mass flow rate, calculated without losses. It is clear that the latter discharge coefficient C_D^+ takes into account also the injection mass flow rate. The analytical model includes also the impact of the injection flow separation at the sharp edges of the injection outlet together with the corresponding channel blockage as well as deviations of the injection flow direction from the channel direction. Since the analytical approach requires some modeling constants, which are a priori not known, simple 2D CFD calculations were undertaken in order to determine these constants. Furthermore the results of the CFD calculations serve for verification of the analytical approach.

4.2. CFD Procedure

The computational domain for the numerical calculations consists of a cross-sectional area of the shrouded tip region with the corresponding inlet region. The geometry as well as the boundary conditions for the inlet were chosen in a dimensionless manner and in compliance with [23] and [30]. The dimensionless inlet velocity was computed applying sink flow with its origin positioned at the casing endwall directly above the sharp inlet edge of the shroud. All other parameters were set up in a dimensionless manner as well.

The RNG k/ϵ -model and the standard k/ω -model were applied for turbulence modeling of the incompressible flow field. However, the results of the standard k/ω -model were taken into further consideration for verification of the analytical approaches and determination of the model constants, which was in compliance with [23]. More details about the CFD calculations are provided in paper 1.

Paper 1

P. Ghaffari and R. Willinger

Impact of Passive Tip-Injection on the Performance of Partially
Shrouded Turbines: Basic Concept and Preliminary Results

ASME paper TBTS2013-2038
ASME Turbine Blade Tip Symposium & Course Week
Hamburg, Germany, 2013

Proceedings of ASME 2013 Turbine Blade Tip Symposium & Course Week
TBTS 2013
September 30 - October 3, 2013, Hamburg, Germany

TBTS2013-2038

**IMPACT OF PASSIVE TIP-INJECTION ON THE PERFORMANCE OF PARTIALLY
SHROUDED TURBINES: BASIC CONCEPT AND PRELIMINARY RESULTS**

Pouya Ghaffari and Reinhard Willinger
Institute for Energy Systems and Thermodynamics
Vienna University of Technology
Getreidemarkt 9/302, A-1060 Vienna, Austria
pouya.ghaffari@tuwien.ac.at
reinhard.willinger@tuwien.ac.at

ABSTRACT

In terms of efficiency improvement many methods for reducing the blade tip-leakage mass flow rate have been proposed. Some of these methods are based on increasing the flow resistance with aid of geometrical modifications of the blade tip (squealers, winglets, shrouded blades, etc.) whereas other methods take advantage of aerodynamical resistance with passive tip-injection as an example. The objective of this paper is a combination of both methods in order to achieve higher reduction in tip-leakage mass flow rate. In the first part of this work necessary characteristic parameters of modern low pressure turbine blades in aircraft gas turbines are estimated. These parameters are taken into consideration to calculate the range of physical quantities influencing tip-leakage flow. Subsequently a two dimensional flow model is obtained with the so called discharge coefficient as the ratio of the actual tip gap mass flow rate to its highest possible value. The investigations are based on dimensionless calculations. In the end the results obtained from dimensionless 2D CFD-simulations are presented and compared with the analytical results. This leads to conclusions regarding the impact of various parameters on the effectiveness of the passive tip-injection.

INTRODUCTION

The main goal in developing new aircraft engines and their components is reducing the overall engine weight and increasing the efficiency, resulting in lower specific fuel consumption.

In modern transport aircraft engines the turbo fan technology reveals high efficiency values. In this spirit higher bypass ratios result in a better performance. In Kurzke [1] the relation between the bypass ratio and the specific fuel consumption is presented. A large fan diameter is related to high circumferential velocity at the fan tip and thus to high noise emission. The low pressure turbine of such a turbofan engine is thus to operate at low rotational speed, as long as no gear box is provided between the low pressure turbine and the fan (Curtis et al. [2]).

An alternative to low speed low pressure turbines is given by the so called geared turbofan. In such a configuration higher blade loads result in a decrease in stage number and consequently in the overall weight. These both arguments lead to the modern design of aerodynamically highly loaded low pressure turbines operating at high rotational speed. The aerodesign of such modern blades is discussed in Malzacher et al. [3]. In Tab. 1 some of the turbine characteristics are included.

The tip section of modern low pressure gas turbine stages features a high degree of reaction whereas the degree of reaction approaches zero in the hub section (Bräunling [4]). In Fig. 1 the impact of the degree of reaction on the tip-leakage losses is presented clearly. As one can see the tip-leakage losses increase by increasing the degree of reaction at constant relative tip gap height. The tip-leakage mass flow rate is responsible for dissipation mechanisms downstream of the blade row and results in lower stage efficiency. The aim is thus to keep the tip-leakage mass flow rate as low as possible. This fact requires effective methods of reducing the tip-leakage mass flow rate.

TABLE 1: MODERN LOW PRESSURE TURBINE CHARACTERISTICS [3].

Loading coefficient at mean section ψ [-]	1.4
Flow coefficient at mean section ϕ [-]	0.55
Reynolds number Re [-]	60000
s/c ratios at tip section [-]	> 1.2

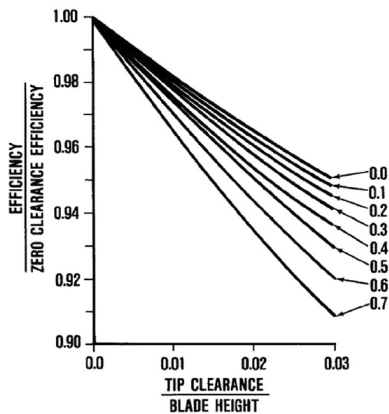


FIGURE 1: EFFICIENCY LOSS DUE TO THE TIP-LEAKAGE FLOW FOR A RANGE OF THE DEGREE OF REACTION FROM ZERO TO 70% (Hong and Groh [5]).

In Curtis et al. [6] an active method of reducing the tip-leakage mass flow rate over shrouded turbine blades is discussed. They could show that the overall mass flow rate at the tip gap exit remained relatively constant whereas the inlet mass flow rate decreased with increasing jet mass flow rate. They could also demonstrate a maximum increase of 1.2% in turbine efficiency. Hogg and Ruiz [7] presented the effect of flow jet barriers in combination with sealing applications using three sealing fins. In the first part of their work the improved effect of inclined injection is presented clearly. Further the influence of inclined injection with guidance in combination with three labyrinth fins is featured of which the middle one is inclined against the main flow direction and serves as injection guidance. The aim of this paper is to show the impact of passive tip-injection on the tip gap mass flow rate based on physical con-

siderations related to flow mechanism in the tip gap region. In order to gain a clear overview assumptions and simplifications have been carried out for both analytical and numerical calculations comprising incompressible flow without rotation and 2D sectional blade geometry. The presented method of injection is called passive as the injection mass flow rate is extracted passively from the total stage mass flow rate.

The first step in the current work consists in estimating relevant performance parameters of modern low pressure turbine stages in aircraft engines. Within the framework of this paper these parameters are estimated with the aid of the presented data in Malzacher et al. [3]. The variable Reynolds number significant for the friction losses in the tip gap region over shrouded blades is then derived respectively. Based on the results analytical 1D models are derived for different positions of the tip-injection outlet over shrouded blades. In the next step 2D CFD-simulations are carried out. Both calculations have the so called discharge coefficient as a measure for the dimensionless tip gap mass flow rate related to a common reference presented later. Both calculations are compared and lead to conclusions regarding the impact of tip-injection on the tip gap mass flow rate.

NOMENCLATURE

a_u	specific blade work
c	chord length
C_D	discharge coefficient at gap inlet
C_D^+	discharge coefficient at gap outlet
C_u	turbulence model constant
f	injection channel width (2D)
F	force
h	blade span
k	constants
l	axial blade length
l_{ch}	injection channel length
p	pressure
P	power
r	radius
r_K	degree of reaction
Re	Reynolds number
s	blade spacing
u	circumferential velocity
w	flow velocity
α	mixing factor
β	rel. flow angle measured from positive circumf. direction
β^+	rel. flow angle measured from negative circumf. direction
γ	dimensionless injection channel width (2D)
γ_s	stagger angle
δ	injection angle
θ	dimensionless injection velocity
λ	friction loss coefficient

- ν kinematic viscosity
- ξ loss coefficient
- κ fin/tip gap height ratio
- ρ density
- σ contraction coefficient
- τ tip gap width
- τ' blade shroud fin clearance
- ϕ flow coefficient
- ψ loading coefficient

Subscripts

- ax axial direction
- b barricade
- c casing section
- c hub
- ch injection channel
- ex tip gap exit
- in inlet
- inj injection
- k kinking
- m mean section
- mix mixing
- t total
- u circumferential component
- δ injection angle
- τ tip gap
- 1 cascade inlet plane
- 2 cascade outlet plane
- ∞ vectorial mean value

PRELIMINARY CONSIDERATIONS

The pressure distribution on the pressure and suction side of turbine blades is responsible for the resulting blade force and thus the stage power. In Fig. 2 the driving pressure difference for the tip-leakage flow is shown for shrouded as well as unshrouded blades.

For estimating the tip gap Reynolds number for 1D analytical considerations a characteristic pressure difference driving the mass flow from the stage inlet to the stage outlet over shrouded blades is needed. According to the basic considerations of *Zweifels* criterion a constant pressure distribution on the pressure and suction side is assumed. The resulting pressure difference is set equal to those between the blade row inlet and outlet especially for blades with a high degree of reaction which applies for the tip region of modern low pressure turbines ([4]).

In this respect the circumferential force can be written as:

$$F_u = \Delta p c h \sin \gamma_s. \quad (1)$$

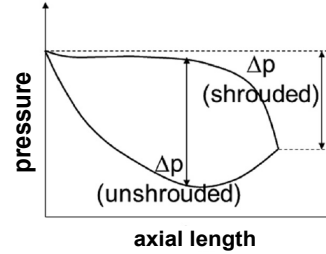


FIGURE 2: DRIVING PRESSURE FOR THE LEAKAGE FLOW (Yoon [8]).

With Δp as the difference between the total pressure at the cascade inlet and the static pressure at the cascade outlet. For further procedure it is preconditioned that the density ρ and axial velocity w_{ax} are constant throughout the whole calculation steps. Considering only the tip region of the blade the quantity h (blade height) refers fictitiously to this section. Subsequently one obtains for the blade power

$$P = \Delta p c h \sin \gamma_s u. \quad (2)$$

On the other hand it is possible to estimate the blade power with the aid of the loading and flow coefficients as follows:

$$\psi = \frac{a_u}{u^2}, \quad \phi = \frac{w_{ax}}{u}, \quad (3)$$

$$P = s h \rho u^3 \phi \psi. \quad (4)$$

It hence yields for the pressure difference

$$\Delta p = \frac{s \rho u^2 \phi \psi}{c \sin \gamma_s}. \quad (5)$$

In view of the fact that this pressure difference is proportional to the theoretical kinetic energy through the tip gap in the case of ideal acceleration one obtains for the theoretical gap velocity w_τ

$$w_\tau = \sqrt{\frac{2 \Delta p}{\rho}} = \sqrt{\frac{2 s u^2 \phi \psi}{c \sin \gamma_s}}. \quad (6)$$

The tip gap Reynolds number can hence be written as

$$Re_\tau = \frac{w_\tau \tau}{\nu} = \frac{u \tau}{\nu} \sqrt{\frac{2 s \phi \psi}{c \sin \gamma_s}}. \quad (7)$$

Taking into account the blade Reynolds number calculated with the blade chord length and relative cascade outlet velocity w_2 one obtains

$$Re_\tau = Re_2 \frac{\tau}{c} \frac{u}{w_2} \sqrt{\frac{2s\phi\psi}{c \sin \gamma_s}}, \quad (8)$$

$$\frac{u}{w_2} = \frac{u}{w_{ax}} \sin \beta_2^+ = \frac{1}{\phi} \sin \beta_2^+, \quad (9)$$

$$Re_\tau = Re_2 \frac{\tau}{c} \sin \beta_2^+ \sqrt{\frac{2s\psi}{c\phi \sin \gamma_s}}. \quad (10)$$

The exit flow angle β_2 can be estimated under simplified conditions from velocity triangles as follows:

$$-\psi = \phi(\cot \beta_2 - \cot \beta_1), \quad (11)$$

$$r_K = -\frac{\phi}{2}(\cot \beta_2 + \cot \beta_1), \quad (12)$$

$$\cot \beta_2 = \frac{-\psi - 2r_K}{2\phi}. \quad (13)$$

For further procedure stagger angle γ_s and mean flow angle β_∞ are set into following relation with good accuracy (Willinger and Haselbacher [9]):

$$\beta_\infty \approx 180^\circ - \gamma_s, \quad (14)$$

$$\tan \beta_\infty = \frac{2}{\cot \beta_1 + \cot \beta_2} = -\frac{\phi}{r_K}. \quad (15)$$

The tip gap width τ refers to the largest radial distance between the blade tip and the casing. In the case of shrouded blades the smallest gap between the shroud fins and the casing has to be considered in regard to smallest possible clearance. With τ' as the tip clearance width between the shroud fins and the casing Eq. 10 forms into

$$Re_\tau = Re_2 \frac{\tau'}{c} \frac{\tau}{\tau'} \sin \beta_2^+ \sqrt{\frac{2s\psi}{c\phi \sin \gamma_s}}. \quad (16)$$

Following Bindon [10] a range of 1.5 to 2.5 % (here 2%) for the ratio of the smallest gap clearance width to the chord length can be assumed. This leads to the final equation for the tip gap Reynolds number with κ as the ratio of the smallest to largest gap clearance width

$$Re_\tau = Re_2 \frac{0.02}{\kappa} \sin \beta_2^+ \sqrt{\frac{2s\psi}{c\phi \sin \gamma_s}}. \quad (17)$$

It has to be mentioned that the loading and flow coefficients presented in Tab. 1 are to be corrected with respect to the blade tip. This can be accomplished with aid of the ratio of the mean section blade radius to the tip radius as follows:

$$\psi_c = \psi_m \left(\frac{r_m}{r_c}\right)^2 \quad \phi_c = \phi_m \frac{r_m}{r_c}. \quad (18)$$

Taking into consideration the tip region of a shrouded blade in a low pressure turbine, it consists of a shroud with two sealing fins in conventional form. In the case of so called partially shrouded blades a weight reduction is achieved by retaining the main configuration and reducing the mass of the shroud appropriately (Porreca et al. [11]). In Fig. 3 a comparison between the two shroud geometries is depicted.

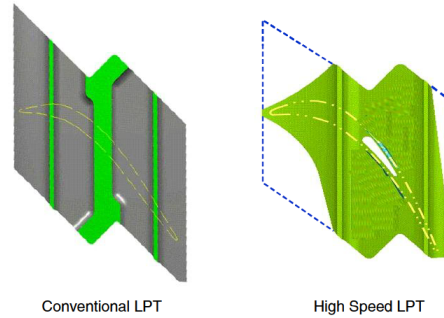


FIGURE 3: CONVENTIONAL VERSUS HIGH SPEED BLADE OUTER SHROUD DESIGN (Riegler and Bichlmaier [12]).

Further considerations relate to a system with passive tip-injection, with injection mass flow rate extracted from the stage mass flow rate participating in stage power (see also Benoni and Willinger [13]). Since the mass flow rate at the tip gap outlet accounts for the dissipation downstream of the blade row, the aim is to reduce the overall mass flow rate at the tip gap outlet. This leads to two different definitions for the discharge coefficient depending on whether only the tip gap or the overall mass flow rate is taken into calculations. Nevertheless the pressure reference for both cases remains the same, as passive injection is considered for all calculations.

1D ANALYTICAL MODEL

In this chapter the effect of passive tip-injection in combination with a blade shroud is analysed with aid of a 1D model. Furthermore the 2D cross-sectional region of a shrouded blade tip is observed. This simplified physical model helps to draw conclusions regarding the effectiveness of the position of tip-injection. It is apparent that two possible injection positions can generally be taken into calculation. These two possibilities are given by the injection in the middle of the cavity between the two fins as well as upstream of the first fin. Figure 4 gives an overview of the geometrical configurations used for the 1D calculations. As one can see, the tip-injection occurs at a variable angle δ . The calculations are carried out under the usage of the equation of flow continuity and balance of momentum for two dimensional incompressible flow. The total tip area is divided into three main control volumes comprising the area between the blade leading edge and the first fin, the cavity between the fins and the area downstream of the second fin to the blade trailing edge at the blade tip. The flow quantities at each control volume outlet serve as inlet conditions for the next control volume. Further assumptions regarding the flow physics in the shrouded tip clearance are listed below:

1. The flow acceleration to the inlet of the tip gap as well as any acceleration process to the sharp edged fins occur without losses in total pressure.
2. The flow acceleration at any sharp edge occurs under flow separation with the contraction coefficient σ equal for each part.
3. The tip mass flow is completely mixed out before entering the sealing fin gaps.
4. The total pressure loss in the cavity between the fins is taken into consideration with the loss factor ξ_{mix} varying between zero and one. This factor takes into account the dissipation extent of the specific kinetic energy in the narrowest cross section over the fin edge. A value of one means total dissipation, as it is common for ideal labyrinth seal flow.
5. Any deviations from a uniform velocity distribution at the gap outlet have been taken into account by the mixing factor α .
6. The friction losses have been taken into calculations with aid of the appropriate theory of pipe flow with 2τ as the hydraulic diameter and l the pipe length for two dimensional considerations. The tip gap velocity w_τ serves as the reference velocity for the calculations.
7. The injection mass flow features constant velocity over the entire injection port at the blade tip in cross-sectional direction and the velocity angle remains consistent with the injection channel angle respectively.

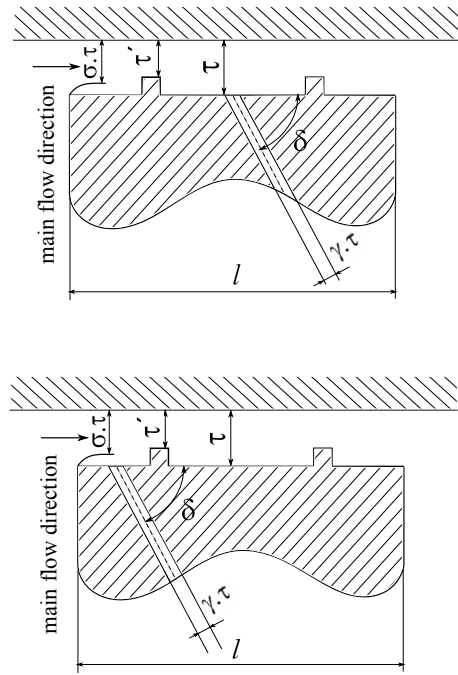


FIGURE 4: 2D TIP SECTION GEOMETRY WITH PASSIVE TIP-INJECTION.

The so called discharge coefficient is obtained as follows:

$$C_D = \frac{w_{\tau, in} \sigma \tau \rho}{\sqrt{\frac{2(p_{t, in} - p_{ex})}{\rho}} \rho \tau} \quad (19)$$

Following factors contain quantities which remain unchanged in their form for both injection positions:

$$A = \frac{1}{\sigma^2} - \frac{2}{\sigma} + 2\gamma\theta^2 \cos \delta, \quad (20)$$

$$B = \frac{1}{\kappa\sigma} + \frac{\gamma\theta}{\kappa\sigma}, \quad (21)$$

$$C = 1 + \gamma\theta. \quad (22)$$

Under the mentioned assumptions following result can be obtained from the calculations:

Injection in the middle of the fins

$$C_D = \frac{1}{\sqrt{A + (1 - \sigma\kappa)^2 B^2 + \left(\frac{2}{\alpha} + \frac{\lambda_\tau l}{2\tau}\right) C^2 + \frac{\xi_{mix}}{\kappa^2 \sigma^2}}}. \quad (23)$$

Injection upstream of the first fin

$$C_D = \frac{1}{\sqrt{A + (1 + \xi_{mix} - 2\sigma\kappa)B^2 + \left(1 + \frac{2}{\alpha} + \frac{\lambda_\tau l}{2\tau}\right) C^2}}. \quad (24)$$

$$\theta = \frac{w_{inj}}{\sigma w_{\tau, in}} \quad (25)$$

Adding the injection mass flow rate to the tip gap mass flow rate leads to following equation containing the overall mass flow rate for further investigations:

$$C_D^+ = \frac{w_{\tau, in} \sigma \tau \rho + w_{inj} \gamma \tau \rho}{\sqrt{\frac{2(p_{t, in} - p_{ex})}{\rho} \rho \tau}} = C_D (1 + \gamma \theta). \quad (26)$$

A closer look to Eq. 23 and 24 suggests that at constant γ and θ values decreasing κ will result in a decrease in C_D and C_D^+ values.

As mentioned above, the injection mass flow rate is ideally meant to be coincident with the injection channel axis at the channel outlet over the entire injection port in cross-sectional direction. Further calculations will prove that this will not apply for real configurations. Flow separation is observable directly before the injection mass flow enters the tip clearance. This fact results in two undesired effects. Firstly injection channel barricade appears immediately upstream of the injection channel outlet and secondly the injection mass flow is deflected in a direction tending to the gap flow main direction. These two effects have been taken into account by two constants k_b as an area ratio for the barricade and k_δ as an angle ratio for the injection flow deflection. The quantity A hence transfers to:

$$A = \frac{1}{\sigma^2} - \frac{2}{\sigma} + 2\gamma\theta^2 \left(\frac{\sin \delta}{k_b \sin(k_\delta \delta)} \right) \cos(k_\delta \delta). \quad (27)$$

The dimensionless injection velocity θ referring to a constant velocity distribution in the injection channel can be estimated for

both injection cases provided that the same static pressure is assumed for both the gap and injection mass flow at the injection outlet. The loss mechanism from the blade leading edge to the injection point concerning the injection flow can be modelled with corresponding loss coefficients. These loss mechanisms are due to the inlet, kinking and friction in the injection channel. A static pressure drop is also to be taken into account due to the flow deflecting as well as channel barricade at the injection channel exit. For the friction losses the formula of *Blasius* has been taken into calculations [14]. For the channel Reynolds number with the corresponding hydraulic diameter $2\gamma\tau$ one obtains

$$Re_{ch} = Re_\tau \frac{2\gamma\theta}{1 + \gamma\theta} \approx Re_\tau \frac{2\gamma}{1 + \gamma} \quad (\text{for } \theta \sim 1), \quad (28)$$

$$\lambda_{ch} \approx 0.3164 \left(\frac{2\gamma}{1 + \gamma} Re_\tau \right)^{-0.25}. \quad (29)$$

Based on considerations above following equation can be derived for θ in both cases:

Injection in the middle of the fins

$$\theta = \sqrt{\frac{\frac{1}{\sigma^2} - \frac{2}{\sigma} + 2 + \frac{\xi_{mix}}{\kappa\sigma}}{\xi_{inj, in} + \xi_k + \lambda_{ch} \frac{l_{ch}}{2\gamma} + \left(\frac{\sin \delta}{k_b \sin(k_\delta \delta)} \right)^2 - 1}}. \quad (30)$$

Injection upstream of the first fin

$$\theta = \sqrt{\frac{\frac{1}{\sigma^2} - \frac{2}{\sigma} + 2}{\xi_{inj, in} + \xi_k + \lambda_{ch} \frac{l_{ch}}{2\gamma} + \left(\frac{\sin \delta}{k_b \sin(k_\delta \delta)} \right)^2 - 1}}. \quad (31)$$

It is apparent that in the case of the injection in the middle of the fins an additional pressure drop is to be taken into account due to the mixing loss in the cavity.

CFD

Based on the presented considerations 2D CFD-simulations have been carried out using dimensionless relations for all governing equations for steady flow. In this manner all kinematic and geometrical quantities are made dimensionless with the aid of the gap velocity w_τ and the gap width τ . For turbulence modelling two kinds of turbulence models (RNG k/ε -model with enhanced wall treatment and k/ω -model) have been applied for every calculation. The numerical calculations were carried out using ANSYS *Fluent 13*.

BOUNDARY CONDITIONS

The computational area upstream of the blade tip gap comprises a square with a side length of 20 gap width. The velocity at the boundary inlet was computed using sink flow with its center positioned over the blade leading edge on the casing end wall. The actual computational area was extended at the gap outlet including the blade and casing wall in order to avoid reverse flow immediately at the boundary outlet. Zero wall shear stress was applied to the wall boundaries in this section in order to eliminate any inaccuracy in terms of friction. At the boundary outlet constant static pressure was applied over the entire gap width. The inlet specific turbulent kinetic energy k was calculated using the velocity contribution at the boundary inlet under the condition of constant turbulence intensity, whereas for the calculation of ϵ and ω two additional quantities C_μ and the characteristic length scale l_m were necessary. l_m was estimated as 1% of the blade spacing (Hah [15]) and made dimensionless with respect to the tip gap width as follows:

$$\frac{l_m}{\tau} = \frac{l_m}{s} \frac{s}{c} \frac{c}{\tau'} \frac{\tau'}{\tau} = 0.6\kappa. \quad (32)$$

Table 2 gives a summary of dimensionless quantities used for all simulations.

TABLE 2: DIMENSIONLESS QUANTITIES FOR THE 2D CFD-SIMULATIONS.

turbulence intensity [-]	5%
C_μ [-]	0.09
Re_τ [-]	2870
κ [-]	0.5
$\frac{l}{\tau}$ [-]	25

COMPUTATIONAL MESH

In Fig. 5 the general configuration of the computational area is depicted (injection in the middle of the fins at an angle of 45°). The dimensionless channel width γ was varied from zero (no injection) to one at 0.5 intervals (three cases on the whole). The calculations refer to three different varieties with regard to the position of the injection port listed below:

1. Injection in the middle of the sealing fins.
2. Injection upstream of the first fin in the middle of the space between the blade leading edge and the edge of the first fin.
3. Guided injection directly upstream of the first sealing fin.

Figure 6 gives an overview of the mentioned injection varieties for the 45° -injection with detailed mesh geometry.

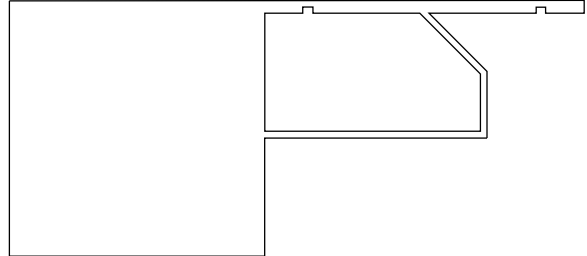


FIGURE 5: 2D BLADE TIP SECTION IN AXIAL DIRECTION WITH TIP-INJECTION IN THE MIDDLE OF THE SEALING FINS.

Mesh refinement was carried out in the vicinity of sharp edges as well as boundary walls in order to take into account the high gradients and resolve the viscous sub layer with the corresponding turbulence model. The first mesh element thickness was chosen pursuant to the requirement of a y^+ value smaller than or equal to one. Investigations concerning grid independency were also carried out for the chosen block structured mesh configuration to make sure that the results are cogent.

Furthermore in the case of guided 45° -injection modification of the fins is observable.

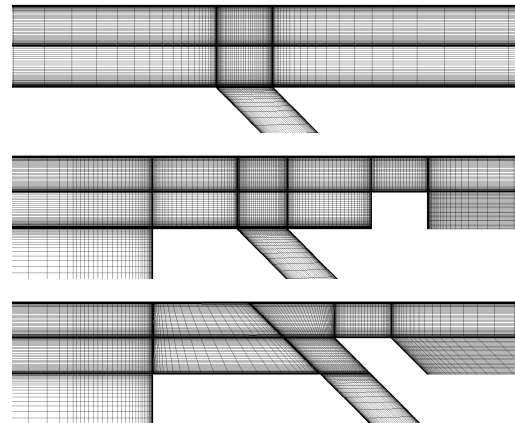


FIGURE 6: DETAILED MESH GEOMETRY AT THE INJECTION SLOT.

RESULTS

Dimensionless 2D CFD-simulations have been carried out for each of the presented meshes with variation of the channel width. Figure 7 shows the streamlines at the blade tip calculated with the k/ω turbulence model for all three injection types specifically for the 45° -injection with a dimensionless channel width $\gamma = 1$.

It is obvious that injection channel barricade appears in all cases due to flow separation at the injection port. The injection flow direction thus tends to distortion and deflection to the direction of the tip gap flow. This effect is approximately of the same order for both unguided injection cases and is reduced in the case of guided injection. The streamlines are besides less deflected in this later case.

The next step is to calculate both discharge coefficients C_D and C_D^+ of all simulation cases and to compare them with the analytical results. Parameter adjustment was carried out only for the k/ω results in order not to lose clarity. These parameters were presented in detail previously and were adjusted according to the calculated results such that the barricade at every point as well as the flow deflection at injection channel exit are approximated properly. The parameter ξ_{mix} was chosen for all cases in a way that the same discharge coefficient was achieved in the case of zero injection.

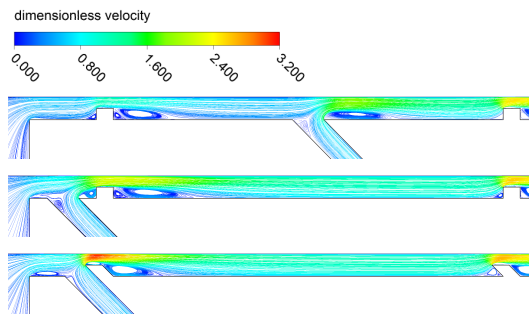


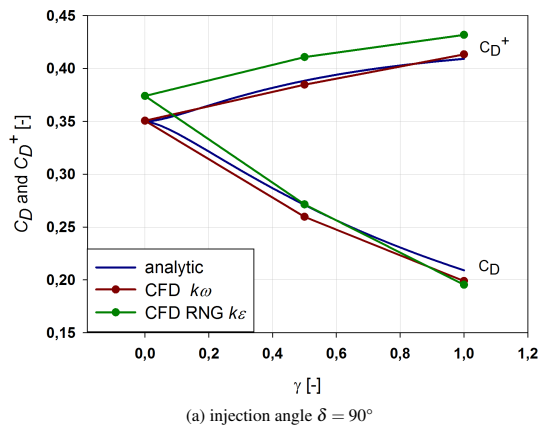
FIGURE 7: STREAMLINES AT THE BLADE TIP (k/ω TURBULENCE MODEL).

In Fig. 8 to 10 results from both the analytical and numerical calculations are depicted. Furthermore various aspects resulting in different discharge coefficients are discussed holistically in the following chapters.

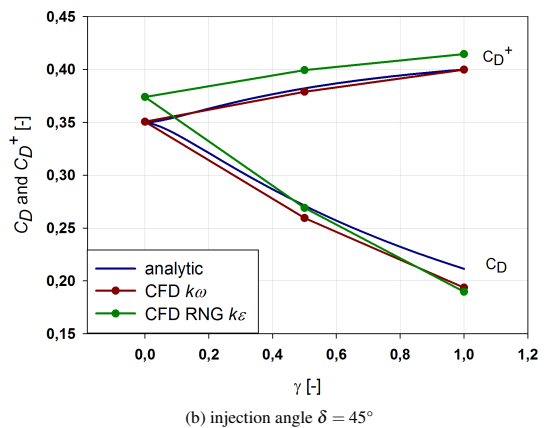
Injection in the Middle of the Fins

The analytical as well as simulation results are depicted in Fig. 8 One can recognise the parameter adjustment of the ana-

lytical results with respect to k/ω simulations. A decrease in C_D -values is observable at both injection angles.



(a) injection angle $\delta = 90^\circ$



(b) injection angle $\delta = 45^\circ$

FIGURE 8: DISCHARGE COEFFICIENT VS. DIMENSIONLESS INJECTION CHANNEL WIDTH FOR INJECTION IN THE MIDDLE OF THE FINS.

However the C_D^+ -values increase with channel width enlargement. Further a good agreement between the results is observable in both cases, even though the discharge coefficient C_D^+ , regarding the overall mass flow rate, seems to be more approximated. This physically means higher injection at lower tip gap

mass flow rate by the simulations. This leads to the conclusion that the calculated flow resistance of the injection mass flow by the simulations is lower than that of the analytical model which results in a higher injection mass flow rate and necessarily higher decrease in the tip gap mass flow rate. Considering the results of the RNG k/ϵ turbulence model, the same tendency in both values of C_D and C_D^+ is remarkable with the sole difference at the point of zero injection which underlines a lower calculated flow resistance by this model.

Injection Upstream of the First Fin

As mentioned before the injection outlet is positioned in the middle of the space between the blade leading edge and the first fin for this configuration. In this case the effect of the injection is overpredicted by the analytical model especially for the 45°-injection as it can be seen in Fig. 9. C_D^+ increases at both turbulence models, however more severely at RNG k/ϵ model. In contrast the analytical model shows a slight decrease in both values of the discharge coefficient in both injection cases.

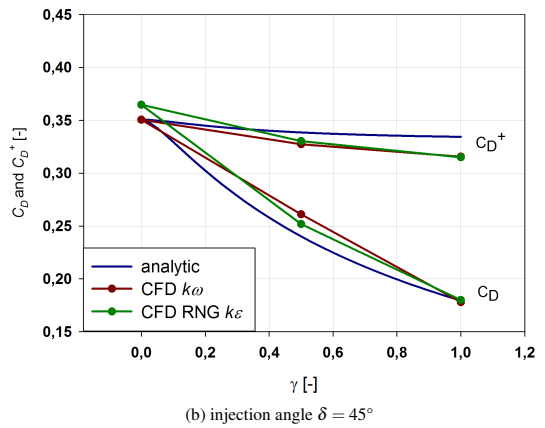
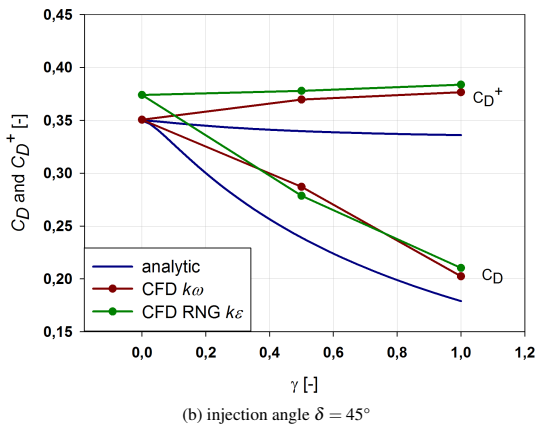
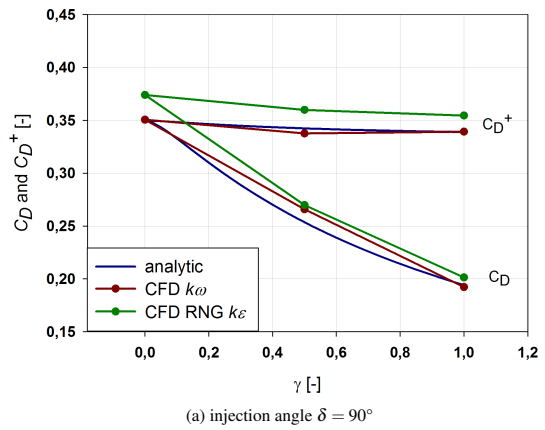
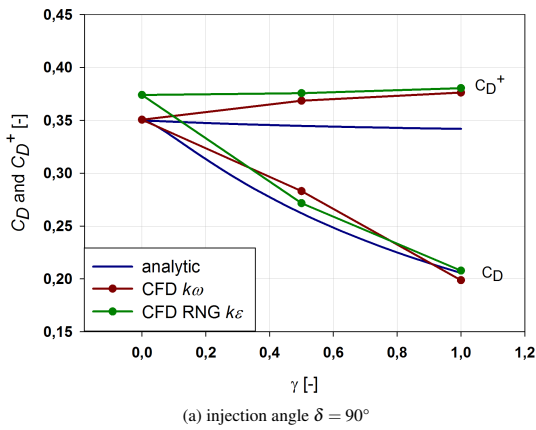


FIGURE 9: DISCHARGE COEFFICIENT VS. DIMENSIONLESS INJECTION CHANNEL WIDTH FOR INJECTION UPSTREAM OF THE FIRST FIN.

FIGURE 10: DISCHARGE COEFFICIENT VS. DIMENSIONLESS INJECTION CHANNEL WIDTH FOR GUIDED INJECTION UPSTREAM OF THE FIRST FIN.

Comparing these results with those of the previous injection type makes it clear that in the case of the 90°-injection almost the same decrease in the value of C_D is observable for all models however C_D^+ increases slightly or remains almost constant depending on the model chosen. This can be attributed to the lower injection mass flow rate resulting to its higher impact on the reduction of the tip gap mass flow rate.

Guided Injection Upstream of the First Fin

The results for the guided injection are depicted in Fig. 10 A higher agreement between the analytical model and the simulations is clearly observable in both cases. The value of C_D^+ decreases with channel width enlargement and is lower in the case of 45°-injection. In this case the influence of the tip-injection on C_D^+ is underpredicted by the analytical model. This means physically higher injection mass flow rate for the same reduction in the tip gap mass flow rate. This fact leads to the conclusion that the impact of the guided injection on the reduction of the tip gap mass flow rate is higher than that of other injection positions.

In comparison to other cases a reduction of approximately 13 % in C_D^+ is achievable at 45°-injection with respect to the case with zero injection.

CONCLUSIONS

A combination of two methods for reducing the tip-leakage mass flow rate were taken into consideration in this work. The blade tip shroud is responsible for increasing flow resistance mechanically, whereas the only tip-injection has an aerodynamic effect. A combination of these methods leads to considerations regarding the position of the injection port with respect to the sealing fins. This effect has been taken into account with the aid of 1D analytical models based on the flow physics at the tip gap over shrouded blades. The so called discharge coefficient C_D , taking into calculation only the tip gap mass flow rate, as well as C_D^+ regarding the overall mass flow rate at the tip gap outlet were calculated as a measure for the effectiveness of tip-injection. The analytical results were compared with those of CFD-simulations calculated with two turbulence models (standard k/ω and RNG k/ϵ).

From the results it emerges that injection upstream of the sealing fins has a higher effect on reducing the tip-leakage mass flow rate especially if the injection is guided through the injection channel. The calculations were solely carried out for a unique dimensionless sealing fin height with regard to the tip gap width. For further investigations the influence of this parameter would also be of interest.

From the analytical considerations it can be inferred that decreasing the value of κ results in a decrease in both discharge coeffi-

cients. Even though the situation of a blade shroud with sealing fins is somehow different from that of labyrinth seals an accurate approach was achieved by the additional parameter ξ_{mix} . It is to be mentioned that the presented results comprise only incompressible steady 2D flow in order not to lose clarity in the presence of many parameters. Modern low pressure turbines particularly those of aircraft engines feature high velocities resulting in transonic flow in many cases. Furthermore the flow field around the blade profiles is mainly three dimensional. These effects may be taken into account by further investigations with knowledge of the efficient injection position. The effect of blade rotation on the injection massflow rate can also be a further point of investigations. Experimental investigations can also be carried out in order to obtain cogent results incorporating various aspects of passive tip injection and its positions at the tip gap.

REFERENCES

- [1] Kurzke, J., 2009. "Fundamental Differences between Conventional and Geared Turbofans". ASME Paper GT2009-59745.
- [2] Curtis, E., Hodson, H., Banieghbal, M., Denton, J., Howell, R., and Harvey, N., 1997. "Development of Blade Profiles for Low-Pressure Turbine Applications". *Journal of Turbomachinery*, **119**, July, pp. 531–538.
- [3] Malzacher, F. J., Gier, J., and Lippl, F., 2006. "Aerode-sign and Testing of an Aeromechanically Highly Loaded LP Turbine". *Journal of Turbomachinery*, **128**, October, pp. 643–649.
- [4] Bräunling, W. J. G., 2009. *Flugzeugtriebwerke*. Springer-Verlag.
- [5] Hong, Y. S., and Groh, F. G., 1966. "Axial Turbine Loss Analysis and Efficiency Prediction Method". *Boeing Report D4-320*.
- [6] Curtis, E. M., Denton, J. D., Longley, J. P., and Rosic, B., 2009. "Controlling Tip Leakage Flow over a Shrouded Turbine Rotor Using an Air-Curtain". ASME Paper GT2009-59411.
- [7] Hogg, S. I., and Ruiz, I. G., 2011. "Fluidic Jet Barriers for Sealing Applications". ASME Paper GT2011-45353.
- [8] Yoon, S., Curtis, E., Denton, J., and Longley, J., 2013. "The Effect of the Degree of Reaction on the Leakage Loss in Steam Turbines". *Journal of Engineering for Gas Turbines and Power*, **135**, February, pp. 1–9.
- [9] Willinger, R., and Haselbacher, H., 2000. "On the Modeling of Tip Leakage Flow in Axial Turbine Blade Rows". ASME Paper 2000-GT-633.
- [10] Bindon, J., 1987. "Pressure Distribution in the Tip Clearance Region of an Unshrouded Axial Turbine as Affecting the Problem of Tip Burnout". ASME Paper 87-GT-230.
- [11] Porreca, L., Behr, T., Schlienger, J., Kalfas, A. I., Abhari, R. S., J.Ehrhard, and Janke, E., 2005. "Fluid Dynamics and

- Performance of Partially and Fully Shrouded Axial Turbines". *Journal of Turbomachinery*, **127**, October, pp. 668–678.
- [12] Riegler, C., and Bichlmaier, C. "The Geared Turbofan Technology-Opportunities, Challenges and Readiness Status". *1st CEAS European Air and Space Conference, CEAS-2007-054*.
- [13] Benoni, A., and Willinger, R., 2012. "Numerical Simulation of Passive Tip-Leakage Flow Control Method for Axial Turbines". In Proceedings of the 6th European Congress on Computational Methods in Applied Sciences and Engineering (ECCOMAS 2012). Paper No. 5429.
- [14] Bohl, W., and Elmendorf, W., 2008. *Technische Strömungslehre*, 14 ed. Vogel Fachbuch Kamprath-Reihe.
- [15] Hah, C., 1984. "A Navier-Stokes Analysis of Three-Dimensional Turbulent Flows Inside Turbine Blade Rows at Design and Off-Design Conditions". *Journal of Engineering for Gas Turbines and Power*, **106**, April, pp. 421–429.

5. Linear Cascade Investigations

In the previous chapter the discharge behavior of shrouded blades under the impact of passive tip-injection was investigated based on 1D analytical considerations and simple 2D CFD calculations. In this regard the guided injection upstream of the first sealing fin turned out to have the best effectiveness. However, no 3D effects were considered in this approach, since it was a first step toward functionality of passive tip-injection.

In this chapter 3D effects are taken into account, though in a linear cascade without rotation and swirl impact. This step is necessary prior to costly CFD calculations in a rotational frame of reference in order to make a preliminary assessment regarding performance of passive tip-injection. In addition to the full shroud, two partially shrouded blades are also included in this estimation procedure to achieve a wide range of comparable cases. Furthermore passive tip-injection has been applied to all shroud geometries. The investigations were all carried out numerically, since on the one hand no adaption of the linear cascade test rig to the shrouded geometry was possible and on the other hand more geometry variations could be studied by means of CFD. The results are presented in paper 2.

5.1. Linear Cascade Geometry

The cascade geometry used for the investigations in this chapter has been the focus of a variety of studies at the department of Fluid-Flow Machinery of the Institute for Energy Systems and Thermodynamics at Technische Universität Wien. The details of the cascade geometry are given in [9] and [29] and presented later in paper 2.

The original unshrouded geometry was provided with a full shroud consisting of three sealing fins (indicated as FS), which was further provided with guided passive tip-injection upstream of the first sealing fin. In the next step the volume of the full shroud was reduced in two ways in order to account for the impact of the pressure distribution on the cavity flow and the leakage flow. First the shroud volume was reduced mostly in the region of the blade leading edge. This case is called PSLE. Subsequently the full shroud volume was reduced mostly in the rear region termed as PSTE. In both cases the number of the fins was reduced to two. The shroud geometries are depicted in Fig. 5.1. Both partial geometries were further provided with guided passive tip-injection upstream of the first sealing fin. An additional injection position was also tested for the

case of the partial shroud reduced at the leading edge due to the profile pressure distribution of the blade (front-loaded). More details about the investigated cases are given in paper 2.

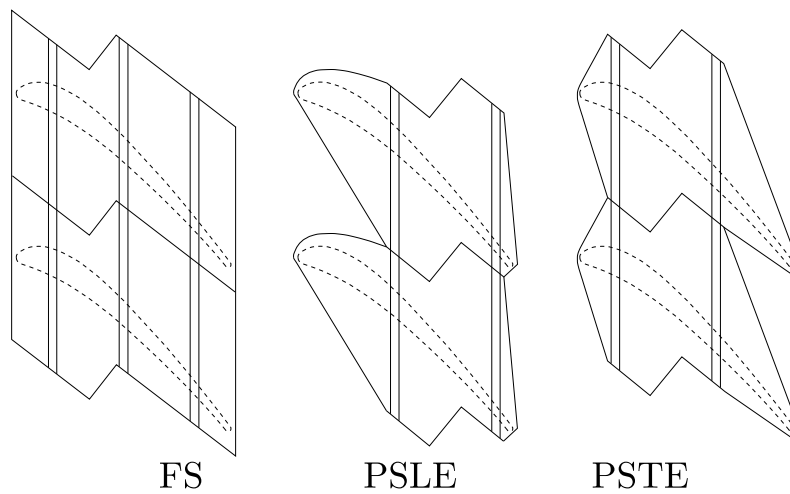


Figure 5.1.: Shroud Geometries for Linear Cascade Investigations

5.2. CFD Calculations

As mentioned before the shroud geometries together with the corresponding injection cases were all studied numerically. The calculations were carried out in ANSYS Fluent 13.0 for a single blade passage and incompressible flow. The realizable k/ϵ -model with enhanced wall treatment was applied for turbulence modeling in compliance with [9]. Furthermore the injection channel was modeled based on a 1D loss correlation. This procedure was also adopted in [9].

The resulted cascade efficiencies were taken into account for assessments regarding the full shroud and the different partial shrouds with and without passive tip-injection. The cascade efficiency penalties with respect to the fully shrouded geometry without tip-injection (as reference) were also evaluated. The computational procedure together with the results are presented in more detail in paper 2.

Paper 2

P. Ghaffari and R. Willinger

Preliminary Investigation of Passive Tip-Injection in a Linear
Turbine Cascade with Shrouded Blades

ETC paper 205
11th European Turbomachinery Conference
Madrid, Spain, 2015

Preliminary Investigation of Passive Tip-Injection in a Linear Turbine Cascade with Shrouded Blades

P. Ghaffari - R. Willinger

Institute for Energy Systems and Thermodynamics
Vienna University of Technology
Getreidemarkt 9/302, A-1060 Vienna, Austria
pouya.ghaffari@tuwien.ac.at, reinhard.willinger@tuwien.ac.at

ABSTRACT

The efficiency of a gas turbine stage depends on various factors. Since tip-leakage losses count for one third of the overall losses in a turbine stage, their reduction is of high importance regarding the stage efficiency. The objective of this paper aims at combination of blade shrouds with the method of passive tip-injection and presents 3D CFD results for incompressible flow without blade rotation using various shroud geometries and injection positions. The originally full shroud is reduced in terms of weight reduction. In this case the negative effect of increasing the tip-leakage losses by partially shrouded blades and its compensation by means of passive tip-injection is investigated. Finally the impact of blade rotation on injection mass flow rate is considered briefly

NOMENCLATURE

c	absolute velocity	w	relative velocity
C	constant	x, y, z	cartesian coordinates
C_p	pressure coefficient	β	relative flow angle
d	injection channel diameter	λ	friction loss coefficient
K	constant	ζ	loss coefficient
l	injection channel length	η_c	cascade efficiency
m	mass	ρ	density
p	pressure	ω	angular velocity
r	radius		

Superscripts

—	pitchwise averaged quantity	=	area averaged quantity
------------	-----------------------------	------------	------------------------

Subscripts

c	casing section	x	axial direction
inj	injection	1	inlet
rel	relative	2	outlet
t	total		

INTRODUCTION

Weight reduction and increasing the overall efficiency of aircraft engines are of high importance in recent investigations. The modern technology of geared turbo fan allows for higher rotational speed of the low pressure turbine driving the fan by providing a gear box between the low pressure turbine and the fan. In Malzacher et al. (2006) the characteristics of a highly loaded low pressure turbine with higher rotational speed are given. The reduced axial length resulting in lower overall weight

implicates higher blade loading of the low pressure turbine and higher tip-leakage losses due to the higher degree of reaction in the tip region (Hong and Groh, 1966). Furthermore high rotational speed results in higher mechanical stress especially in the blade root. This leads to mass reduction from fully shrouded to partially shrouded blades (Riegler and Bichlmaier, 2007).

The impact of passive tip-injection on the tip-leakage flow in unshrouded axial blades has been investigated in linear turbine cascades with various injection angles against the tip flow direction. Furthermore CFD calculations as well as analytical considerations have been carried out in this field. In Benoni and Willinger (2013) experimental data regarding passive tip-injection with an angle of 45° against the tip-leakage flow are presented. In Curtis et al. (2009) an active method of reducing tip-leakage mass flow rate over shrouded turbine blades is discussed. It can be shown that the overall mass flow rate at the tip gap exit remains relatively constant whereas the inlet mass flow rate decreases with increasing the jet mass flow rate. A maximum increase of 1.2% in turbine efficiency could also be featured in the results. Hogg and Ruiz (2011) presented the effect of flow jet barriers in combination with sealing applications using three sealing fins. In the first part of their work the improved effect of inclined injection is presented clearly. Furthermore the influence of inclined injection with guidance in combination with three labyrinth fins is investigated.

A combination of shrouded blades with passive tip-injection was investigated in Ghaffari and Willinger (2013) analytically as well as by means of 2D CFD calculations. The tip mass flow rate showed high dependency on the axial injection position over the blade shroud. Due to this fact three injection positions over the blade shroud with two fins were studied. Among these positions the guided injection upstream of the first fin turned out to have the best effectiveness.

Since the impact of passive tip-injection at partially shrouded blades is dominated by three dimensional effects, various combinations of blade shroud geometries and tip-injection are investigated by means of 3D CFD calculations in this paper. In the end the effect of blade rotation is studied analytically.

GEOMETRY CONFIGURATIONS

The cascade geometry used for the CFD calculations is the same as in Benoni and Willinger (2013). The same geometry was also used in Hamik and Willinger (2008) for detailed tip-leakage flow investigations. In this work the blade used in the cascade was provided by a generic full shroud with three fins followed by a reduction of the shroud mass as well as the number of the fins due to lack of axial space. The geometrical relations of the generic shroud were chosen based on Riegler and Bichlmaier (2007) as well as a real shrouded blade geometry from the second turbine stage of a heavy duty gas turbine. The main dimensions of the shroud used for the calculations as well as the cascade characteristics are given in Fig. 1.

The originally fully shrouded blade (**FS**) was reduced in two ways. First the shroud mass was mainly reduced at the leading edge of the blade (**PSLE**). Since the investigated blade is front loaded, based on the blade pressure distribution at midspan, a second variation with most of the reduction at the blade trailing edge (**PSTE**) was also studied. In Fig. 2 the full shroud as well as the related partial shrouds are depicted. One recognizes the periodical borders of the shroud for CFD calculations. Furthermore it has to be mentioned that the geometrical modifications were assumed based on the given cascade geometry. Since the cascade is linear and serves for flow investigations no structural mechanics assessment was carried out.

The geometries presented in this paper relate to those used for the CFD calculations with periodic boundaries. In designing the full as well as partial shrouds realistic shroud geometries were taken into consideration. The front shape of the partial shroud in the case of **PSLE** is due to the high solidity value of the investigated cascade resulting in less space in pitchwise direction for shroud reduction. In Tab. 1 the percental reduction in the shroud mass is presented for each of the partial shrouds. Furthermore it has to be mentioned that the changes in mechanical stress in the blade root

due to centrifugal forces are proportional to the mass reduction of the shroud.

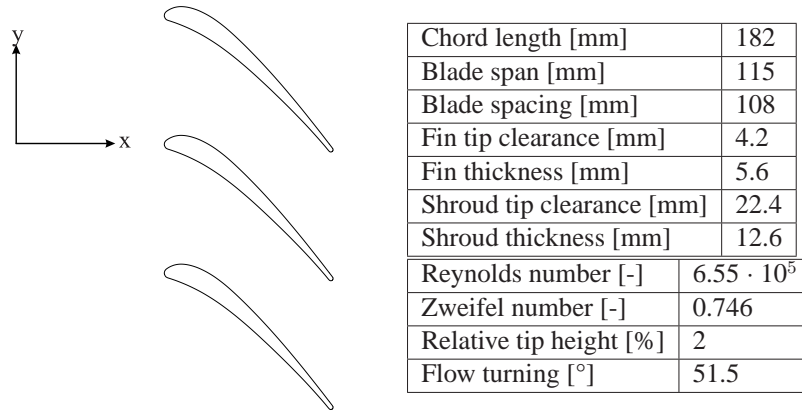


Figure 1: Geometrical and operational parameters of cascade and generic shroud

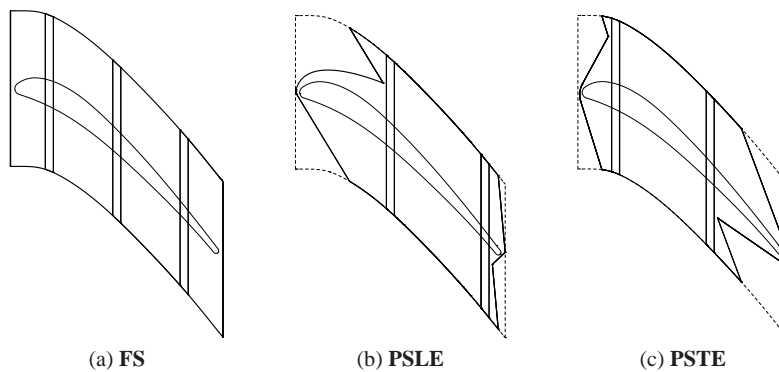


Figure 2: Investigated shroud geometries

Partial shroud	$\Delta m / m$ [%]
PSLE	-11.3
PSTE	-12.1

Table 1: Relative mass reduction from full to partial shroud

In the next step each shroud geometry was provided by inlet and outlet injection bores with a diameter of 5 mm. The injection inlet at the blade leading edge was positioned at a distance of 30 mm in spanwise direction under the blade shroud in order to catch the flow outside of the boundary layer. The injection outlet was positioned depending on the injection case being chosen. According to Ghaffari and Willinger (2013) guided passive tip-injection upstream of the first fin has the highest effectiveness. This means that the injection outlet is manufactured by a groove in the first fin, by means of which the injection flow is guided resulting in better effectiveness. For this reason every shroud geometry was provided by guided injection (**GI**). In this case the bore center was positioned

in the middle of the blade thickness over the shroud with an axial distance of 1.5 mm from the front edge of the first fin. In addition to the cases with guided injection the shroud geometry reduced at the leading edge was also investigated in combination with unguided injection (**UGI**). In this case the injection outlet was located at the place with the highest profile pressure difference. In order not to lose clarity the two injection cases mentioned above are depicted in Fig. 3 for the shroud reduced at the leading edge.

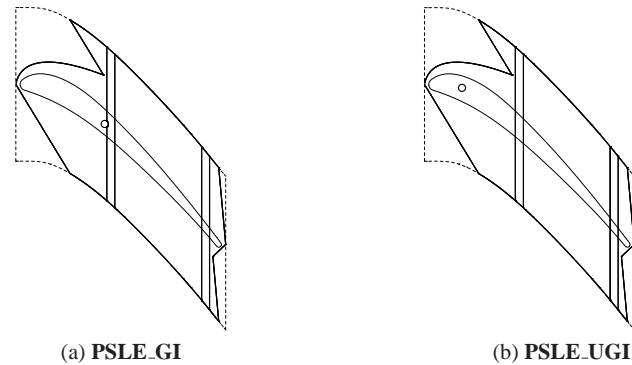


Figure 3: Investigated injection cases for shroud geometry reduced at the leading edge

CFD CALCULATIONS

Computational Mesh

The generated geometries were all meshed in ICEM 13.0. The difficulty was in meshing the sharp edges at the leading or trailing edge of the shroud caused by the periodic boundaries. In compliance with Benoni and Willinger (2012) the injection channel except for its inlet and outlet was not meshed and the injection channel flow was modeled based on loss correlations as mentioned later. Mesh refinement was carried out in the vicinity of every wall providing sufficient resolution of the boundary layer ($y^+ < 1$). The mesh independence of the CFD calculations was further proved for each mesh. In Tab. 2 the cell number of each geometry is presented. Furthermore the generated mesh is depicted in the vicinity of the sharp edges and the tip as well as the injection bores in Fig. 4 for **PSLE_GI**.

Without injection		With injection	
FS	4.12 million	FS_GI	4.84 million
PSLE	4.71 million	PSLE_GI	6.57 million
		PSLE_UGI	7.39 million
PSTE	4.14 million	PSTE_GI	6.01 million

Table 2: Cell number of investigated calculation meshes

Boundary Conditions

All calculations were carried out in Fluent 13.0 for incompressible and steady flow without blade rotation. Since the calculation domain comprises one blade spacing, periodic boundary conditions were applied. For the inlet boundary condition constant velocity distribution was chosen in order to take into consideration the tip-leakage flow isolated from the secondary flow. For turbulence at the inlet an intensity of 5% and a turbulent length scale of 0.021 m were set as constant values.

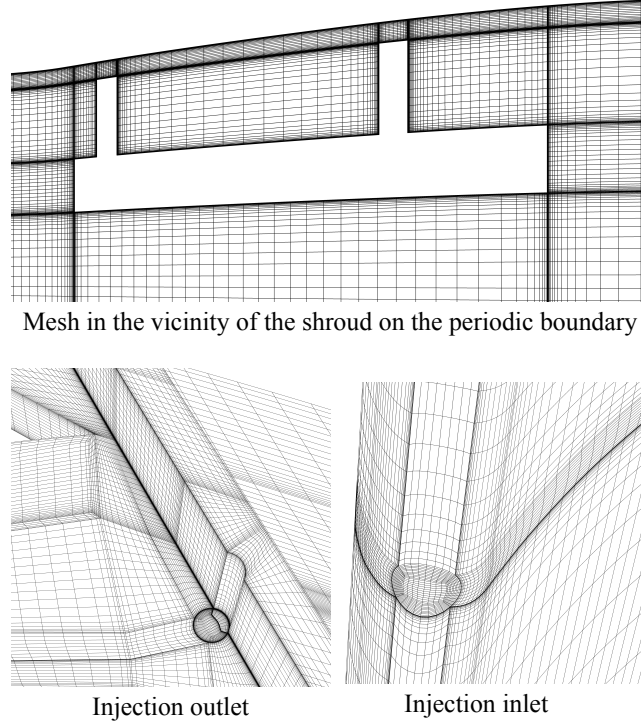


Figure 4: Investigated injection cases for shroud geometry reduced at the leading edge

The turbulent length scale was measured upstream of the cascade by means of hot wire anemometry and indicated good agreement with the turbulent length scale calculated by means of the hydraulic diameter of the channel. At the boundary outlet constant static pressure was applied. For turbulence modeling realizable $k\epsilon$ -model with enhanced wall treatment was chosen.

Since the injection channel was modeled via analytical considerations the injection inlet and outlet had to be specified by boundary conditions. In this spirit pressure outlet was assigned to the injection inlet with target mass flow rate being calculated during the iterations. In this manner the static pressure is a result of the calculation. At the injection outlet the mass flow rate calculated via channel modeling for each investigated case was assigned.

Injection Channel Modeling

The modeling of the injection channel was carried out according to Benoni and Willinger (2012) with appropriate adjustments regarding the shrouded blade. The main idea is to calculate the injection mass flow rate by means of a 1D model. Applying the Bernoulli-equation for incompressible channel flow with losses leads to

$$p_{inj,2} + \frac{1}{2}\rho w_{inj}^2 + \frac{1}{2}\rho w_{inj}^2 \left(\lambda \frac{l}{d} + \Sigma\zeta \right) = p_1 + \frac{1}{2}\rho w_1^2 \quad (1)$$

$$C_{p,inj} = \frac{p_{inj,2} - p_1}{\frac{1}{2}\rho w_1^2} = 1 - \left(\frac{w_{inj}}{w_1} \right)^2 \left[1 + \lambda \frac{l}{d} + \Sigma\zeta \right] \quad (2)$$

In this equation p_1 and w_1 correspond to static pressure and velocity at the inlet of the cascade. $C_{p,inj}$ is thus the static pressure coefficient corresponding to the pressure difference between the cascade

inlet and the injection position over the blade shroud. This value was calculated with respect to each shroud geometry and was adjusted for each of the injection cases. $\Sigma\zeta$ characterizes the sum of the losses except for the friction losses being included in the preceding term. The injection velocity can thus be calculated as follows:

$$\frac{w_{inj}}{w_1} = \sqrt{\frac{1 - C_{p,inj}}{1 + \lambda_d^l + \Sigma\zeta}} \quad (3)$$

The target mass flow rate at the injection inlet as well as the mass flow rate at the injection outlet were hence calculated via Eqn. 3 and applied properly.

Results

The numerical results showed that the flow field around the blade shroud was greatly influenced by the shroud geometry. The y^+ values however indicated less dependence on shroud geometry. A range of $0.01 < y^+ < 0.6$ was evident on the blade surface for the mesh chosen and each shroud geometry with and without tip-injection. The tip-injection turned out to have no impact on the range of y^+ on the blade as well as shroud surface including the sealing fins. The y^+ values on the shroud surface together with the sealing fins are between 0.001 and 0.7 for **FS**, 0.001 and 0.96 for **PSLE** as well as 0.001 and 0.8 for **PSTE**.

Although the tip gap flow is mainly in axial direction in the case of full shroud 3D effects dominate the tip gap flow in partially shrouded configurations. In Fig. 5 the streamlines around both types of the shrouded blades are depicted. The viewing direction is spanwise from hub to tip. As one can clearly see a part of the tip gap flow is turned onto the blade suction side in the front region of the partial shroud and is accelerated in the case of **PSLE**. It is then mixed to the tip gap flow at the outlet. This appearance is missing in the case of **PSTE** as the main part of the shroud reduction is dislocated to the trailing edge, where profile pressure difference is lower. In this case the tip gap flow is mixed to the passage flow at the blade trailing edge. These deviations will affect the exit flow angle as presented later. In Fig. 6 2D streamlines of tip-leakage flow with passive injection are depicted in a meridian

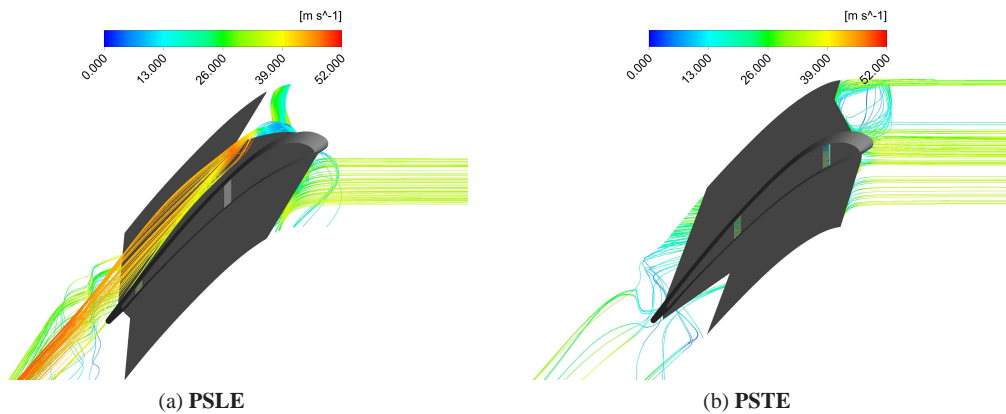


Figure 5: Streamlines of **PSLE** and **PSTE**

plane for **FS_GI** and **PSLE_GI**. As one can clearly see passive tip-injection reinforces the vortex over the blade shroud in the case of **FS_GI** as it is located close to the leading edge. Furthermore the guidance of the first fin is obvious. In the case of **PSLE_GI** the vortex is built up in the vicinity of the leading edge. Due to the shroud reduction concentrated at the leading edge the first fin is positioned

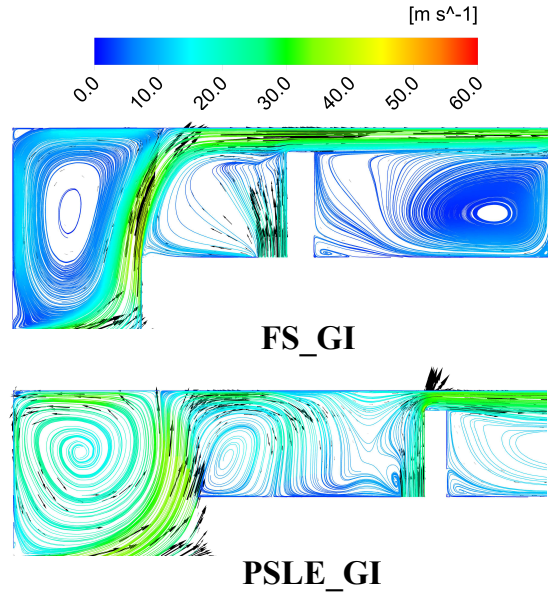


Figure 6: 2D streamlines of tip-leakage flow with passive injection

further downstream. Due to this fact the guided injection does not have the possibility of reinforcing the vortex over the shroud and contributes to further increasing the tip-leakage mass flow rate at the tip gap outlet. Based on this fact additional injection position close to the leading edge was taken into consideration for this shroud geometry. The impact of passive tip-injection on cascade efficiency will become clear later.

For comparison the pitchwise averaged value of the exit flow angle $\bar{\beta}_2$ as well as total pressure coefficient \bar{C}_{pt2} were evaluated at the outlet in an axial distance of 140 mm from the blade trailing edge in 13 different positions in spanwise direction. It has to be mentioned that $\bar{\beta}_2$ was calculated with respect to the negative circumferential direction. For calculating \bar{C}_{pt2} the total pressure at the inlet of the cascade was taken into calculation and the difference was made dimensionless by the dynamic pressure at the cascade inlet as indicated in Eqn. 4.

$$\bar{C}_{pt2} = \frac{p_{t1} - \bar{p}_{t2}}{\frac{\rho}{2} w_1^2}. \quad (4)$$

It has to be mentioned that higher \bar{C}_{pt2} values correspond to higher losses since the total pressure drops from the inlet to the outlet of the cascade. Furthermore the cascade efficiency η_c was calculated by means of following equation for turbine cascades and incompressible flow and mass flow averaged quantities:

$$\eta_c = \frac{\overline{w_2^2}}{\frac{2}{\rho} (\bar{p}_1 - \bar{p}_2) + \overline{w_1^2}}. \quad (5)$$

Full Shroud

In Fig. 7 the pitchwise averaged exit flow angle $\bar{\beta}_2$ and total pressure coefficient \bar{C}_{pt2} are depicted for different positions of dimensionless channel height for the full shroud with and without

tip-injection. Deviations in the flow angle are visible in the vicinity of the tip gap outlet in comparison to the midspan due to the tip-leakage flow mixing into the main flow resulting in an overturning. Taking into account the changes in total pressure one can clearly recognize that total pressure losses decrease due to passive tip-injection in the vicinity of the tip gap outlet whereas \overline{C}_{pt2} values remain unchanged in the midspan region.

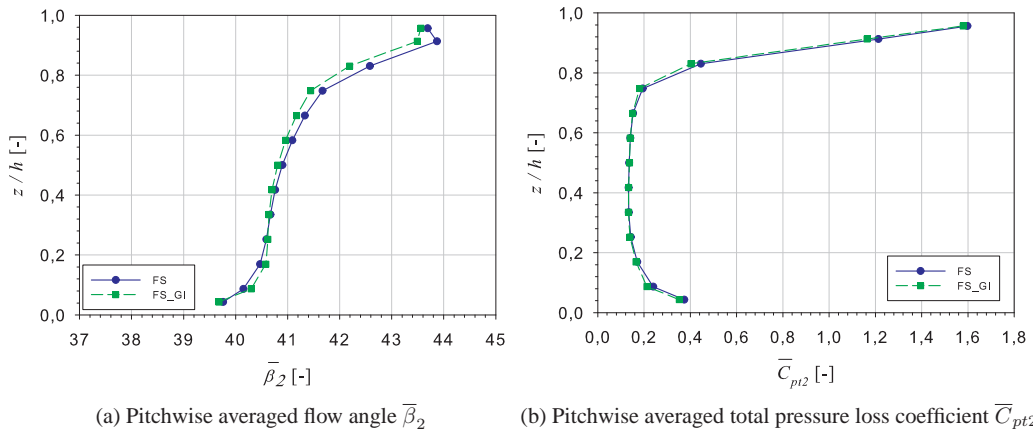


Figure 7: $\overline{\beta}_2$ and \overline{C}_{pt2} of full shroud with and without tip-injection

Partial Shroud Reduced at the Leading Edge

The results of the calculations regarding the case with the partial shroud reduced at the leading edge are demonstrated in Fig. 8.

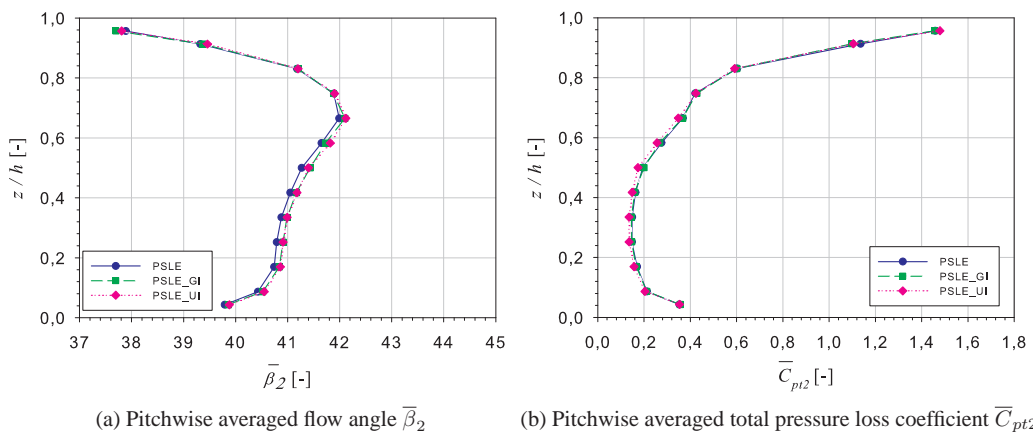


Figure 8: $\overline{\beta}_2$ and \overline{C}_{pt2} of partial shroud reduced at the leading edge with and without tip-injection

One can clearly see the impact of tip-leakage flow on the exit flow angle in the vicinity of the tip gap

outlet resulting in an overturning extending down in spanwise direction to a larger area in comparison to the previous case with full shroud. It is also clear that no large changes are achievable applying passive tip-injection. This can be explained by the fact that the tip gap flow is deflected mostly to the blade suction side before the injection mass flow is mixed properly. On the contrary in the case of fully shrouded blade the flow rolls up to a vortex of larger scale over the shroud. In this case the blockage effect can be enhanced by means of passive injection.

Partial Shroud Reduced at the Trailing Edge

Shifting the shroud reduction to the trailing edge makes it possible to locate the first fin close to the leading edge and to perform guided injection in this place. Furthermore the front region of the blade with the maximum pressure difference is covered by the shroud which prevents flow deflection to the blade suction side. In Fig. 9 the pitchwise averaged exit flow angle $\bar{\beta}_2$ and total pressure coefficient \bar{C}_{pt2} are depicted.

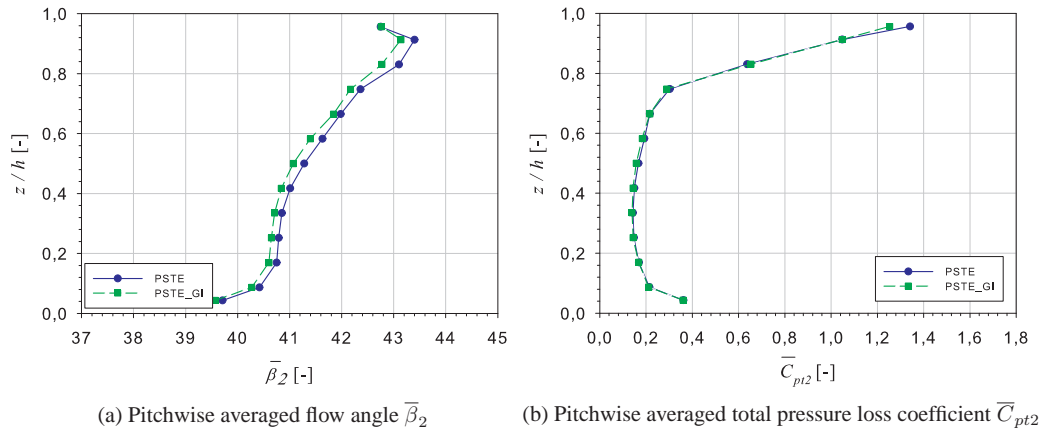


Figure 9: $\bar{\beta}_2$ and \bar{C}_{pt2} of partial shroud reduced at the trailing edge with and without tip-injection

Compared to the fully shrouded blade the flow angle features similar tendency in the region of the tip gap outlet. In addition the impact of tip-injection is more dominant than in the previous case. This can be explained by the higher blockage effect of the tip-injection due to the larger vortex in the vicinity of the leading edge.

The cascade efficiencies of the various cases investigated in this paper are depicted in Tab. 3. **FS** has been taken as reference in order to characterize the efficiency changes respectively. As one can clearly see the cascade efficiency increases by 0.34 % due to passive tip-injection in the case of **FS**. Furthermore the negative effect of shroud reduction on cascade efficiency is evident. In the case of **PSLE_GI** guided tip-injection contributes to further reducing the cascade efficiency. Because of the partial shroud geometry of this configuration the first fin features larger distance to the leading edge. On the other hand the vortex built up over the blade shroud is mostly concentrated at the leading edge. Due to this fact the injection mass flow is not able to generate a blockage effect and contributes to additional tip gap mass flow rate mixing to the main flow at the outlet increasing the tip-leakage losses. This negative effect can be compensated by positioning the injection outlet at the place with the highest profile pressure difference over the shroud. With this new injection position it is possible to improve the cascade efficiency. However it is not possible to compensate the efficiency decrease due to the shroud reduction completely and achieve the same efficiency as in the case of fully shrouded

blade. In the case of **PSLE** shroud reduction also increases the tip-leakage losses although to lower extent in comparison to **PSLE**. An increase in efficiency due to tip-injection is also visible. Moreover **PSLE** features higher shroud mass reduction.

Investigated case	η_c [-]	$\Delta\eta_c/\eta_c$ [%] (with FS as reference)
FS	0.881	-
FS_GI	0.884	+0.34
PSLE	0.867	-1.59
PSLE_GI	0.866	-1.70
PSLE_UI	0.868	-1.48
PSLE	0.876	-0.57
PSLE_GI	0.877	-0.45

Table 3: Cascade efficiency η_c and relative efficiency changes $\Delta\eta_c/\eta_c$

EFFECT OF ROTATION

Regarding the effect of blade rotation on the tip-injection it has to be taken into consideration that the pressure distribution upstream of the injection slot and the blade tip inlet varies with respect to the radius in the case of swirled flow. Assuming both free vortex flow and radial equilibrium at the inlet one obtains

$$rc_u = K, \quad (6)$$

$$\frac{c_u^2}{r} = \frac{1}{\rho} \frac{dp}{dr}. \quad (7)$$

Under the assumption of constant axial velocity in radial direction as well as zero radial velocity component following equation results for the radial static pressure distribution:

$$p(r) = C - \rho \frac{K^2}{2} \frac{1}{r^2}, \quad (8)$$

with C as a constant. Considering the velocity consisting of constant axial component and radial distribution resulting from the free vortex one obtains following result for the total pressure distribution:

$$p_t(r) = C + \frac{\rho}{2} c_x^2. \quad (9)$$

Since both the previous and following considerations are carried out with respect to the rotating system, Eqn. 9 is transformed to the relative total pressure distribution. In this manner the circumferential velocity resulting from the blade rotation has to be subtracted from the absolute velocity and one obtains

$$p_{t,rel}(r) = C + \frac{\rho}{2} (c_x^2 - 2K\omega + r^2\omega^2). \quad (10)$$

Considering the difference between the radius at the tip and the injection inlet slot one obtains following total pressure difference:

$$p_{t,rel}(r_c) - p_{t,rel}(r_{inj,1}) = \frac{\rho}{2} \omega^2 (r_c^2 - r_{inj,1}^2). \quad (11)$$

Taking into consideration the Bernoulli-equation for rotating systems and $p_{inj,2}$ as the static pressure at the injection outlet one obtains

$$p_{t,rel}(r_{inj,1}) - p_{inj,2} = \frac{\rho}{2}w^2(1 + \zeta) - \frac{\rho}{2}\omega^2(r_c^2 - r_{inj,1}^2), \quad (12)$$

$$p_{t,rel}(r_c) - p_{inj,2} = \frac{\rho}{2}w^2(1 + \zeta). \quad (13)$$

As one can see the same results can be achieved as in the case without blade rotation as long as the relative total pressure at the blade tip is taken as the reference pressure. This means that the blade rotation and therefore the spanwise position of the injection inlet have a secondary effect regarding the injection mass flow rate. Nevertheless blade rotation influences the injection channel flow and possibly the losses resulted in comparison to a stationary system.

CONCLUSIONS

Current investigations were carried out for incompressible steady flow in a linear cascade. The results showed that blade shroud reduction has a negative impact regarding the cascade efficiency. Furthermore it could be shown that the type of shroud reduction has a considerable influence on the tip-leakage losses. Considering the aspect of reducing the weight of rotating components as blade shrouds in support of mechanical stress one also has to take into consideration the blade aerodynamic. A proper choice of how the blade shroud is to be reduced is of great importance. While the partial shroud reduced at the trailing edge features higher mass reduction in comparison to the partial shroud reduced at the leading edge it results in higher cascade efficiencies.

The method of passive tip-injection proved to be capable of reducing the tip-leakage losses. Its highest effectiveness could be reached in the case of fully shrouded blade. In comparison to unshrouded blades investigated in previous works more options are given regarding the injection position in the case of shrouded blades with sealing fins. According to previous basic considerations guided injection upstream of the first fin proved to be most effective. Current calculations taking into account the 3D effects of tip gap flow show to which extent the effectiveness of this type of injection depends on the shroud reduction. The CFD results showed that it is possible to enhance the cascade efficiency of the fully shrouded and at the trailing edge reduced partially shrouded blade by 0.34% and 0.11% respectively via guided injection. On the contrary guided injection would reduce the cascade efficiency by 0.12% in the case of the partial shroud reduced at the leading edge. In this case unguided injection at the place of maximum pressure difference would enhance the cascade efficiency by 0.12%.

Due to high rotational speed of modern low pressure turbines the impact of blade rotation and thus the spanwise position of the injection inlet on the passive tip-injection was also studied analytically. In this spirit some assumptions such as free vortex flow and radial equilibrium were necessary. The results showed that under these assumptions the spanwise position of the injection inlet does not influence the tip-injection mass flow rate appreciably. It can thus be concluded that under different circumstances the blade rotation and therefore the spanwise position of the injection inlet have a secondary effect on passive tip-injection according to the analytical considerations.

Forthcoming works could include real applications with real blade and shroud geometry taking into account blade rotation and compressible flow. Different injection positions over the blade shroud could be taken into calculation in order to investigate the impact of the position more cogently. Moreover the blade aerodynamic being affected by the injection bore at the leading edge can be taken into consideration. In this spirit various diameters of the injection channel could be considered in order to gain a better understanding regarding the injection mass flow rate and its capability of reducing tip-leakage losses. For completeness structural mechanics assessments can be the topic of further investigations.

ACKNOWLEDGEMENTS

The authors would like to acknowledge the Austrian Research Promotion Agency FFG for supporting the project in the framework of the Aeronautics Research and Technology Programme TAKE OFF.

REFERENCES

- Benoni, A. and Willinger, R. (2012). Numerical Simulation of Passive Tip-Leakage Flow Control Method for Axial Turbines. In *ECCOMAS 2012*, Vienna. Paper No. 5429.
- Benoni, A. and Willinger, R. (2013). Design modification of a passive tip-leakage control method for axial turbines: Linear cascade wind tunnel results. ASME Paper TBTS2013-2056.
- Curtis, E. M., Denton, J. D., Longley, J. P., and Rosic, B. (2009). Controlling Tip Leakage Flow Over a Shrouded Turbine Rotor Using an Air-Curtain. ASME Paper GT2009-59411.
- Ghaffari, P. and Willinger, R. (2013). Impact of passive tip-injection on the performance of partially shrouded turbines: Basic concept and preliminary results. ASME Paper TBTS2013-2038.
- Hamik, M. and Willinger, R. (2008). An innovative passive tip-leakage control method for axial turbines: Linear cascade wind tunnel results. ASME Paper GT2008-50056.
- Hogg, S. I. and Ruiz, I. G. (2011). Fluidic Jet Barriers for Sealing Applications. ASME Paper GT2011-45353.
- Hong, Y. S. and Groh, F. G. (1966). Axial Turbine Loss Analysis and Efficiency Prediction Method. *Boeing Report D4-320*.
- Malzacher, F. J., Gier, J., and Lippl, F. (2006). Aerodesign and Testing of an Aeromechanically Highly Loaded LP Turbine. *Journal of Turbomachinery*, 128:643–649.
- Riegler, C. and Bichlmaier, C. (2007). The Geared Turbofan Technology-Opportunities, Challenges and Readiness Status. *1st CEAS European Air and Space Conference, CEAS-2007-054*.

6. Investigations on a Real Application

In the previous chapters the impact of passive tip-injection on the discharge behavior as well as the cascade efficiency was investigated. It could be concluded that in the case of a full shroud the method of guided passive tip-injection upstream of the first sealing fin features the highest effectiveness in spite of the fact that the full shroud with three sealing fins already has a satisfactory sealing effect. However, the evaluations do not take into account the effect of rotation on the injection flow and its contribution to specific stage work.

These effects are subject of the investigations presented in this chapter. For this purpose a LPT rotor with shrouded blades provided with guided passive tip-injection was studied. For comparison cases without clearance were also considered. The method of guided passive tip-injection upstream of the first sealing fin was, however, investigated only numerically due to manufacturing restrictions. The CFD calculations regarding the original shrouded configuration with and without guided passive tip-injection as well as the cases without clearance together with the results are presented in paper 3.

In addition to the guided passive tip-injection, a further injection position was also taken into consideration. This case together with the original shrouded configuration were studied experimentally and numerically. Furthermore the impact of passive tip-injection on the specific stage work was considered analytically. This approach is capable of estimating the effect of injection on the rotor performance with respect to geometrical parameters and inflow conditions. In this regard off-design calculations can be carried out. The analytical approach together with the numerical and experimental results are content of paper 4 in this chapter.

For more clarity the LPT rotor studied in this chapter is described briefly below.

6.1. LPT Rotor

The LPT rotor considered in this thesis belongs to a test facility at the laboratory of the Institute for Thermal Turbomachinery and Machine Dynamics at Graz University of Technology. The test section of the facility consists of a high pressure (HP) vane, a transonic HPT rotor, a S-shaped turning mid turbine frame (TMTF) and a counter rotating shrouded LPT rotor, which is the focus of the investigations. Two compressor systems consisting of a compressor station and a brake compressor serve as air suppliers for the test facility. The brake compressor is driven by the HPT and the outflow is uncooled. The two mass flows are merged in a mixer as well as a tandem cascade at the inlet of a mixing chamber. This system was optimized in order to achieve

a quite homogenous mass flow and temperature at the inlet of the test section ([49]). By cooling the air coming from the compressor station it is possible to adjust the temperature at the stage inlet. Due to the presence of the brake compressor it is possible to provide an overall mass flow rate of up to $22 \frac{\text{kg}}{\text{s}}$. However, the inlet pressure is limited by the mixing chamber to 4.5 bar. In order to obtain higher pressure ratios a suction blower can reduce the pressure at the facility exit up to 200 mbar below the ambient pressure ([49]). The power of the LPT is absorbed by a water brake with a maximum power of 700 kW and a maximum rotational speed of 4500 rpm ([49]). More detailed information can be found in Hubinka [32].

In Fig. 6.1 the meridional plane of the test arrangement with corresponding measurement planes is depicted. For the current investigations only the LPT rotor section is of interest. The planes E, D and F serve for acquisition of test data.

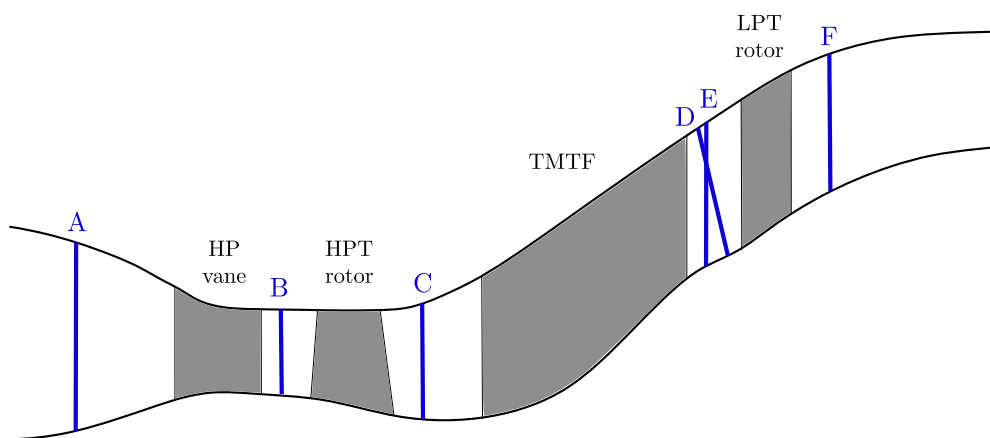


Figure 6.1.: Meridional Plane of the Test Arrangement

The LPT rotor consists of 72 shrouded blades. The shroud is provided with two labyrinth seals. The shroud cavity features small axial and radial gaps so that a high sealing efficiency can be expected. Further information about the operational conditions of the LPT are provided later in paper 3 and paper 4.

6.2. Application of Passive Tip-Injection

The initial idea of passive tip-injection out of the blade leading edge, as discussed in previous chapters, depends highly on the profile geometry. Small blade leading edge thickness allows for smaller injection channel diameters due to higher stress peaks at sharp edges. Furthermore high injection channel diameters would cause larger geometry degeneration in case of small leading edge thickness resulting in higher aerodynamic losses. As a fact the material removal for manufacturing the injection bore reduces the surface responsible for blade torque in the vicinity of the leading edge. In this spirit the injection channel diameter should be chosen with caution as a compromise between acceptable mechanical stress and aerodynamic losses as well as losses due

to the finite channel diameter.

Stress analysis regarding the initial idea of passive tip-injection extracted from the blade leading edge featured high stress peaks even at a bore diameter of 1 mm. The operation of the LPT would hence have been critical. Too small bore diameters on the other hand would increase the friction losses in the injection channel, which further reduce the injection mass flow rate and the injection effectiveness. Furthermore guided passive tip-injection with a groove in the first sealing fin presents a manufacturing challenge. Due to these reasons the initial type of passive tip-injection was not pursued by measurements. Nevertheless guided passive tip-injection was investigated numerically for better understanding of this type of injection in real applications. This case is further called leading edge injection and the corresponding results are presented in paper 3. Additionally two cases without clearance were also studied in paper 3. In the one case the blade tip ends directly at the casing. This case corresponds to a configuration without radial gap and is called clearance free. In the other case the configuration features no axial gaps. The shroud section attached to the blade tip rotates with the same speed as the blade. This case is referred to as clearance free with adjusted tip.

A further injection type, called through-shroud injection, was studied numerically and experimentally. In this case the injection channel passes directly through the shroud. The injection channel could be manufactured with reasonable effort in this case and the functionality was not limited by the mechanical stress due to the injection bore. A further advantage of this injection type was a larger channel diameter compared to the leading edge injection. Details about the position of the injection bore over the shroud together with the results are presented in the framework of paper 4 in this chapter.

6.3. Measurement Instrumentation

For each measurement the LPT was operated at constant reduced quantities in order to obtain the same operational point. The data were acquired in planes E and F with different measurement techniques. The measurements in plane E served as upstream flow condition and were basically applied to the CFD calculations as boundary conditions. These measurements were carried out using a pneumatic five-hole probe (FHP) being able to acquire time-mean flow variables, since such data were of interest concerning the steady-state CFD calculations. The FHP, which is also able to measure the temperature, was manufactured and calibrated at the Institut für Strahlantriebe und Turboarbeitsmaschinen at the Rheinisch Westfälische Technische Hochschule (RWTH) Aachen. For more information about the FHP refer to Arnold and Eifel [5] and Santner [49].

In plane F a single-hole fast response aerodynamic pressure probe (FRAPP) was applied, being able to measure the unsteady flow field downstream of the rotor at a high sampling rate. The geometrical as well as aerodynamic specifications of the FRAPP are presented in Gaetani [22]. The pressure sensor is mounted in a single hole on the aerodynamic section of the probe.

Despite the existence of a single hole only, a virtual three-hole reconstruction is carried out by of symmetrical probe rotation with respect to its axis. Static calibration is performed by means of three pressure readings at different yaw angles and Mach numbers. The readings are carried out at a step of 45° considered as the central pressure and the ones measured on the left and right angular stations symmetrically with respect to the central pressure. In this manner the calibration matrix is defined. More information about the calibration procedure can be found in Persico et al. [38] and Gaetani [22]. It should be noted that flow separation on the probe cylindrical head occurs at yaw angles of $68^\circ - 70^\circ$ as reported in [22]. For this reason the calibration measurements should be performed in a range of -22.5° to $+22.5^\circ$ taking into consideration the 45° -step. In order to guarantee that the yaw angle is within the calibrated range 3 or 5 rotations are performed for each measurement point.

The probe is insensitive to the pitch angle within a range which is not symmetrical with respect to zero due to the probe head. Standard errors including the static calibration uncertainty are also reported in [22] based on validation tests for various flow Mach numbers. Furthermore Schrempf [51] elaborates on calibration sensitivity of pneumatic three-hole probes to the pitch angle.

Due to the unsteady character of the flow in turbomachinery applications the dynamic behavior of measurement techniques for transient flow is of high importance. The transfer behavior of the FRAPP was tested in a low pressure shock tube with frequency dependent phase functions as well as amplitude functions. For more information about the dynamic calibration of the FRAPP see also Persico et al. [38, 39].

Acquiring measurement data downstream of the LPT rotor required appropriate positioning and traversing of the FRAPP. The radial traversing system was additionally able to rotate the probe with respect to its axis ensuring data acquisition in a virtual three-hole probe mode within the calibration range. Furthermore the probe was traversed with respect to the rotor axis by rotating the casing providing radial data acquisition at different circumferential positions.

The data were measured for several revolutions of the rotor at each measurement point. After the acquisition process a transfer function was applied to the raw pressure data to get the corrected time-resolved data. Subsequently the data set of each rotational position was phase-averaged to eliminate the stochastic fluctuations due to the turbulence. The calibration matrix was then applied to the transferred and phase-averaged data determining the yaw angle, Mach number, total and static pressure in an iterative procedure. See also [22] for more information about the probe application and the calibration matrix. After this procedure the results were time-averaged, which was necessary for comparison with the results of the steady-state CFD calculations.

6.4. CFD Procedure

In the framework of the investigations not only the reference geometry of the shrouded blade but also cases without tip clearance were taken into consideration in order to be able to examine the differences in the flow field and in the vicinity of the tip gap outlet. All calculations were carried out for a compressible flow in a rotating frame of reference. The realizable k/ϵ -model with enhanced wall treatment as well as the SST k/ω -model were applied to the calculations. However, the results of the realizable k/ϵ -model are only presented in paper 3 and paper 4 due to missing rotation-curvature correction of the SST k/ω -model in ANSYS Fluent 13.0 and the associated discrepancy as described in [52]. Nevertheless the results of the SST k/ω -model for the same quantities presented in paper 3 and paper 4 are provided later in the appendix of this thesis for the sake of completeness. According to [3] the realizable k/ϵ -model includes rotational effects. Due to the limitation of the realizable k/ϵ -model regarding non-physical production of turbulent viscosity in situations with rotating and stationary fluid zones (multiple reference frames), the entire domain was calculated in a single rotating frame of reference. The non-moving walls were provided with zero rotational speed. Furthermore the RSM model was not used despite its accuracy for 3D flows for following reasons:

1. Due to modeling of six components of the Reynolds stress tensor accurate and detailed flow conditions including turbulence have to be assigned to the inlet boundary, which were missing.
2. The RSM model consists of a large number of model constants requiring exact knowledge regarding their application. In this manner this model is suitable for verification of measurements and recalculation of a well-known flow field rather than for an a priori evaluation
3. The RSM model features high instability concerning convergence especially at higher discretization orders.
4. The RSM model requires high computational resources.

Further calculations regarding the influence of absolute or relative velocity formulation with the realizable k/ϵ -model were also carried out in the framework of the evaluations. This process was performed on the original shrouded design without tip-injection. These results together with the evaluation of the SST k/ω -model are presented later in paper 4.

It should also be mentioned that the second order upwind scheme was chosen for spatial discretization of all transport quantities except for pressure, which was interpolated using the standard scheme. Nevertheless comparative calculations using the second order interpolation scheme for the pressure resulted in a relative deviation of less than 0.03% for the calculated torque.

In order to guarantee convergence of the final solution the calculations were started for incompressible flow without the energy equation with a lower order of discretization (power law), which was then switched to the second order upwind (except for the pressure) ensuring higher accuracy. Furthermore the calculations were started with a lower rotational speed of the domain which was successively increased to the main rotational speed. After guaranteeing stable solution for incompressible flow the state equation of incompressible ideal gas was chosen, which calculates the density depending on the temperature only. In the last step ideal gas was chosen for calculating the final solution. The convergence was observed in addition to the residuals by calculating the mass-averaged total pressure and the mass-averaged absolute static pressure as well as the integral pressure of the entire blade.

Furthermore the material properties such as the specific heat, thermal conductivity and viscosity were assumed constant and were calculated as mean values based on the measurement data acquired by the FHP. The assumption of constant viscosity is justified by the fact that the eddy viscosity is by some orders of magnitude higher than the molecular viscosity. Verifications with the variable viscosity model of Sutherland showed a relative deviation of less than 0.02% in the calculated torque. Table 6.1 gives an overview of the material constants chosen for the CFD calculations.

Specific heat at constant pressure	$[\frac{\text{J}}{\text{kg K}}]$	1007.83
Thermal conductivity	$[\frac{\text{W}}{\text{m K}}]$	0.028082
Dynamic viscosity	$[\text{Pa s}]$	$1.9635 \cdot 10^{-5}$

Table 6.1.: Material Constants

Paper 3

P. Ghaffari, R. Willinger, S. Bauinger, A. Marn

Impact of Passive Tip-Injection on Tip-Leakage Flow in Axial Low Pressure Turbine Stage

ASME paper GT2015-42226
ASME Turbo Expo
Montreal, Canada, 2015

Proceedings of ASME Turbo Expo 2015: Turbine Technical Conference and Exposition
GT2015
June 15 - 19, 2015, Montreal, Canada

GT2015-42226

**IMPACT OF PASSIVE TIP-INJECTION ON TIP-LEAKAGE FLOW IN AXIAL LOW
PRESSURE TURBINE STAGE**

**Pouya Ghaffari
Reinhard Willinger**

Institute for Energy Systems and Thermodynamics
Vienna University of Technology
Getreidemarkt 9/302, A-1060 Vienna, Austria
pouya.ghaffari@tuwien.ac.at
reinhard.willinger@tuwien.ac.at

**Sabine Bauinger
Andreas Marn**

Institute for Thermal Turbomachinery
and Machine Dynamics
Graz University of Technology
Inffeldgasse 25A, A-8010 Graz, Austria
sabine.bauinger@tugraz.at
andreas.marn@tugraz.at

ABSTRACT

In addition to geometrical modifications of the blade tip for reducing tip-leakage mass flow rate the method of passive tip-injection serves as an aerodynamic resistance towards the tip-leakage flow. The impact of this method has been investigated thoroughly at unshrouded blades in linear cascades. Furthermore combinations of shrouded blades with passive tip-injection have been investigated analytically as well as via numerical simulations for incompressible flow in linear cascades. The objective of this paper is to consider a real uncooled low pressure turbine stage with shrouded blades and to investigate the effect of passive tip-injection on various operational characteristics. CFD calculations have been carried out in a rotational frame taking into consideration compressible flow and serve for evaluating the method of passive tip-injection in the given turbine stage. Experimental data obtained from the machine without tip-injection serve as boundary conditions for the CFD calculations.

NOMENCLATURE

c absolute velocity
 h specific enthalpy
 \dot{m} mass flow rate
 M_t torque

p pressure
 r radius
 r' dimensionless channel height
 R specific gas constant
 T temperature
 u circumferential velocity
 w relative velocity
 α absolute yaw angle
 η efficiency
 κ specific heat ratio
 θ circumferential angle
 ω angular velocity

Superscripts

— pitchwise averaged quantity
= mass flow averaged quantity

Subscripts

i injection
 s isentropic
 t total
 u circumferential component
 τ tip gap
1 rotor inlet
2 rotor outlet

Abbreviations

CFD	computational fluid dynamics
HPT	high pressure turbine
LPT	low pressure turbine
TMTF	turning mid turbine frame

INTRODUCTION

The modern technology of geared turbofan aims at increasing the rotational speed of the Low Pressure Turbine (LPT) driving the fan by decoupling of the two components by means of a gear box. Higher rotational speed of the LPT results in lower stage number and highly loaded blades. Basic characteristics of geared turbofans are presented in Kurzke [1]. In Malzacher et al. [2] the design of aeromechanically highly loaded LPT blades operating at high rotational speed is discussed.

High blade loads as well as a higher degree of reaction in the tip section of modern LPTs lead to higher tip-leakage losses (Hong and Groh [3]). Considering the tip-leakage mass flow rate responsible for dissipation mechanisms downstream of the blade row, its reduction results in higher stage efficiencies. A conventional method is given by blade shrouds with a number of sealing fins increasing the flow resistance.

The method of passive tip-injection in unshrouded turbine blades has been previously investigated experimentally as well as by means of CFD calculations. In Benoni and Willinger [4] experimental data regarding passive tip-injection with an angle of 90° as well as 45° against the tip-leakage flow are presented. The measurement data show a decrease in losses due to tip-injection. Further decrease is obvious in the case of inclined tip-injection with an angle of 45° . Moreover the strength of tip-leakage vortex is reduced by tip-injection, while this reduction is stronger in the case of inclined injection. In Benoni and Willinger [5] corresponding CFD results to the test rig are introduced. It is argued that the Realizable k/ϵ -model shows an advantage calculating flows with strong streamline curvature and vortices. In this paper the injection channel was modeled by an 1D analytical model taking into calculation various losses. The CFD calculations could prove a decrease in tip-leakage losses due to inclined tip-injection.

Regarding the effect of tip-injection in combination with sealing fins active injection over shrouded blades is discussed in Curtis et al. [6]. With the injection nozzle positioned at the casing wall it could be shown that tip-injection can reduce the tip-leakage mass flow rate. The overall mass flow rate at the tip gap exit depends however on the mass flow rate injected into the gap. It could be further shown that a maximum increase of 0.4% in turbine efficiency was achieved at an injection rate of approximately 1.2% of the main mass flow rate. Further a decrease of about 0.6% in turbine efficiency could be stated at the point of perfect

sealing at an injection rate of approximately 3.5% of the main mass flow rate. Similar results were obtained by Behr et al. [7] using active casing-air injection as well. It was shown that at an injection rate of 0.7% of the turbine mass flow rate the isentropic efficiency could increase by around 0.5%. They could further show that at an injection rate of 1% of the turbine mass flow rate the isentropic efficiency would decrease and even fall under the efficiency value of the case without injection depending on the tip clearance.

The effect of flow jet barriers in sealing applications is further studied in Hogg and Ruiz [8]. They investigated the impact of injection jet inclination on the tip-leakage mass flow rate as well as the overall mass flow rate at the tip gap outlet. It could be shown that an inclination of the injection jet could result in a decrease in tip-leakage as well as the overall tip gap mass flow rate at the outlet whereas the perpendicular injection resulted in an increase in the overall tip gap mass flow rate. Hogg and Ruiz [8] further investigated the effect of inclined injection in combination with labyrinth sealing fins numerically in a way that the middle fin of three labyrinth fins was inclined by 45° towards the tip-leakage flow direction. Furthermore the middle fin served as injection guidance. In this case it could be shown that higher reduction potential was obvious compared to the previous case using injection jet flow alone. They could achieve a reduction of around 25% in total tip-leakage mass flow rate which points out an enhancement by means of injection guidance.

In contrast to unshrouded blades with given profile pressure distribution in tip region many possible injection positions over the blade shroud are available. In Ghaffari and Willinger [9] analytical calculations supported by 2D CFD simulations show that guided injection upstream of the first sealing fin has the highest effectiveness.

Taking into consideration 3D tip gap flow over shrouded blades Ghaffari and Willinger [10] present CFD results of passive tip-injection in combination with fully as well as partially shrouded blades. It can be shown that highest effectiveness can be achieved in the case of full shroud provided with guided injection. It has to be mentioned that the CFD calculations were carried out for incompressible flow in a linear cascade without blade rotation.

In this paper a real LPT application is taken into consideration. Measurements carried out in a test rig without injection serve as boundary conditions as well as comparison between measurement and CFD calculations. In comparison to previous works the effect of compressibility and blade rotation on the passive tip-injection are investigated in this paper. Furthermore the injection channel was meshed and simulated as a part of the calculation domain.

LPT STAGE

The shrouded LPT rotor considered in this paper belongs to a test rig consisting of a transonic high pressure turbine (HPT) and a counter rotating LPT connected by the Turning Mid Turbine Frame (TMTF). The LPT rotor is driven at a lower speed compared to the HPT and has a larger mean radius as usual in real engine configurations (Santner [11]). The flow leaves the test section through a duct with support struts and a diffuser recovering part of outlet pressure before entering into the exhaust casing. For absorption of the LPT power a waterbrake is used. In Fig. 1 the LPT as well as the TMTF upstream of the LPT are presented in a meridional cut. The TMTF further turns the flow and provides the LPT with swirled flow.

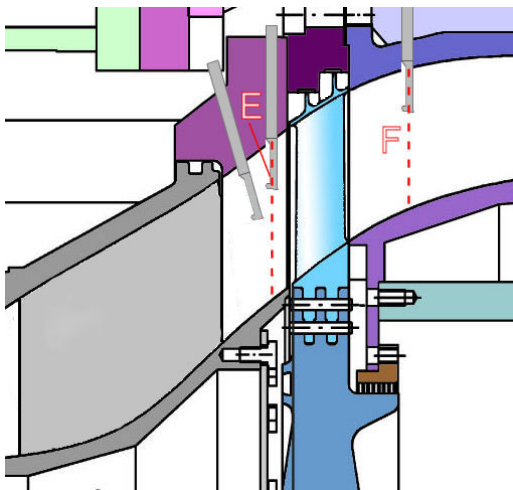


FIGURE 1: MERIDIONAL CUT OF LPT AND TMTF

The measurement planes are also depicted. Plane E serves as inlet and the measurement data as boundary condition for the CFD calculations. Plane E is positioned at a distance of 59% axial chord length upstream of the blade leading edge. Plane F is positioned at a distance of 77% axial chord length downstream of the blade trailing edge. The LPT outlet at a distance of 6 times the axial chord length serves as the boundary outlet for the CFD calculations. The operating conditions of the LPT are summarised in Tab. 1. The values are all mean values of the tests performed.

TABLE 1: OPERATION DATA OF LPT.

Reduced inlet mass flow [$\frac{kg\sqrt{K}}{s\ bar}$]	214.6
Mechanical speed [$\frac{1}{min}$]	3549.3
Reduced speed [$\frac{1}{min\sqrt{K}}$]	194.0
Stage total pressure ratio [-]	1.3

Measurement System

All measurements were carried out with a 5-hole probe manufactured and calibrated at the Institute of Jet Propulsion and Turbomachinery, RWTH Aachen. The probe has a hemispherical head with a diameter of 2.5 mm and a shaft diameter of 7 mm. Due to the strong slope of the duct in both planes E and F, which are mainly considered in this paper, a probe with an inclined head of 115° relative to the probe shaft axis was used. In order to perform traverses in circumferential direction the probe was mounted on the rotatable outer casing of the LPT while the radial measurement positions were realized using a traverse gear rotating the probe around the shaft axis of the probe and positioning it in radial direction. The measurement system includes 15 multi-channel pressure transducers PSI 9016 with a total amount of 240 channels and an accuracy of 0.05% full scale, four Field Point FP-TC-120 eight-channel thermocouple input modules of National Instruments and one FP-RTD-122 resistance thermometer input module. Tab. 2 presents the measurement uncertainties of the five-hole probe measurements in a confidence interval of 95%.

The measurements were carried out for 23 radial and 45 angular positions in plane E and 21 radial and 45 angular positions in plane F with an angular increment of 0.5°.

TABLE 2: MEASUREMENT UNCERTAINTIES.

Mach number [-]	-0.004	0.005
Yaw angle α [°]	-0.3	0.3
Pitch angle γ [°]	-0.4	0.5
Total pressure p_t [bar]	$-3 \cdot 10^{-3}$	$3 \cdot 10^{-3}$
Static pressure p [bar]	$-5.1 \cdot 10^{-3}$	$5.4 \cdot 10^{-3}$
Total temperature T_t [K]	-0.5	0.6
Static temperature T [K]	-0.8	0.7

METHOD OF PASSIVE TIP-INJECTION

The idea behind passive tip-injection is to extract a small amount of the stage mass flow rate and to inject it into the tip clearance over the blade shroud in order to produce more

blockage and to reduce the overall tip-leakage mass flow rate. In this spirit the injection inlet is positioned at the blade leading edge with high level of total pressure and besides appropriate flow conditions. The injection flow is then turned by a perpendicular bore realizing tip-injection perpendicular to the tip-leakage flow. Further an inclined injection could be considered provided that manufacturing possibilities are given. At first sight it might seem paradoxical that the method of passive tip-injection would enhance the stage efficiency, since a part of the stage mass flow is transported from a smaller to a higher radius acting as a compressor. In this case the stage efficiency would deteriorate taking into account that a part of the overall tip-leakage mass flow rate leaving at the tip gap outlet detracts specific work from the stage work. Provided that the overall tip-leakage mass flow rate remains unchanged in the case without tip-injection it would leave the tip gap with zero specific work. Following analytical considerations will however show that depending on operational parameters of passive tip-injection two different cases result. For this reason the equation of momentum is taken into consideration for the tip-injection with flow angles given at the injection inlet and outlet. For reasons of clarity velocity triangles are depicted schematically in Fig. 2.

$$a_{ui} = u_{\tau}c_{u\tau} - u_i c_{ui}. \quad (1)$$

Considering the injection case with an injection angle of 90° with respect to the tip-leakage flow one obtains

$$c_{ui} = w_{ui} + r_i \omega, \quad (2)$$

$$c_{u\tau} = r_{\tau} \omega \quad (3)$$

and further

$$a_{ui} = r_{\tau}^2 \omega^2 - (r_i^2 \omega^2 + r_i \omega w_{ui}) \quad (4)$$

$$= r_i^2 \omega^2 \left[\left(\frac{r_{\tau}}{r_i} \right)^2 - \left(1 + \frac{w_{ui}}{r_i \omega} \right) \right]. \quad (5)$$

Taking into consideration that positive a_{ui} would detract specific work while negative a_{ui} contributes to stage work one can clearly recognise the operation point at which the situation would reverse. The point corresponding to negative a_{ui} is

$$\left(\frac{r_{\tau}}{r_i} \right)^2 < \left(1 + \frac{w_{ui}}{r_i \omega} \right). \quad (6)$$

One can clearly see that higher injection inlet radii and values of the circumferential component of the relative inlet velocity

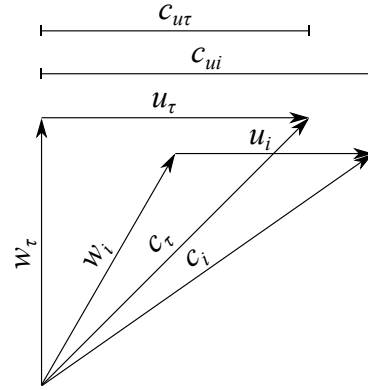


FIGURE 2: VELOCITY TRIANGLES DESCRIBING THE INJECTION FLOW SCHEMATICALLY

as well as lower rotational speed both allow for a negative a_{ui} . Furthermore it has to be mentioned that the velocity distribution directly at the injection outlet is responsible for relative velocity $w_{u\tau}$ which was assumed equal to zero in current considerations. In this spirit changes in inflow angle would influence the performance of passive tip-injection and have to be considered more closely.

CFD CALCULATIONS

For CFD calculations the original geometry was adjusted in order to obtain higher mesh quality. The manufacturing radii were eliminated since they reduce the mesh quality in their vicinity. In Fig. 3 the shrouded geometry used for the CFD calculations is depicted. In order to evaluate the shrouded geometry in comparison to the case without tip clearance the shroud was eliminated in a way that the tip section runs congruently with the bottom side of the shroud. Additionally two variations were taken into consideration. In the first case the rotating blade tip ends directly at the casing brushing past the end wall. In the second case the blade rotates with its associated casing section as in the shrouded case without axial gap. For reasons of simplicity this case is further called clearance free with adjusted tip.

The shrouded geometry was subsequently provided with injection bores in a way that guided passive injection upstream of the first sealing fin was ensured. Due to the fact that the blade is twisted the radius of the injection inlet was chosen in such a way as to avoid adverse wall thickness. On the other hand it has to be taken into consideration that high level of total pressure is necessary at the injection inlet and thus the positioning within the boundary layer underneath the blade

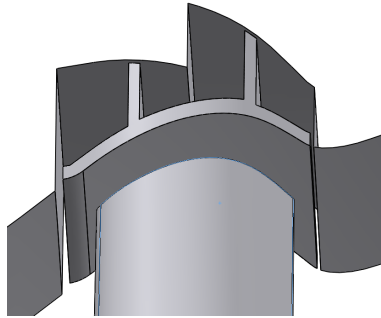


FIGURE 3: SHROUDED GEOMETRY USED FOR CFD CALCULATIONS

shroud should be avoided. Both considerations led to a position of 13.5 mm radius difference between the shroud bottom surface and injection inlet centre. The direction of the injection channel was chosen in accordance with the circumferential inlet flow angle at the corresponding radius. In compliance with previous works the centre of the injection outlet was positioned in a way that a groove emerged in the first sealing fin acting as injection guidance.

In this manner the outlet bore was centred at an axial distance of 0.2 mm from the edge of the sealing fin against the axial direction. Fig. 4 shows the geometrical proportions of the injection bores considered in this paper. It has to be mentioned that the choice of the injection channel diameter must be a compromise between flow losses in the injection channel and the modification of the leading edge of the blade affecting the profile pressure distribution but also the manufacturing capability. Too small channel diameters would result in high friction losses in a way that the passive injection would lose its effectiveness. Large diameters however would affect the aerodynamic of the blade in the vicinity of the injection inlet so that the positive effect of passive injection is counteracted by unfavourable flow conditions. As a compromise a diameter of 2 mm was chosen for the investigations.

In this spirit four geometrical cases were calculated: Clearance free, clearance free with adjusted tip, shrouded and shrouded with injection.

Computational Mesh

The computational domain was meshed via block structures in ICEM 14.5. The generated mesh features high quality regarding the determinant as well as skewness of the elements. The mesh was refined in the vicinity of the walls in order to

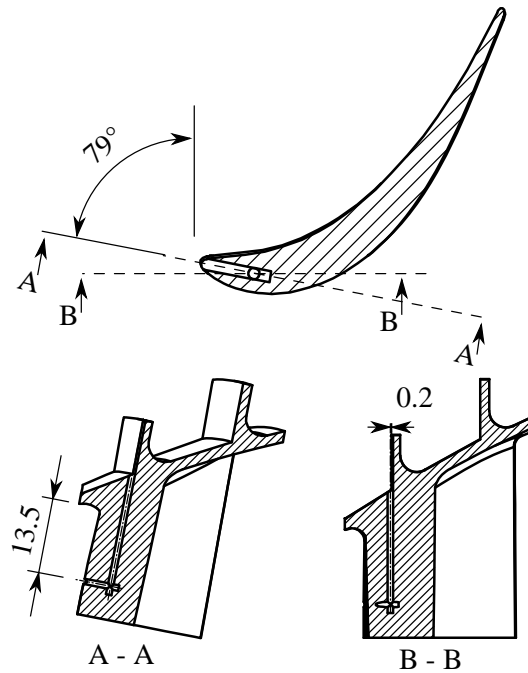


FIGURE 4: MAIN GEOMETRICAL PROPORTIONS OF SHROUDED BLADE WITH PASSIVE TIP-INJECTION

achieve a high wall resolution with $y^+ < 1$. The injection channel was meshed properly based on previous investigations taking into consideration the injection channel only. In Fig. 5 the details of the generated mesh are depicted in the region of the blade tip as well as injection inlet and outlet. The tip region features 30 cells over the first fin and 36 cells over the second fin. In Tab. 3 the cell number of the investigated cases are presented. One can recognise increasing number of cells in the computational domain with increasing complexity. Mesh study was carried out for every case calculated in this paper and independence of the CFD results was ensured.

TABLE 3: CELL NUMBER OF THE INVESTIGATED CASES.

Cases without tip clearance	4.4 million
Case with blade shroud	9.6 million
Cases with blade shroud and injection	18.0 million

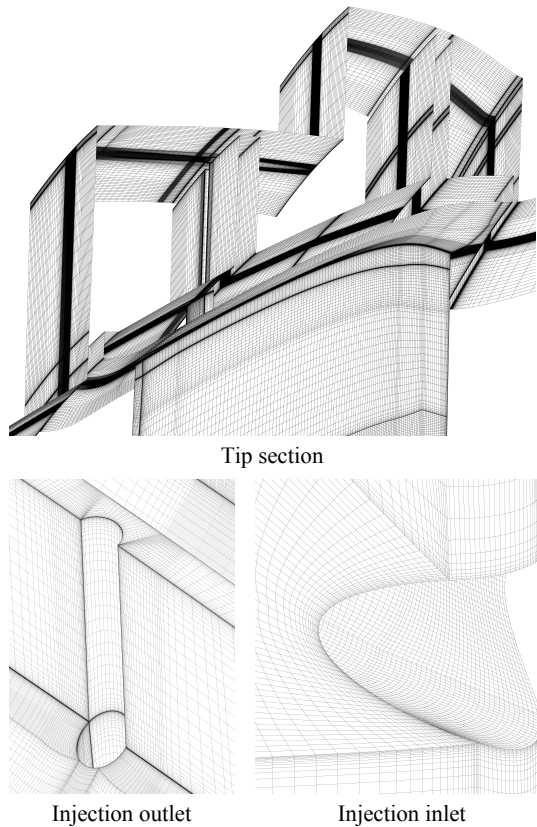


FIGURE 5: DETAILS OF THE GENERATED MESH

Boundary Conditions

The CFD calculations were carried out using Fluent 13 with finite volume method for solving the discretized governing equations.

The calculations were carried out in a rotating frame with corresponding rotational speed. The compressible flow was calculated using ideal gas law. Realizable k/ϵ -model with enhanced wall treatment was set up for the turbulence modeling to achieve high wall resolution of the boundary layers. This turbulence model and its reliability for tip-leakage as well as injection flow has been investigated in previous work ([5]).

In Tab. 4 the quantities necessary for the CFD calculations are presented. The turbulent intensity of the flow at the inlet was assumed whereas the turbulent length scale was calculated by means of the hydraulic diameter of the inlet.

Since no large temperature changes were obvious from the

measurement data the physical properties of the air such as specific heat capacity, thermal conductivity and viscosity were assumed constant and calculated at an average domain temperature. As boundary condition pressure inlet was taken for the inlet and pressure outlet for the outlet since velocity inlet boundary condition would cause unphysical results in the case of compressible flow calculations. Since the TMTF upstream of the LPT features a vane number of 16 in comparison to the LPT investigated with 72 blades deviating periodicity results for both components. Due to the fact that the cell number is high for the shrouded case with tip-injection only one flow passage of the LPT was simulated in the frame work of this paper. For this reason the measurement data in plane E were averaged in circumferential direction in 23 radial positions. As usual for compressible flow calculations with pressure inlet as boundary condition total pressure p_t and temperature T_t were applied. Furthermore the flow direction had to be specified at the pressure inlet. For this reason the flow direction was calculated from the velocity and assigned. Since it was unclear if the resulting flow at the pressure outlet would be completely swirl free, radial equilibrium pressure distribution was set up for all calculations. Periodic boundaries were also assigned with 5° with respect to the axis of rotation.

TABLE 4: NUMERICAL SETUP.

Turbulent intensity [%]	5
Turbulent length scale [m]	0.0063
Rotational domain speed [1/s]	59.2
Operating pressure [Pa]	95000

Further it has to be mentioned that second order discretisation was set up for all transport quantities.

Since starting the calculations immediately with compressible setups would cause convergence problems all cases were calculated with incompressible setups in order to obtain stable calculations which were then switched to compressible ones.

Mass flow averaged total and static pressure at the outlet as well as the integral pressure distribution of the blade were evaluated during the iterations in order to ensure convergence of the calculations.

Results

In Fig. 6 the streamlines of the injection path are depicted. As one can clearly see the shroud fin serves as a guidance for the injection mass flow. Further it is clear that part of the injection mass flow swirls in the vicinity of the injection outlet while the other part flows through the tip gap over the first fin. Taking into consideration different directions of the chamber

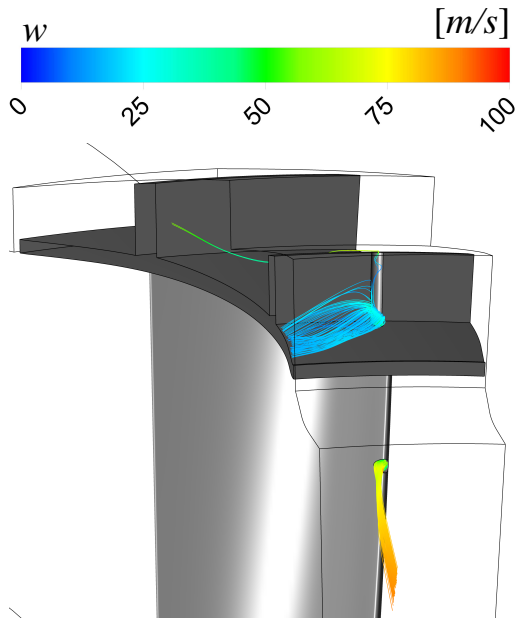


FIGURE 6: STREAMLINES OF THE INJECTION PATH.

swirl and the swirl induced by the injection, it is obvious that the passive injection reinforces the blockage effect. Furthermore the streamlines at the injection outlet feature a tendency opposite to the rotational direction which affects the performance of passive tip-injection positively (see Eqn. 1).

In order to show the blockage effect of passive tip-injection more clearly the 2D streamlines are depicted in Fig. 7 at a cross sectional plane through the bore centre of the injection outlet. In comparison to the shrouded case the injection flow crowds out the tip-leakage mass flow by disposing the vortex in the labyrinth chamber. The impact of passive tip-injection on the reduction of the tip-leakage mass flow rate will become clear later.

For the sake of completeness the pressure distribution in the injection channel is depicted in Fig. 8. As one can clearly see higher pressure on the top side of the channel inlet is visible. This appearance is due to the fact that the incoming flow features radial components. Due to manufacturing simplicity the injection channel inlet was solely oriented with respect to the circumferential direction of the inlet flow. This causes flow separation on the bottom side of the injection inlet surface. This fact is evident considering the pressure distribution pointing out flow stagnation on the inlet top surface.

In order to evaluate the simulated cases the isentropic stage efficiency (rotor only) was calculated. For this reason mass

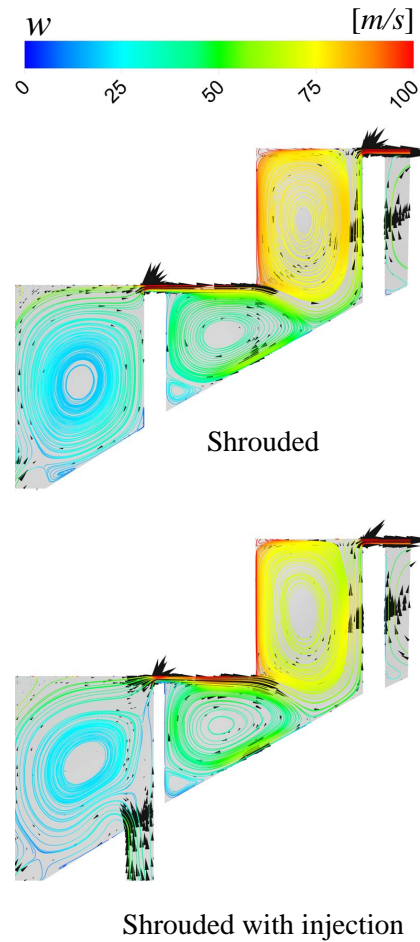


FIGURE 7: 2D STREAMLINES AT INJECTION OUTLET.

flow averaged quantities were taken into calculations. Under assumption of constant specific heat ratio κ as well as specific gas constant R one obtains following equation for isentropic enthalpy change with given state variables mass flow averaged at the inlet as well as at the outlet:

$$\Delta h_s = \frac{\kappa}{\kappa - 1} R \bar{T}_1 \left[\left(\frac{\bar{p}_1}{\bar{p}_2} \right)^{\frac{\kappa-1}{\kappa}} - 1 \right]. \quad (7)$$

Taking into consideration the change in specific kinetic energy the isentropic efficiency is calculated as followed by means of

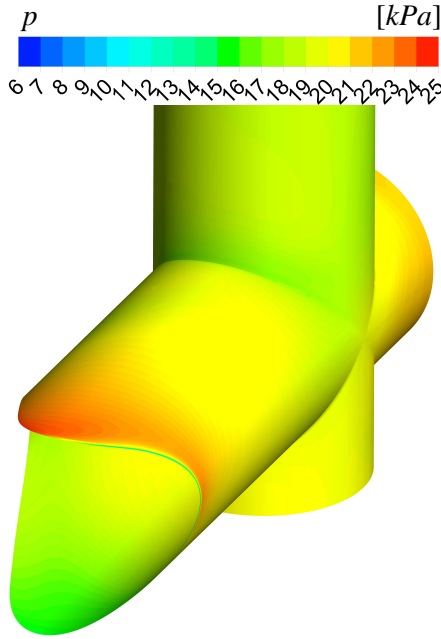


FIGURE 8: STATIC PRESSURE DISTRIBUTION ON THE INJECTION CHANNEL WALL

total quantities at plane E and F:

$$\eta_s = \frac{\bar{h}_{t1} - \bar{h}_{t2}}{\Delta h_s + \frac{1}{2} (\bar{c}_1^2 - \bar{c}_2^2)}. \quad (8)$$

Additionally the overall torque affecting all rotating parts was calculated in post processing procedure. It has to be mentioned that in the case of passive tip-injection the resulting torque affecting the injection channel accounts for 0.09% of the overall torque and thus for 0.09% of the stage power. Compared to the tip-leakage mass flow dissipating without participating on stage power an improvement can be achieved by passive tip-injection. For the investigated stage with given rotational speed and blade number the passive tip-injection accounts for approximately 0.31 kW. The results regarding the isentropic stage efficiency as well as the resulting torque are presented in Tab. 5.

As one can clearly see the highest isentropic efficiency is achieved in the case without tip clearance though with adjusted tip. However it has to be mentioned that the rotational casing section acts as additional rotating surface with friction forces. Taking into consideration that the pressure distribution does not

TABLE 5: η_s AND M_t OF INVESTIGATED CASES.

Cases	η_s [%]	M_t [Nm]
Clearance free	94.0	12.772
Clearance free with adjusted tip	94.2	12.773
Shrouded	93.5	12.705
Shrouded with injection	93.7	12.721

have any impact on the resulting torque the shear forces reduce the resulting torque as clear from the data. Furthermore it can be seen that both the resulting torque and the isentropic efficiency increase by means of passive tip-injection. For reasons of completeness the tip-leakage mass flow rate was evaluated from the CFD results of the cases with shrouded blade with and without passive tip-injection. It has to be mentioned that the tip-leakage mass flow rate was calculated at the tip gap inlet separately from the injection mass flow rate. The corresponding results are depicted in Tab. 6.

TABLE 6: TIP-LEAKAGE AND INJECTION MASS FLOW RATE

Cases	\dot{m}_τ [kg/s]	\dot{m}_i [kg/s]
Shrouded	$1.35 \cdot 10^{-3}$	-
Shrouded with injection	$1.20 \cdot 10^{-3}$	$1.43 \cdot 10^{-4}$

Although the mass flow rate at the tip gap outlet as overall mass flow rate remains approximately constant passive tip-injection contributes to a reduction of tip-leakage mass flow rate at the tip gap inlet by 11%. The positive effect of passive tip-injection is due to the fact that the injection mass flow follows a different path. While the tip-leakage flow does not participate on the specific stage work the injection flow conducts specific work. In order to analyse the flow in every investigated case the pitchwise averaged flow angle $\bar{\alpha}_2$ with respect to the direction of rotation was evaluated at plane F in 21 different radial positions. The coordinate was made dimensionless by means of the overall radial channel gap at plane F so that $r' = 0$ corresponds to the hub and $r' = 1$ corresponds to the casing. The results are depicted in Fig. 9. Taking into consideration the direction of rotation of the rotor angles smaller than 90° relate to circumferential components contrary to the rotational direction while an angle of 90° corresponds to swirl free flow.

Since the measurement data refer to a shrouded blade geometry good accordance between measurement and CFD results is obvious compared to the simulated shrouded case. The outlet flow angle features likewise tendency in both cases apart from a small offset.

Furthermore one recognises deviations of the flow angle in the

vicinity of the blade tip comparing the various cases simulated. In both cases without tip clearance $\bar{\alpha}_2$ features lower values near the casing. However $\bar{\alpha}_2$ is lower in this region in the case without adjusted tip. Moreover the flow angle in hub region remains unchanged in every investigated case as expected.

Regarding tip-leakage losses the pitchwise averaged total temperature \bar{T}_t at plane F is depicted in Fig. 10. Since higher total temperature is a sign for less specific work it is an indicator for the performance of the stage.

One can clearly see the regions of higher total temperature in the vicinity of the casing in the case with blade shroud. In contrast the total temperature is lower in this region in the cases without tip clearance and even lower in the case of adjusted tip. Furthermore likewise tendency in the CFD results as well as the measurement data is obvious. However deviations between measurement and CFD are apparent in the results. Maximum total temperature differences of around 4 K are evident in the middle of the channel. The reason for this discrepancy is due to the averaging of the measurement data at the boundary inlet. As the number of the vanes of the TMTF differ significantly from the blade number of the LPT disturbances of large scale are transmitted through out the LPT stage to plane F causing dissipation but also nonuniform flow field over an angle of greater than 5°. These disturbances are not visible in CFD results due to circumferential averaging in plane E over an angle of 22.5° corresponding to two flow passages of the TMTF. In order to be consistent the measurement data were also averaged in circumferential direction over an angle of 22.5° in plane F. Higher total temperatures corresponding to higher dissipation are hence apparent in the measurement results. Furthermore one can recognise a more uniform temperature distribution of the measurement data in the middle of the channel in comparison to the CFD results. This could be due to higher radial mixing in the real application. The extent of mixing processes could also be affected by the turbulence modeling chosen.

For more clarity two measured not averaged temperature curves in radial direction with an angular increment of 10° are depicted in Fig. 11. Although the angular increment corresponds to exactly two passages deviating results are apparent due to the flow disturbances upstream of the rotor.

Since the flow field downstream of a stage affects the inlet flow conditions of the subsequent stage it is important to take into consideration the influence of different tip geometries as well as the passive tip-injection on the downstream flow field. The effect of passive tip-injection is dominant in the vicinity of the tip gap outlet, which is not obvious in Fig. 9 due to the fact that the averaged flow angle $\bar{\alpha}_2$ is depicted over the entire channel height. For this reason contour plots of yaw angle α_2 at plane F are depicted in Fig. 12 however in the vicinity of the casing. Also velocity vectors are presented. Because of the limitations caused by the geometrical dimensions of the probe on the one hand but also the error susceptibility in the boundary layer on

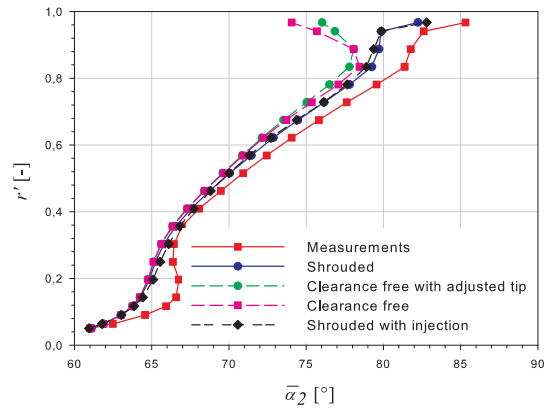


FIGURE 9: $\bar{\alpha}_2$ AT PLANE F

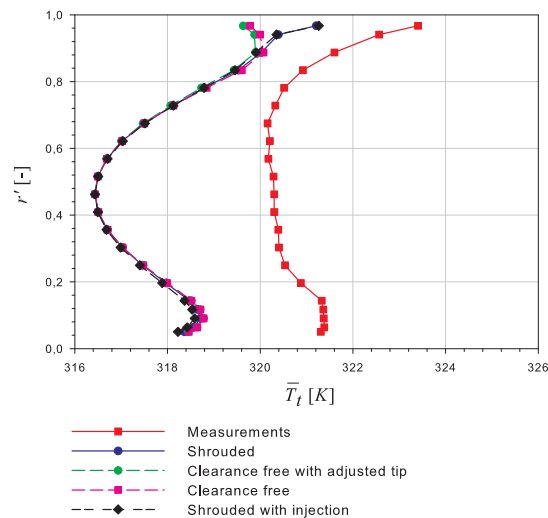


FIGURE 10: \bar{T}_t AT PLANE F

the other hand the measurement data were acquired up to a dimensionless channel height of 0.97. The region at the tip gap outlet in the vicinity of the casing is however relevant regarding investigations of flow structures and details comparing different

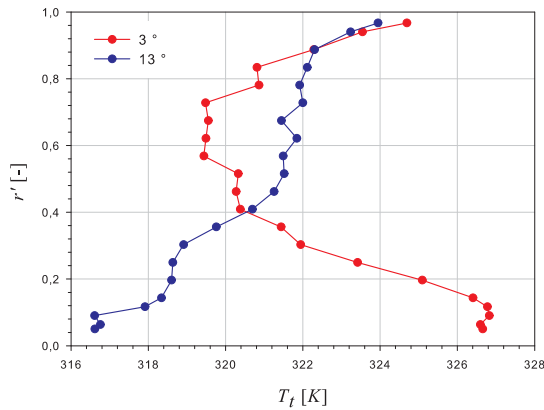


FIGURE 11: T_t AT PLANE F

blade tip geometries. Since no measurement data were acquired in the immediate vicinity of the casing only CFD results are depicted.

One can recognise regions of higher α_2 in the vicinity of the tip gap of the shrouded case. Reversal of velocity vectors is present in this region. This appearance is not clear from Fig.9 since the measurement data do not comprise regions close to the casing. Similar results are present in the case of shrouded blade with passive tip-injection however to a lower extent which means the flow field seems more uniform close to the casing which has an improved effect regarding flow condition of the downstream stage. In comparison both cases without tip-clearance do not feature a reversal of the velocity vectors close to the casing and the flow field is more uniform.

CONCLUSIONS

The objective of this paper was to evaluate the effect of passive tip-injection on tip-leakage mass flow rate in combination with blade shrouds. Previous investigations have already been carried out on unshrouded blades. Preliminary considerations regarding passive tip-injection with shrouded blades have also been carried out by means of analytical calculations as well as 2D CFD simulations and 3D simulations in linear cascades. In contrast to unshrouded blades more possibilities are given regarding positioning of the injection outlet. In this paper a real LPT geometry was investigated with various tip geometries at which the shrouded geometry was additionally provided by an injection channel connecting the blade leading edge with a high level of total pressure with the

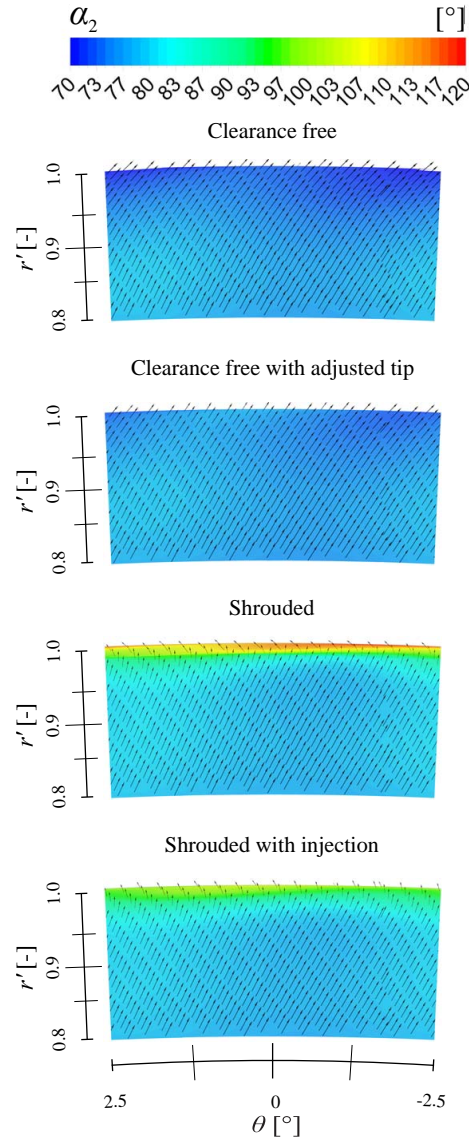


FIGURE 12: YAW ANGLE α_2 AT PLANE F

shroud tip. Furthermore the first sealing fin was used as guidance for the tip-injection. According to previous investigations guided tip-injection proved to be most effective. It has to be mentioned that the design parameters of the injection channel depend on

many factors affecting on the one hand the aerodynamic of the blade and on the other hand the losses in the channel. Changes in profile pressure distribution in the vicinity of the injection inlet degrading the blade aerodynamic have to be compensated by the effect of decreasing the tip-leakage mass flow rate improving the stage efficiency. The main goal of the considerations is hence to achieve high isentropic stage efficiencies at high specific stage work.

The CFD calculations were carried out for compressible flow in a rotational frame of reference. Experimental data at the inlet were applied as boundary condition for the CFD calculations. It could be shown that small changes of the blade tip influence the flow condition downstream of the stage considerably. As a result deviations in absolute flow angle were obvious. The highest isentropic efficiency could be achieved in the case of blade geometry without tip clearance with adjusted tip in which the corresponding section of the casing rotates with the blade. Nevertheless no great changes were obvious in the resulting torque since the additional rotating section causes friction forces operating contrary to the rotational direction.

It could also be shown that passive tip-injection has the potential to decrease the tip-leakage mass flow rate at the tip gap inlet. Even if the overall mass flow rate at the tip gap outlet remains almost constant it could be reasoned that the injection flow contributes to the specific work of the stage contrary to the tip gap flow as it causes positive torque in the rotational direction. Moreover it could be shown that the outlet flow condition in the vicinity of the tip gap was enhanced by means of passive tip-injection. This issue is important regarding flow condition of the downstream stage.

Future investigations could include various LPT blade geometries with higher blade leading edge radius making larger injection bores possible. Moreover the orientation of the channel inlet could be revised and adjusted. In order to verify the CFD results experiments could be carried out regarding blade shrouds with passive tip-injection. Also various positions of the injection inlet could be taken into consideration. One of possibilities would be positioning of the injection inlet on the bottom side of the blade shroud. Therefore higher injection inlet radii could be realized affecting the performance positively. Further investigations could take into consideration the impact of various inlet flow angles upstream of the rotor on the performance of passive tip-injection.

In addition real partial shroud geometries could be provided by passive injection channels and investigated regarding compensating the negative effect of shroud reduction by the method of passive tip-injection. In this manner the overall weight of the stage could be reduced with no or little change in stage efficiency.

ACKNOWLEDGEMENTS

The authors would like to acknowledge the Austrian Research Promotion Agency FFG for supporting the project in the framework of the Aeronautics Research and Technology Programme TAKE OFF.

References

- [1] Kurzke, J., 2009. "Fundamental Differences between Conventional and Geared Turbofans". ASME Paper GT2009-59745.
- [2] Malzacher, F. J., Gier, J., and Lippl, F., 2006. "Aerodesing and Testing of an Aeromechanically Highly Loaded LP Turbine". *Journal of Turbomachinery*, **128**, October, pp. 643–649.
- [3] Hong, Y. S., and Groh, F. G., 1966. "Axial Turbine Loss Analysis and Efficiency Prediction Method". *Boeing Report D4-320*.
- [4] Benoni, A., and Willinger, R., 2013. "Design modification of a passive tip-leakage control method for axial turbines: Linear cascade wind tunnel results". ASME Paper TBTS2013-2056.
- [5] Benoni, A., and Willinger, R., 2012. "Numerical Simulation of Passive Tip-Leakage Flow Control Method for Axial Turbines". In ECCOMAS 2012. Paper No. 5429.
- [6] Curtis, E. M., Denton, J. D., Longley, J. P., and Rosic, B., 2009. "Controlling Tip Leakage Flow over a Shrouded Turbine Rotor Using an Air-Curtain". ASME Paper GT2009-59411.
- [7] Behr, T., Kalfas, A. J., and Abhari, R. S., 2008. "Desensitization of the flowfield from rotor tip-gap height by casing-air injection". Vol. 24. JOURNAL OF PROPULSION AND POWER.
- [8] Hogg, S. I., and Ruiz, I. G., 2011. "Fluidic Jet Barriers for Sealing Applications". ASME Paper GT2011-45353.
- [9] Ghaffari, P., and Willinger, R., 2013. "Impact of passive tip-injection on the performance of partially shrouded turbines: Basic concept and preliminary results". ASME Paper TBTS2013-2038.
- [10] Ghaffari, P., and Willinger, R. "Preliminary investigation of passive tip-injection in a linear turbine cascade with shrouded blades". Submitted to 11th European Turbomachinery Conference, March 23 - 27, 2015, Madrid, Spain.
- [11] Santner, C., 2008. "Experimental investigation of turning mid turbine frame designs". PhD thesis, Graz University of Technology.

Paper 4

P. Ghaffari and R. Willinger

On the Impact of Passive Tip-Injection on the Downstream Flow
Field of a Shrouded LP-Turbine: CFD and Experimental Results

ASME paper GT2016-56196
ASME Turbo Expo
Seoul, South Korea, 2016

GT2016-56196

ON THE IMPACT OF PASSIVE TIP-INJECTION ON THE DOWNSTREAM FLOW FIELD OF A SHROUDED LP-TURBINE: CFD AND EXPERIMENTAL RESULTS

Pouya Ghaffari and Reinhard Willinger
 Institute for Energy Systems and Thermodynamics
 Technische Universität Wien
 Getreidemarkt 9/302, A-1060 Vienna, Austria
 pouya.ghaffari@tuwien.ac.at
 reinhard.willinger@tuwien.ac.at

ABSTRACT

Using shrouded blades with fins is a common method to reduce the leakage mass flow rate through the clearance between rotor and stator. A variety of methods have been developed improving the discharge behaviour of this sealing application. The leakage mass flow rate and its interaction with the main flow resulting in mixing losses and deviations in turning is also an important issue and has to be taken into consideration. The objective of this paper is to present a method aiming at reduction of tip-leakage mass flow rate and its high angular momentum by means of passive tip-injection. The results include analytical study followed by CFD calculations for compressible flow in a rotational frame of reference as well as experimental data. An uncooled low pressure air turbine with shrouded blades is considered for the CFD and the measurements. Three passive tip-injection configurations are investigated numerically out of which one configuration is also examined experimentally in the framework of this study.

NOMENCLATURE

a_u	specific circumferential stage work	[J / kg]
A	area	[m ²]
c	chord length	[m]
C	absolute velocity	[m / s]
C_D	inlet discharge coefficient	[-]
C_D^+	outlet discharge coefficient	[-]

\dot{m}	mass flow rate	[kg / s]
Ma	Mach number	[-]
p	pressure	[Pa]
r	radius	[m]
s	spacing	[m]
s	specific entropy	[J / kg K]
T	temperature	[K]
w	axial velocity (tip clearance section)	[m / s]
α	absolute flow angle measured from positive circumferential direction	[°]
α'	absolute flow angle based on exit main flow axial velocity measured from positive circumferential direction	[°]
γ	dimensionless injection channel width	[-]
γ_s	stagger angle	[°]
δ	inclination angle	[°]
η	hub to tip radius ratio	[-]
θ	dimensionless injection velocity	[-]
ρ	density	[kg / m ³]
ϕ	flow coefficient	[-]
ψ	loading coefficient	[-]
σ	contraction ratio	[-]
ω	angular velocity	[rad / s]

Superscripts

$\tilde{}$	mixed out quantity
$+$	flow angle measured from positive circumferential direction

— pitchwise averaged quantity
 ^ dimensionless

Subscripts

c casing
h hub
i injection
id ideal
m mean value
t total
u circumferential component
 τ tip clearance section
 1 inlet
 2 outlet

Abbreviations

AVF absolute velocity formulation
 CFD computational fluid dynamics
 FRAPP Fast Response Aerodynamic Pressure Probe
 LPT low pressure turbine
 RKE Realizable k/ϵ
 RVF relative velocity formulation
 SST Shear Stress Transport
 TMTF turning mid turbine frame

INTRODUCTION

In general tip-leakage reduces the mass flow through the blade passages contributing to stage work. It further contributes to mixing losses downstream of the rotor. The re-entry of the tip-leakage flow with deviating meridional as well as circumferential velocity affects the flow field in the vicinity of the casing of a rotor. It also affects the downstream stator and the associated secondary flow. Many geometrical shroud configurations aim at reduction of tip-leakage mass flow rate. Improvement of re-entry conditions of leakage flow by means of geometrical modifications has also been investigated in the past.

In Denton [1] various loss mechanisms in turbomachinery including tip-leakage losses in the case of shrouded blades are described and investigated analytically. It is stated that the entropy generation due to mixing losses caused by tip-leakage flow is primarily associated with the mixing process between the leakage flow and the main flow downstream of the blade row. It is further stated that the swirl velocity of the leakage flow is retained throughout the shroud clearance.

Anker and Mayer [2] and Giboni et al. [3] investigated the interaction of labyrinth seal flow and main flow in a 1.5 stage axial turbine numerically and experimentally. The results in [2] show that higher clearance results in a negative incidence of greater magnitude in the vicinity of the casing of the following stator. In [3] an increase in the strength of the leakage jet could be ob-

served towards the suction side, where it enters the main flow with high radial components, separating at the casing edge and forming a large zone of recirculation. The circumferential flow unsteadiness due to the leakage flow affects the stator incidence angle as well as the size and position of its casing side passage vortex.

Rosic and Denton [4] investigated the effect of turning the leakage flow into the axial direction on the downstream flow field experimentally. A low speed three stage air turbine with low aspect ratio blading was used for this study. Three turning vane configurations consisting of two, four and eight turning vanes per rotor blade pitch respectively were mounted into the downstream shroud exit cavity and studied in the framework of the investigations. It could be shown that the distribution of the absolute exit flow angle was increasingly improved with increasing the vane number in the vicinity of the casing but also towards the midspan. Furthermore the configuration with eight turning vanes resulted in an efficiency improvement of 0.4% at the design point.

The same turbine was also taken into consideration in Rosic et al. [5] and [6]. In their studies various shroud as well as cavity parameters and configurations were investigated numerically and experimentally. It was found that reduction of the length of both the inlet and the exit shroud cavity (by rearranging the axial casing end wall position and expansion of the shroud overhang in the inlet cavity) is beneficial. They further concluded that improvement of interaction between the mainstream and the cavity flow can improve the efficiency rather than reduction in tip-leakage fraction only. Furthermore the highest efficiency improvement by 0.75% of the optimized geometry could be achieved at higher tip clearance.

In Curtis et al. [7] the impact of active tip-injection on tip-leakage flow as well as overall turbine efficiency has been studied analytically, numerically and experimentally. A single stage low speed intermediate pressure air turbine was used for the investigations. The jet was inclined by 45° against the leakage flow direction. It could be shown that the highest efficiency increase of 0.4% could be achieved at an injection ratio of 1.2% of main flow. Perfect sealing could be achieved at an injection ratio of 3.5% of main flow. This case however resulted in a decrease in efficiency of 0.6%.

Hogg and Ruiz [8] investigated the influence of active fluid injection on the leakage flow numerically. In this spirit sealing applications consisting of fluidic jet barrier only and in combination with labyrinth seals were examined. It is concluded that a simple air curtain sealing application has only limited potential regarding leakage flow reduction. Significantly greater potential could be achieved in the case of labyrinth seal consisting of three fins provided by active injection along the upstream surface of the central fin which was inclined by 45° against the oncoming leakage flow.

The combination of passive tip-injection and shrouds has been

studied in Ghaffari and Willinger [9] and Ghaffari et al. [10]. In [9] the injection position over the blade shroud has been investigated analytically as well as by means of 2D numerical simulations. In the framework of the analytical considerations an overall discharge coefficient describes the ratio of the overall tip-leakage mass flow rate at the tip gap outlet to its ideal value calculated without losses. The results show that the highest effectiveness can be achieved in the case of guided passive tip-injection along the upstream surface of the first sealing fin. The investigations were extended to include three dimensional effects and blade rotation in [10]. In this study a low pressure turbine (LPT) geometry was used for the investigations. The measurement data obtained from the original shrouded configuration were applied as boundary conditions for the CFD calculations. The passive tip-injection was examined only numerically. In this study the injection mass flow is extracted at the blade leading edge at an appropriate distance from the shroud bottom surface and injected into the shroud clearance along the upstream surface of the first fin provided with a groove as guidance for the injection. The results show a reduction in tip-leakage mass flow rate at the tip gap inlet. It is further shown that the injection mass flow contributes to stage work.

The investigations in [10] are extended by an additional injection channel diameter as well as injection configuration in the framework of the current study. Furthermore measurements have been carried out for the injection case which could be implemented with no great manufacturing restrictions. The measurements have been undertaken in the same LPT test rig described in [10].

PASSIVE TIP-INJECTION

The mixing of tip-leakage flow with the main flow results on the one hand in increased entropy generation and on the other hand in modified incidence angle of the subsequent blade row. Since the extent of the losses can be considered related to the tip-leakage mass flow rate at the tip gap outlet, many methods aim at tip-leakage reduction directly. It is also conceivable to improve the mixing condition resulting in lower losses as well as enhancement of the incidence conditions of the subsequent blade row. The studies mentioned before present some methods regarding enhancement of mixing conditions of tip-leakage flow. The impact of passive tip-injection on leakage mass flow rate is presented in [9]. In this method the injection mass flow is extracted from the stage main flow and injected into the shroud cavity. For calculation of the overall tip-leakage mass flow rate in [9] the influence of the circumferential velocity component is neglected. In Rosic et al. [11] it is stated that the leakage flow is driven by the difference between the total pressure based on the meridional velocity component at the tip gap inlet and the static pressure at the outlet. In this spirit two discharge coefficients C_D and C_D^+ are defined in [9] which describe the ratio of the real tip-leakage

mass flow rate to the mass flow rate without losses at the tip gap inlet and outlet respectively.

In this section the impact of the circumferential velocity component is taken into account regarding calculation of mixing losses since it affects the outlet swirl and thus the associated reduction in stage work and incidence angle of the subsequent blade row. Different approaches can be applied to calculation of the mixing losses due to tip-leakage flow. In [1] the entropy generation caused by the mixing process has been taken into consideration. In this study the considerations are based upon incompressible flow conditions. The reduction in specific stage work due to leakage flow and the impact of passive tip-injection can be investigated clearly in this approach.

Basically, it is assumed that the angular momentum of the flow is preserved across the shroud cavity in the case of no injection. This results in high circumferential velocity components in the rotational direction. Taking into consideration the flow turning in turbine blades, inclination of the injection direction opposite to the rotational direction could further enhance the effectiveness of passive tip-injection. In accordance with [9] the injection slot is assumed to be extended over the entire circumference in the current study. In this spirit the considerations can be undertaken in a meridional section taking into account the circumferential flow components. Furthermore all calculations are undertaken in dimensionless terms. The subscripts τ and i refer to tip-leakage and injection quantities respectively. According to [9] θ is the dimensionless injection velocity with respect to the tip-leakage velocity at the inlet.

$$\theta = \frac{w_i}{\sigma w_{\tau,1}} \quad (1)$$

σ is the contraction ratio due to the shroud sharp edge so that $\sigma w_{\tau,1}$ refers to the tip-leakage velocity extended over the entire tip gap inlet. γ is defined as the dimensionless injection slot width with respect to the inlet clearance. $\gamma\theta$ thus characterizes the dimensionless injection mass flow rate based on the inlet tip-leakage mass flow rate. The leakage velocity $w_{\tau,1}$ is made dimensionless with respect to the exit axial velocity component of the main flow, which is further assumed constant over the blade height and taken into account as reference velocity for the investigations. According to [9] one obtains following relationship:

$$\frac{\sigma w_{\tau,1}}{C_x} = C_D \sqrt{\frac{2s\psi_c}{c \sin \gamma_s \phi_c}} \quad (2)$$

with ψ_c and ϕ_c as loading and flow coefficients at casing section and C_D as discharge coefficient taking into account the inlet tip gap mass flow rate only. Similarly one obtains following equa-

tions:

$$\frac{w_i}{C_x} = \theta \frac{\sigma w_{\tau,1}}{C_x}, \quad \frac{\sigma w_{\tau,2}}{C_x} = C_D^+ \sqrt{\frac{2s\psi_c}{c \sin \gamma_s \phi_c}}. \quad (3)$$

w_i and $w_{\tau,2}$ are the injection velocity and the leakage velocity at the outlet respectively. The relationship between the discharge coefficients C_D and C_D^+ is

$$C_D^+ = (1 + \gamma\theta) C_D, \quad (4)$$

where C_D^+ takes into account the injection mass flow rate as well. Applying the conservation equation of angular momentum for the tip-leakage flow including the injection flow results

$$\dot{m}_{\tau,1} C_x \cot \alpha_{\tau,1} + \dot{m}_i (r_c \omega - w_i \cos \delta_\tau) = \dot{m}_{\tau,2} C_x \cot \alpha'_{\tau,2}. \quad (5)$$

It should be mentioned that the circumferential velocity component of the leakage flow at the tip gap outlet is built based on the axial velocity of the main flow at the outlet resulting in $\alpha'_{\tau,2}$. Furthermore δ_τ is the relative inclination angle measured from the negative rotational direction. For more clarity the relationships are depicted in Fig. 1 in more details in a plane immediately downstream of the rotor.

$$C_{u,\tau 2} = C_x \cot \alpha'_{\tau,2}, \quad (6)$$

$$C_{u,\tau 2} = w_{\tau,2} \cot \alpha_{\tau,2}. \quad (7)$$

In this figure r_τ refers to the beginning of the radius affected by the leakage flow and r_c to the casing. Subsequently one obtains following equation in dimensionless terms:

$$\cot \alpha'_{\tau,2} = \frac{\cot \alpha_{\tau,1}}{1 + \gamma\theta} + \frac{\gamma\theta}{1 + \gamma\theta} \left(\frac{1}{\phi_c} - \frac{w_i}{C_x} \cos \delta_\tau \right). \quad (8)$$

As one can clearly see in the case of no injection ($\gamma\theta = 0$) the inlet angular momentum remains preserved

$$\cot \alpha'_{\tau,2} = \cot \alpha_{\tau,1}. \quad (9)$$

In case of variable radius in the tip section from inlet to outlet Eqn. 8 is transformed into

$$\cot \alpha'_{\tau,2} = \frac{r_{c,1}}{r_{c,2}} \frac{\cot \alpha_{\tau,1}}{1 + \gamma\theta} + \frac{r_i}{r_{c,2}} \frac{\gamma\theta}{1 + \gamma\theta} \left(\frac{1}{\phi_{c,i}} - \frac{w_i}{C_x} \cos \delta_\tau \right). \quad (10)$$

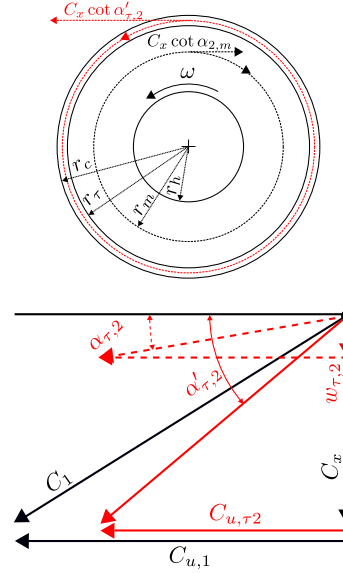


FIGURE 1: VELOCITY RELATIONSHIPS

In the next step it is assumed that mixing between the under-turned leakage flow and the main flow takes place in a short distance downstream of the rotor. In this spirit conservation of angular momentum is applied to the control volume comprising the annular area immediately downstream of the rotor without mixing and the area where the flow filed is completely mixed out. Applying the integral equation of conservation of angular momentum yields

$$\int_{r_h}^{r_\tau} C_x (r \times C_{u,2}) \rho dr + \int_{r_\tau}^{r_c} C_x (r \times C_{u,\tau 2}) \rho dr = \int_{r_h}^{r_c} C_x (r \times \tilde{C}_{u,2}) \rho dr. \quad (11)$$

The quantities with a tilde refer to quantities after the mixing process. Furthermore the flow field at the inlet as well as the outlet of the control volume is characterized by mass flow averaged quantities with the subscript "m". The mean radius r_m as well as axial velocity C_x downstream of the rotor are taken as reference. Under the assumption of small clearance one obtains

$$\tilde{C}_x \approx C_x + \frac{\dot{m}_{\tau,2}}{(r_c^2 - r_h^2) \pi \rho}. \quad (12)$$

The conservation equation of angular momentum is hence trans-

formed into

$$(1 - \eta^2) \cot \alpha_{2,m} + 2 \frac{\tau}{r_m} \frac{w_{\tau,2}}{C_x} \cot \alpha'_{\tau,2} = \quad (13)$$

$$= \cot \tilde{\alpha}_{2,m} \left[(1 - \eta^2) + \frac{\tau}{r_c} + \frac{w_{\tau,2}}{C_x} \right],$$

with η as the hub to tip radius ratio. Applying Eqn. 3 and 8 one obtains following relationship between the flow angle resulting after mixing the tip-leakage flow and the undisturbed flow angle:

$$\frac{\cot \tilde{\alpha}_{2,m}}{\cot \alpha_{2,m}} = \frac{2 \frac{\tau}{r_m} C_D^+ \sqrt{\frac{2s\psi_c}{c\phi_c \sin \gamma_s} \cot \alpha'_{\tau,2} + 1 - \eta^2}}{2 \frac{\tau}{r_c} C_D^+ \sqrt{\frac{2s\psi_c}{c\phi_c \sin \gamma_s} + 1 - \eta^2}}. \quad (14)$$

It can thus be concluded that the deficit in outlet flow angle disappears if

1. the tip-leakage mass flow rate or the tip clearance disappears

$$\tau C_D^+ = 0, \quad (15)$$

2. or the tip leakage flow features the same swirl as the main flow. Taking into account the fact that the swirl of the leakage flow was calculated based on the axial velocity of the main flow this results in

$$r_m \cot \alpha_{2,m} = r_c \cot \alpha'_{\tau,2}. \quad (16)$$

The relative reduction of specific stage work can further be calculated applying Eqn. 14 as follows:

$$\frac{\Delta a_u}{a_{u,id}} = \frac{\frac{\cot \tilde{\alpha}_{2,m}}{\cot \alpha_{2,m}} - 1}{\frac{\cot \alpha_{1,m}}{\cot \alpha_{2,m}} - 1}, \quad (17)$$

with $a_{u,id}$ as the specific stage work without tip-leakage losses. The above equations were evaluated for the LPT under investigation in this paper taking into account also the variable tip section radius. The results are depicted in Fig. 2. For calculation of the discharge coefficients as well as the dimensionless injection velocity the relationships in [9] were applied. As one can clearly see inclination of the injection channel towards the rotational direction (in the relative frame of reference) enhances the effectiveness of passive tip-injection. It can further be stated that the

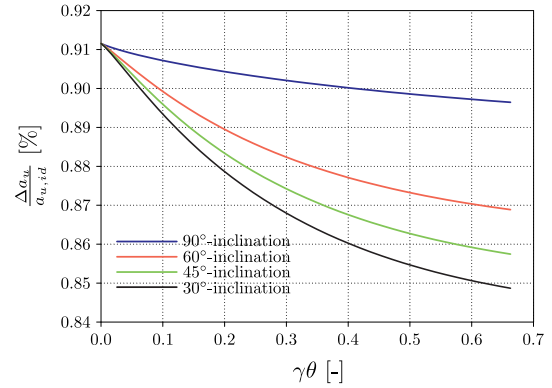


FIGURE 2: RELATIVE REDUCTION OF STAGE WORK (ORIGINAL CONFIGURATION)

analytical model is well able to predict the relationship between the geometrical parameters and the associated penalty in specific stage work. Higher clearances as well as hub to tip radius ratios result in higher penalty in specific stage work. A clearance enlargement to a 5 mm gap results in a penalty increase from 0.91 (Fig. 2) to 5.45% for the current geometry without passive injection. Furthermore it should be mentioned that special care has to be taken in case of variable tip section radius since the impact of passive tip-injection is sensitive to the injection mass flow rate as well as main flow swirl. Higher injection mass flow rates and lower inclination angles can even result in further increase of the penalty in specific stage work for non-moderate radius increase from the inlet to the outlet of the shroud cavity. Lower inlet main flow swirl can also turn the effect of passive tip-injection and result in lower specific stage work. For more clarity the original configuration was modified by enlarging the radius increase from the cavity inlet to the outlet and reducing the inlet swirl. The results are depicted in Fig. 3. One can clearly recognize the enhancement in the case of no injection due to lower inlet swirl since this model does not take into account the profile losses which can also be accounted for by defining adjusted flow angles. Due to the passive injection, taking place at higher outer diameter, 90°-injection has a negative effect on specific stage work. This can be explained by the fact that higher injection radii further reinforce the swirl in rotational direction when no inclination is provided. Furthermore it can be recognized that higher injection mass flow rate also impairs the effectiveness of passive tip-injection even in the case of highly inclined injection. It should be mentioned that affecting the inlet swirl by passive injection has to be considered in combination with the impact on reducing the leakage flow. In the case that the negative influence of reinforcing the inlet swirl by passive injection is overcome by

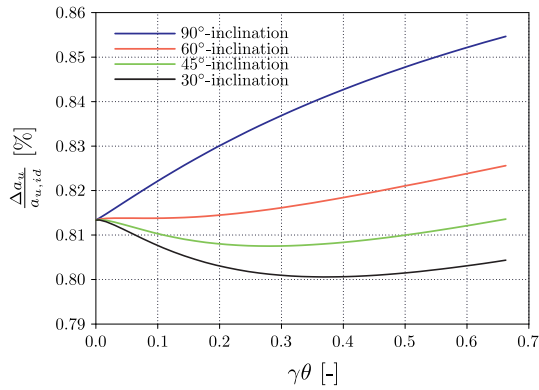


FIGURE 3: RELATIVE REDUCTION OF STAGE WORK (MODIFIED CONFIGURATION)

strong reduction in overall tip-leakage mass flow rate the overall impact is positive. Higher inclination suppresses inlet swirl strengthening in a way that the flow angle deficit is reduced at lower injection mass flow rate values.

Based on variable inlet swirl in combination with profile losses accounted for in terms of modified exit flow angle this model can thus be applied for off-design calculations.

LPT STAGE

The LPT stage for the investigations is the same as described in [10]. The shrouded LPT rotor considered in this paper belongs to a test rig consisting of a transonic high pressure turbine (HPT) and a counter rotating LPT with 72 shrouded blades connected by the Turning Mid Turbine Frame (TMTF). The TMTF further turns the flow and provides the LPT with swirled flow. For more information about the facility see also Santner [12]. The inlet measurement plane E is positioned at a distance of 59% axial chord length upstream of the blade leading edge and serves as the inlet for the CFD calculations. The exit measurement Plane F is positioned at a distance of 77% axial chord length downstream of the blade trailing edge and serves as the evaluation plane for the measurements and CFD. The outlet defined for the CFD is positioned further downstream with ambient static pressure. The TMTF and LPT configurations as well as the measurement planes are depicted in Fig. 4 schematically. The operational conditions of the LPT are summarized in Tab. 1.

Injection Channel

In [10] the injection channel inlet is positioned at the blade leading edge. The injection channel consists of two perpendicu-

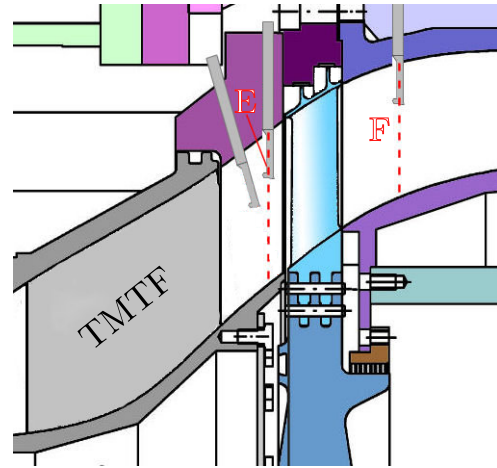


FIGURE 4: MERIDIONAL CUT OF LPT AND TMTF

TABLE 1: OPERATIONAL DATA OF THE LPT

Reduced inlet mass flow [$\frac{\text{kg}\sqrt{\text{K}}}{\text{s bar}}$]	214.6
Mechanical speed [$\frac{1}{\text{min}}$]	3549.3
Reduced speed [$\frac{1}{\text{min}\sqrt{\text{K}}}$]	194.0
Stage total pressure ratio [-]	1.3

lar channels per blade led through the blade and the shroud. The injection channel outlet is manufactured with a groove in the first sealing fin in order to realize guided tip-injection. Due to manufacturing restrictions on the one hand and high mechanical stress at the sharp edges of the injection inlet on the other hand no measurements could be carried out for this injection method and the considerations are limited to numerical calculations only, which are presented in this paper as well. For more information regarding the leading edge injection, as it is named for specification, and the corresponding numerical setups see [10].

The injection channel in this study is manufactured by means of a single hole through the shroud with the advantage that shorter injection channel lengths and higher diameters can be manufactured. This configuration is further named as through-shroud injection. Prior to manufacturing and testing of the final injection position many positions were tested numerically. The final position of the injection channel is schematically depicted in Fig. 5. Furthermore the shroud configuration and vortex structure of the tip section are presented in this figure. The axial position of the injection bore center coincides with the cavity edge in the

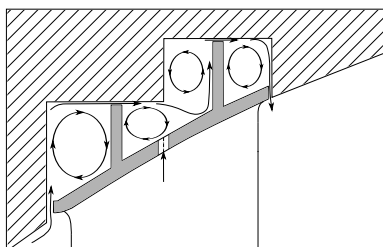


FIGURE 5: TIP SECTION OF THE LPT

casing in order to achieve high mixing of the injection flow. The circumferential position of the channel was chosen near the pressure side in order to ensure higher inlet pressure. The shrouded blade including the injection channel is presented in Fig. 6 in more details

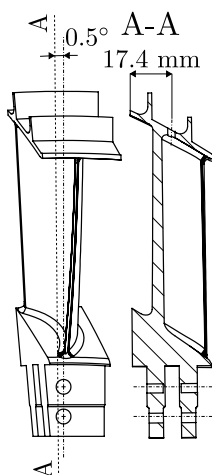


FIGURE 6: THROUGH-SHROUD INJECTION CHANNEL

Measurement Instrumentation

The data are obtained from two sets of measurements carried out with a 5-hole probe with integrated temperature sensor and a single-hole Fast Response Aerodynamic Pressure Probe (FRAPP).

For more information about the 5-hole probe and the associated uncertainties see [12, 10]. The 5-hole probe measurements were

carried out for 23 radial and 46 angular positions in the inlet measurement plane and 21 radial and 46 angular positions in the exit measurement plane with an angular increment of 0.5° . The measurement data in the inlet plane were applied as boundary conditions for the CFD calculations and those in the exit plane were used for evaluation of the numerical settings.

The FRAPP is a cylindrical high response probe operated as a virtual three sensor probe. Pressure readings are acquired by three to five rotations of the probe around the probe axis. Dynamic calibration is necessary in order to correct the data. After phase averaging for eliminating the stochastic fluctuations, the static calibration matrix is applied to the raw data in order to obtain the time resolved flow field. The presented data in this paper are further time averaged. More information about the FRAPP and its dynamic calibration can be found in Persico et al. [13, 14]. The probe is insensitive to the pitch angle within a range that is not symmetrical with respect to the zero position. The standard errors due to the pitch angle are presented in Tab. 2. The pitch angle is declared with respect to the probe axis and is counted as negative if the probe head is rotated opposite to the flow direction.

The use of FRAPP allows for better refinement in the vicinity of the casing, which is the region of interest. A distance of at least 6 mm from the hub results from the position of the probe hole. Data were acquired in the exit measurement plane for 29 radial and 46 circumferential positions covering an angular sector of 22.5° . The measurement grid has a radial increment of 3 mm towards the hub since this region was not modified for the investigations. The grid was refined to an increment of 1 mm towards the casing for higher resolution.

TABLE 2: STANDARD ERRORS OF THE FRAPP

	Pitch angle -10°	Pitch angle $+10^\circ$
Yaw angle [°]	0.3	0.2
Total pressure [% kinetic head]	0.5	0.4
Static pressure [% kinetic head]	3	13
Mach number [-]	0.006	0.06

Experimental Results

The LPT test rig is operated at constant reduced quantities. Based on the measurement technique and the associated calibration applied for the current study both static and total pressure, absolute yaw angle and the Mach number can be evaluated. Meaningful interpretation of the results is however based on the absolute yaw angle and Mach number. Due to the time frame between the measurements of the rotor before and

after manufacturing the injection bore the absolute values of static and total pressure are affected by the deviating operational conditions.

In this section the circumferential averaged results acquired by FRAPP in the exit measurement plane are presented. Since the region next to the casing is of interest in the framework of the investigations all quantities are depicted from a dimensionless channel height of 0.7.

In Fig. 7 the deviations in circumferential averaged exit flow angle from the averaged exit flow angle at midspan are depicted in order to avoid possible offsets. α_2^+ refers to the absolute

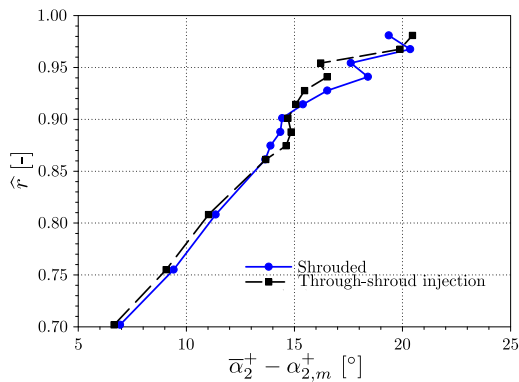


FIGURE 7: MEASURED EXIT FLOW ANGLE

exit flow angle with respect to the negative rotational direction. Nonuniform distribution is observable in the vicinity of the casing in both cases. This can be attributed to some extent to the pitch angle sensitivity of the probe but also to the unsteady behavior of the flow in this region. Generally it can be said that the flow angle features higher values in the case without passive tip-injection in the casing region which is a sign of higher swirl in the rotational direction associated with tip-leakage flow. Closer to the casing higher values of the exit flow angle are due to lower axial velocities associated with lower tip leakage mass flow rate. Further away from the casing the secondary flow effects are more pronounced in the case with passive tip-injection. This can be considered as a result of lower tip-leakage mass flow rate at the outlet which further results in less interaction between secondary and tip-leakage flow.

In the end it can be stated that the contribution of the exit flow angle is more uniform in the case with passive tip-injection and follows the trend of the main flow towards the casing. Further away from the casing the circumferential averaged flow angle still features lower values in the case with passive tip-injection

which is a positive effect concerning the flow turning. Further it has to be mentioned that there is an ingress of the tip region flow field affected by tip-injection into the main flow.

These predictions are supported taking into account further flow quantities in the exit measurement plane. Since no temperature acquisition was possible by the FRAPP used for the current investigations the circumferential averaged Mach number is considered and presented in Fig. 8. Tip leakage flow is characterized

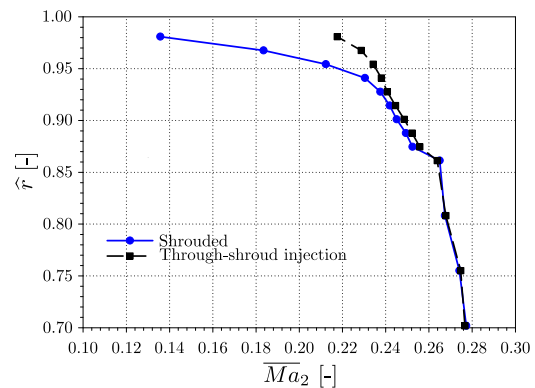


FIGURE 8: MEASURED EXIT MACH NUMBER

by low axial velocities and higher temperatures caused by not participating in stage work. This results in lower Mach number values in the vicinity of the casing as it can be observed for the case without passive tip-injection. Almost no difference can be seen between both cases further away from the casing near the midspan featuring main flow Mach number. Considerably lower Mach number values can be observed in the vicinity of the casing in the case without passive tip-injection. It can further be stated that higher tip-leakage mass flow rate in this case affects the mixing of the tip-leakage flow to the main flow. This results in further extension of the region featuring lower Mach number into the main flow. In contrast the case with passive tip-injection features Mach number values close to the values of the main flow in the vicinity of the casing. It can further be stated that the flow field is mixed out to a higher extent than in the case without tip-injection which can be attributed to lower tip-leakage mass flow rate.

CFD CALCULATIONS

In order to achieve higher mesh quality the manufacturing radii of the original geometry were eliminated for meshing. The

mesh was created via ICEM CFD 14.5 and was refined towards the solid walls in a way that $y^+ < 1$ holds. Due to the fact that the geometry under investigation features a large number of wall associated regions the cell number rapidly increased. In addition the TMTF consists of 16 turning vanes resulting in a high cell number for unsteady numerical calculations. Due to the limitations of the computational resources only one blade passage was simulated in this study. In this spirit the impact of passive tip-injection could be studied in isolation. The cell number of different cases is presented in Tab. 3. As it was mentioned addi-

TABLE 3: CELL NUMBER OF INVESTIGATED CASES

Case	Cell number
Shrouded (original geometry)	4.4 million
Leading edge injection 1mm / 2 mm	18.0 million
Through-shroud injection	15.7 million

tional results are presented in this paper referring to the leading edge injection as described in [10] extended by the extra injection channel diameter of 1 mm. In Fig. 9 the computational mesh for the through-shroud injection is depicted. For details about the mesh of the leading edge injection see [10]. A mesh study was also undertaken in order to ensure that the results are mesh independent. The results of the finest mesh were taken into further consideration and are presented in this paper.

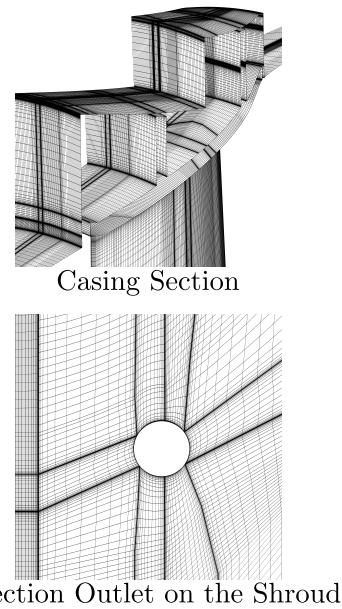
The numerical calculations were carried out via Fluent 13.0 for compressible flow with ideal gas law in a rotational frame of reference. The stationary walls were provided with no motion. A number of numerical calculations were carried out in order to evaluate two turbulence models Realizable k/ϵ (RKE) and Shear Stress Transport (SST) k/ω in terms of suitability for the cases considered in this study. In this spirit the original shrouded geometry without injection was taken as reference. The important numerical setups are presented in Tab. 4

TABLE 4: NUMERICAL SETUP.

Turbulent intensity [%]	5
Turbulent length scale [m]	0.0063
Rotational domain speed [1 / s]	59.2
Operating pressure [Pa]	95000

Model Evaluation

Calculation of flow field in a rotational frame of reference offers two options regarding velocity formulation. These two

**FIGURE 9: DETAILS OF THE GENERATED MESH**

options are velocity formulation in either absolute or relative frames and can affect the results depending on the conditions being investigated. Since the flow through the shrouded gap and the main flow are subject to different turning both formulations were tested and evaluated for this study. For evaluation of different numerical options the measurement data obtained from the 5-hole probe were taken into consideration. Figure 10 shows the circumferential averaged exit flow angle with respect to the negative circumferential direction ($\bar{\alpha}_2^+$) in the exit measurement plane. The ordinate is specified by the dimensionless channel height with respect to the channel height in the exit measurement plane. This specification is also used for the following descriptions in this paper. The abbreviations AVF and RVF stand for absolute and relative velocity formulation respectively. Good agreement between measurement and CFD is observable especially at midspan. The SST k/ω model overestimates the effect of overturning and under turning due to the passage vortex in the vicinity of the hub. The same effect can be encountered in the casing region. Due to this reason the results of the Realizable k/ϵ -model with enhanced wall treatment were taken into consideration although all cases were additionally calculated also with a SST k/ω -model. Furthermore one can clearly see that very good agreement in the hub region exits between the measurement and the results calculated applying RVF. However the results are

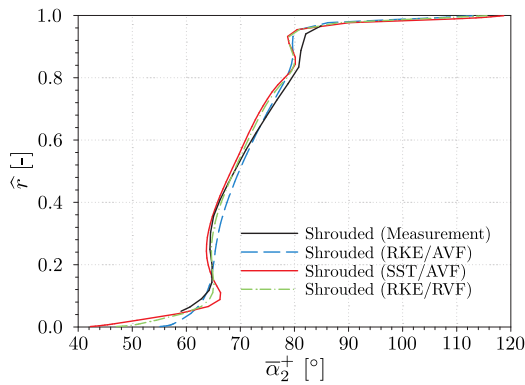


FIGURE 10: EXIT FLOW ANGLE

similar to those calculated with the SST k/ω -model in the casing region. Since this area is of interest the AVF was chosen for all cases investigated in this study.

CFD Results

In this section the CFD results in the exit measurement plane are presented. Figure 11 shows the circumferential exit flow angle for different cases investigated in this study. As already mentioned this angle is calculated with respect to the negative circumferential direction. Higher values in the casing region are a sign of overturning which is more pronounced in the case of shrouded geometry without tip-injection. Further away from the casing slight overturning associated with the passage vortex can be observed. This appearance is not well pronounced since the exit measurement plane is positioned downstream of the rotor and the flow field is mixed out to some extent. The SST k/ω model and RVF however overpredict this effect as can be observed in Fig. 10. In [10] two additional cases without axial and radial gaps are also presented. Higher flow overturning can be observed in the case without radial gap since the blade tip ends directly at the stationary casing. In the case without axial gap the flow overturning is less pronounced since the moving casing section contributes to flow turning in the rotational direction.

According to the analytical investigations, lower α_2^+ values result in lower $\cot \alpha_2'$ values which subsequently result in lower penalty in specific stage work. It can further be observed that the leading edge injection features higher effectiveness in comparison to the through-shroud injection even at smaller injection channel diameters. This can be contributed to better mixing of the injection flow with the tip-leakage flow in this case since the first sealing fin serves as a guidance for the injection. It can further be stated that larger channel diameter of the leading edge injection does not affect the effectiveness significantly. Compared to the mea-

surement results one recognizes no ingress of the affected flow field in the tip section into the main flow. It can be assumed that this effect is a result of the unsteady flow character which is reflected in the measurement data.

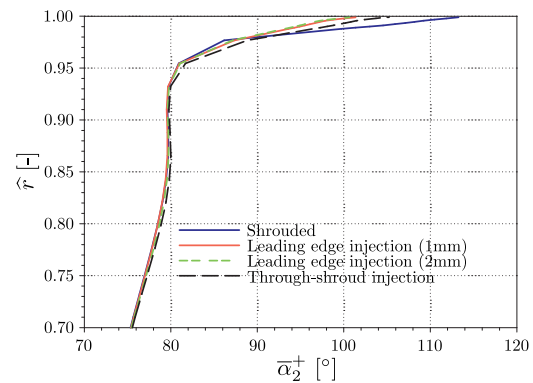


FIGURE 11: EXIT FLOW ANGLE

Since specific entropy is an indicator for loss mechanisms, the calculated specific entropy with respect to the standard state is depicted in Fig. 12 for the different cases. Strong increase in specific entropy is observable in the casing region due to the mixing of the leakage flow. Passive tip-injection results in decrease in entropy generation. Small differences are observable between the individual injection cases. It can thus be stated that different injection cases differ negligibly regarding entropy generation associated with tip-leakage flow. Nevertheless the aerodynamical behavior of the blading can be affected differently by various injection types. Due to small deviations these effects are reflected globally in entropy generation of the stage and can not be taken into account observing the tip section in an isolated manner.

Figure 13 shows the circumferential averaged total temperature. Increase in total temperature in the vicinity of the casing is an indicator for lower specific stage work due to higher total enthalpy values. It has to be mentioned that two different mechanisms are responsible for lower total temperature values of different injection types. In the case of leading edge injection the injection flow contributes to positive stage work as it is explained in [10]. In the case of through-shroud injection however fluid is extracted from the stage flow after it has partially participated in the stage work due to its turning. In both cases passive tip-injection positively affects the specific stage work which is reflected in lower total temperature values in the vicinity of the casing.

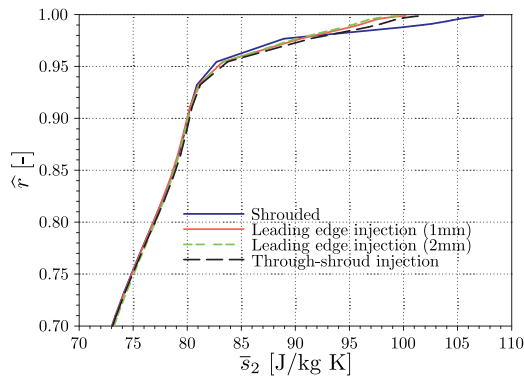


FIGURE 12: SPECIFIC ENTROPY

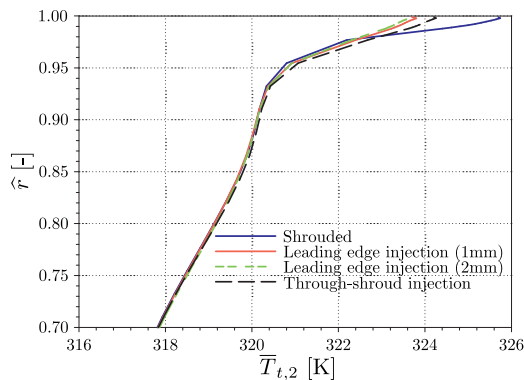


FIGURE 13: TOTAL TEMPERATURE

CONCLUSION

The impact of passive tip-injection on the downstream flow field was investigated in this study taking into consideration a shrouded LPT configuration representative of a real application. In contrast to previous investigations on the impact of guided passive tip-injection with the injection flow extracted at the blade leading edge the injection channel for this study was manufactured by means of a bore through the shroud. This type of injection channel is advantageous due to its manufacturing feasibility. An analytical model has been derived in the framework of the investigations estimating the applicability of passive tip-injection and its impact on the exit flow angle and associated enhancement of specific stage work. Furthermore experimental and numerical studies have been undertaken.

Based on the measurement data it can be stated that passive tip-

injection reduces the overall tip-leakage mass flow rate. It can further be stated that it contributes to more uniform exit flow angle and less deviation from the main flow which is a positive effect for the downstream blade row. Furthermore the flow field is mixed out to a higher extent in the casing region in the case with passive tip-injection.

The numerical results present the current injection channel type together with previous results of leading edge tip-injection. Improvement of the downstream flow field is observable in all injection cases. The leading edge tip-injection however features slightly higher effectiveness in comparison to the through-shroud injection reflected in lower entropy values and lower deviations in exit flow angle. This can be attributed to the guided injection and better mixing of injection and leakage flow.

The feasibility of leading edge tip-injection is given for higher blade leading edge thickness with less impact on blade aerodynamics. In this spirit a numerical and experimental study on configurations with higher blade leading edge thickness could be a topic for further investigations. Application of measurement techniques acquiring temperature and the effect of pitch angle could also be desirable. Furthermore off-design measurements and simulations could contribute to better understanding of applicability of passive tip-injection.

ACKNOWLEDGMENT

The authors would like to acknowledge the Institute for Thermal Turbomachinery and Machine Dynamics in Graz University of Technology for performing the measurements as well as the Austrian Research Promotion Agency FFG for supporting the project in the framework of the Aeronautics Research and Technology Programme TAKE OFF.

REFERENCES

- [1] Denton, J. D., (October 1993). "Loss Mechanisms in Turbomachines.". *ASME Journal of Turbomachinery*, Vol. 115, 621-656.
- [2] Anker, J. E., and Mayer, J. F., (2002). "Simulation of the Interaction of Labyrinth Seal Leakage Flow and Main Flow in an Axial Turbine". *ASME Paper GT2002-30348*.
- [3] Giboni, A., Wolter, K., Menter, J. R., and Pfof, H., (2004). "Experimental and Numerical Investigation into the Unsteady Interaction of Labyrinth Seal Leakage Flow and Main Flow in a 1.5-Stage Axial Turbine". *ASME Paper GT2004-53024*.
- [4] Rosic, B., and Denton, J. D., (April 2008). "Control of Shroud Leakage Loss by Reducing Circumferential Mixing". *ASME Journal of Turbomachinery*, Vol. 130,.
- [5] Rosic, B., Denton, J. D., and Curtis, E. M., (October 2008). "The Influence of Shroud and Cavity Geometry on Turbine Performance: An Experimental and Computational Study -

- Part I: Shroud Geometry”. *ASME Journal of Turbomachinery*, Vol. 130.
- [6] Rosic, B., Denton, J. D., and Curtis, E. M., (October 2008). “The Influence of Shroud and Cavity Geometry on Turbine Performance: An Experimental and Computational Study - Part II: Exit Cavity Geometry”. *ASME Journal of Turbomachinery*, Vol. 130.
- [7] Curtis, E. M., Denton, J. D., Longley, J. P., and Rosic, B., (June 2009). “Controlling Tip Leakage Flow over a Shrouded Turbine Rotor Using an Air-Curtain”. *ASME Paper GT2009-59411*.
- [8] Hogg, S. I., and Ruiz, I. G., (June 2011). “Fluidic Jet Barriers for Sealing Applications”. *ASME Paper GT2011-45353*.
- [9] Ghaffari, P., and Willinger, R., (October 2013). “Impact of Passive Tip-Injection on the Performance of Partially Shrouded Turbines: Basic Concept and Preliminary Results”. *ASME Paper TBTS2013-2038*.
- [10] Ghaffari, P., Willinger, R., Bauinger, S., and Marn, A., (June 2015). “Impact of Passive Tip-Injection on Tip-Leakage Flow in Axial Low Pressure Turbine Stage”. *ASME Paper GT2015-42226*.
- [11] Rosic, B., Denton, J. D., and Pullan, G., (October 2006). “The Importance of Shroud Leakage Modeling in Multi-stage Turbine Flow Calculations”. *ASME Journal of Turbomachinery*, Vol. 128, 699-707.
- [12] Santner, C., (2008). “Experimental Investigation of Turning Mid Turbine Frame Designs, Graz University of Technology, PhD thesis”.
- [13] Persico, G., Gaetani, P., and Guardone, A., (2005). “Design and Analysis of New Concept Fast-Response Pressure Probes”. *Meas. Sci. Technol.*, Vol. 16, 1741-1750.
- [14] Persico, G., Gaetani, P., and Guardone, A., (2005). “Dynamic Calibration of Fast-Response Probes in Low-Pressure Shock Tubes”. *Meas. Sci. Technol.*, Vol. 16, 1751-1759.

6.5. Mesh Study

Mesh study and estimation of the discretization errors is a common practice in validation of CFD results. Applying CFD for calculation of the flow physics faces many sources of errors such as turbulence modeling, truncation and round-off errors as well as errors due to discretization and interpolation schemes. In general it is a sophisticated task to quantify and differentiate the sources of error in a CFD calculation. There are, however, well-established methods for quantifying the discretization error and ensuring mesh independence of the results. The discretization error depends essentially on the mesh size and its distribution as well as the discretization scheme. The method used in this thesis is called Richardson-Extrapolation for estimation of a mesh-independent quantity calculated with a infinitely fine mesh. Due to the high complexity of the CFD carried out in this chapter, the mesh study is presented for these results briefly. The procedure of Richardson-Extrapolation is also described in Schäfer [50] and Celik et al. [13].

This procedure is presented for spatial discretization only, since the calculations in this thesis are steady-state calculations. Φ_h is the value of a characteristic quantity important to the objective of the simulations calculated with a representative finite mesh size h . For estimating the distretization error the mesh is coarsened (or refined) systematically. For a refinement factor of 2, Φ_{2h} and Φ_{4h} represent the values calculated with increasing mesh size. In this regard Φ_h and Φ_{4h} signify the values calculated with the finest and coarsest mesh respectively. In the next step the error of the mesh size h and the mesh-independent solution Φ_∞ can approximately be calculated as

$$e_h \approx \frac{\Phi_h - \Phi_{2h}}{2^p - 1} \quad \Phi_\infty \approx \Phi_h + \frac{\Phi_h - \Phi_{2h}}{2^p - 1}. \quad (6.1)$$

In this equation p is the order of the procedure which can be calculated approximately as

$$p \approx \frac{\ln \left(\frac{\Phi_{2h} - \Phi_{4h}}{\Phi_h - \Phi_{2h}} \right)}{\ln 2}. \quad (6.2)$$

The mass-averaged values of absolute exit flow angle $\bar{\alpha}_2^+$ (with respect to the negative circumferential direction), total temperature $\bar{T}_{t,2}$ and specific entropy \bar{s}_2 in the exit measurement plane F (see Fig. 6.1) were considered for validation of the discretization error. The blade torque was not used in this procedure, since it produces additional uncertainty due to integration of the circumferential component of the pressure distribution over the blade surface. This uncertainty would increase with increasing mesh size (due to the skewness). In Tab. 6.2 the order of the procedure is given for the quantities mentioned above.

In Fig. 6.2 and Fig. 6.3 the relative errors of the individual quantities with respect to the mesh independent (exact) solution and the ratios of the quantities to the exact solution are depicted respectively for different mesh sizes. Generally it can be concluded that the discretization error of the selected mesh is below 0.1% for all quantities. One can clearly see that the total tempera-

$p(\bar{s}_2)$	$p(\bar{\alpha}_2^+)$	$p(\bar{T}_{t,2})$
4.36	2.21	3.46

Table 6.2.: Procedure Order

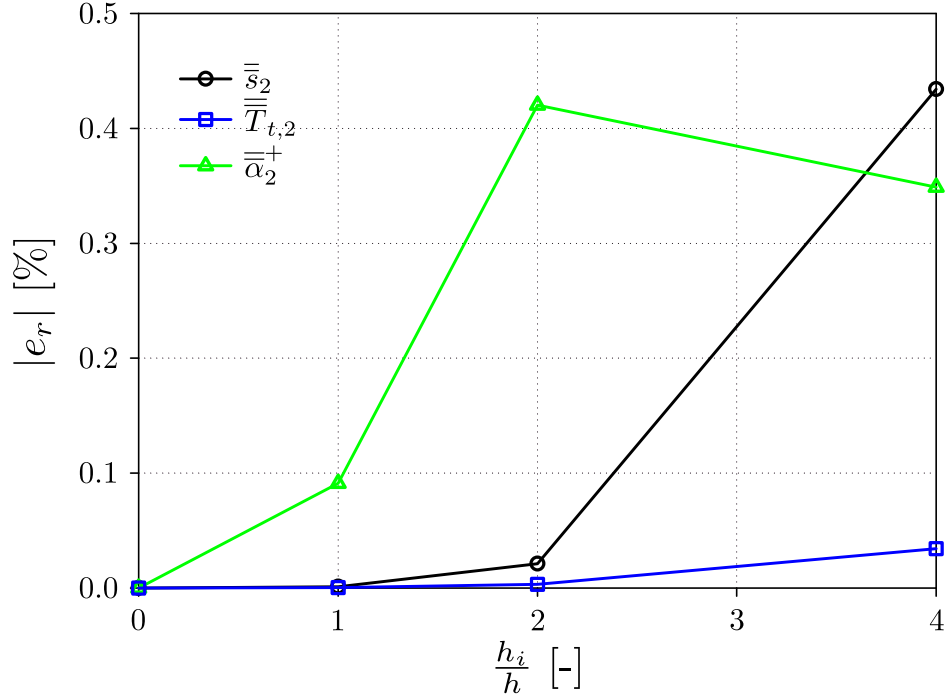


Figure 6.2.: Relative Errors

ture and the specific entropy feature convergent behavior toward the exact solution. In contrast the errors in the absolute flow angle feature an increasing tendency up to the mesh size $2h$ and decrease to the mesh size $4h$. It is assumed that the combination of two velocity components with individually different discretization errors for calculating the flow angle is responsible for this behavior.

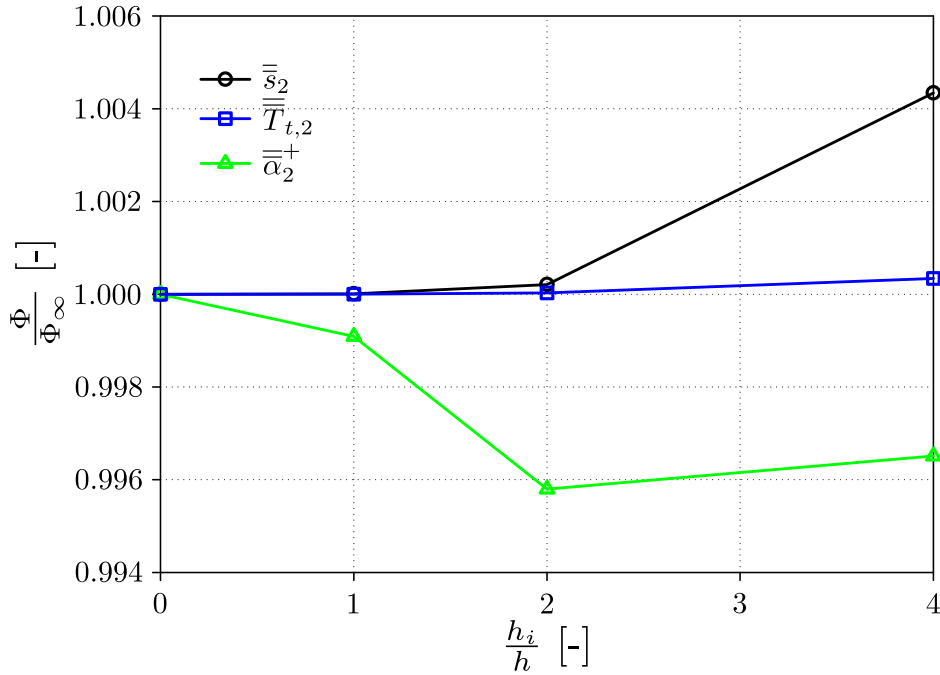


Figure 6.3.: Richardson Extrapolation

6.6. Additional Information

In this section additional information containing contour plots and streamlines are provided for a better understanding of the leakage flow as well as the injection flow of the LPT rotor under investigation in the last chapter of this thesis.

6.6.1. CFD Contour Plots

6.6.1.1. Cavity Flow of the Shrouded Geometry without Injection

In Fig. 6.4 the contour plots of radial velocity are depicted in different circumferential positions at the cavity inlet for the shrouded case without passive tip-injection. As one can clearly see the main flow ingress into the cavity is non-uniform in circumferential direction. Considering the rotational direction of the rotor the main flow enters the cavity to a higher extent upstream of the pressure side featuring higher radial velocity components. The main flow ingress decreases in rotational direction approaching the inlet area upstream of the suction side.

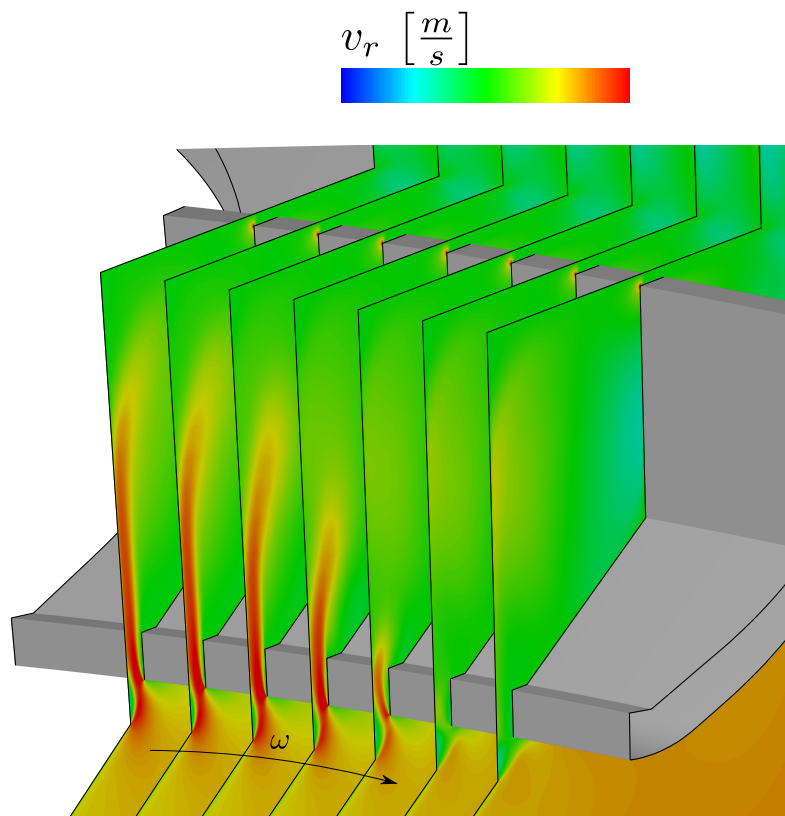


Figure 6.4.: Contour Plots of Radial Velocity at the Cavity Inlet

In Fig. 6.5 the contour plots of radial velocity are depicted in different circumferential positions at the cavity outlet. As in the previous plots the cavity flow ingress into the main flow occurs non-uniformly in circumferential direction. The blue color illustrates negative radial velocity components. Approaching the suction side the cavity flow features higher negative radial velocity components indicating higher ingress into the main flow.

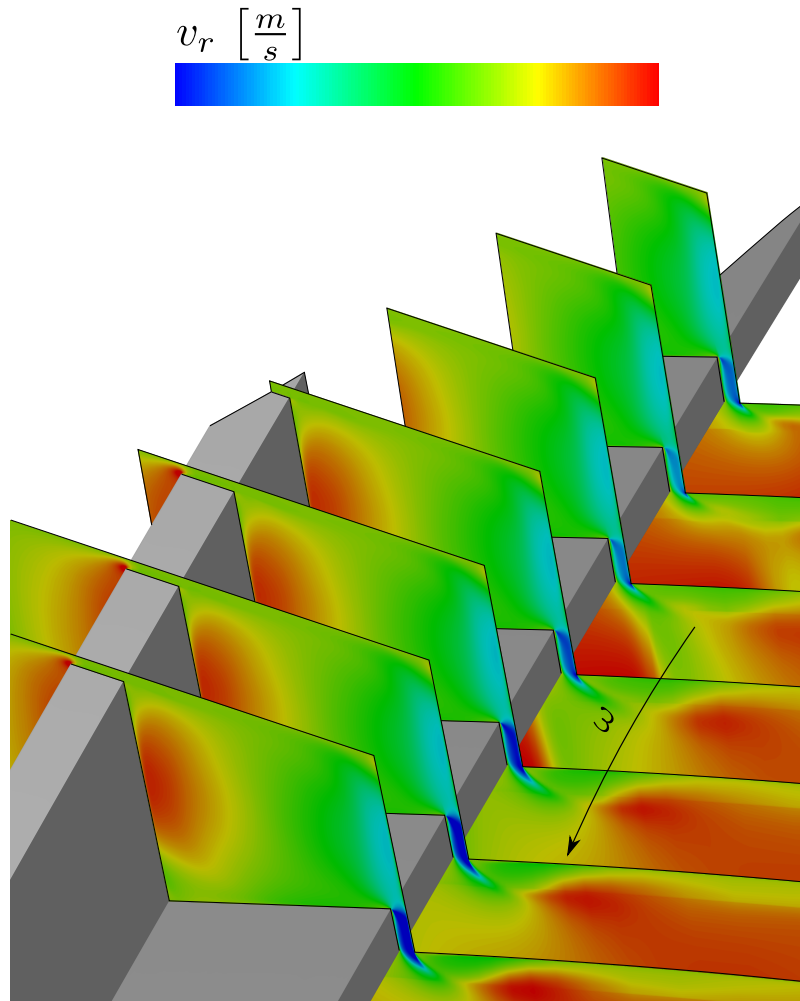


Figure 6.5.: Contour Plots of Radial Velocity at the Cavity Outlet

6.6.1.2. Circumferential Velocity

In Fig. 6.6 and 6.7 the contour plots of the absolute circumferential velocity component are depicted for the leading edge injection in a meridional plane and an axial plane through the cavity and the injection bore center respectively. The injection channel diameter is 2 mm in this case. In Fig. 6.8 and 6.9 the contour plots of the absolute circumferential velocity component are depicted for the through-shroud injection.

Due to the small gaps in the cavity area high mixing is observable between the cavity flow and both the injection flow and the main flow entering the cavity. In the case of leading edge injection higher circumferential velocities are apparent in the vicinity of the upstream surface of the first fin due to wall friction. In the case of through-shroud injection higher circumferential velocities can be observed in the vicinities of the surrounding injection channel walls.

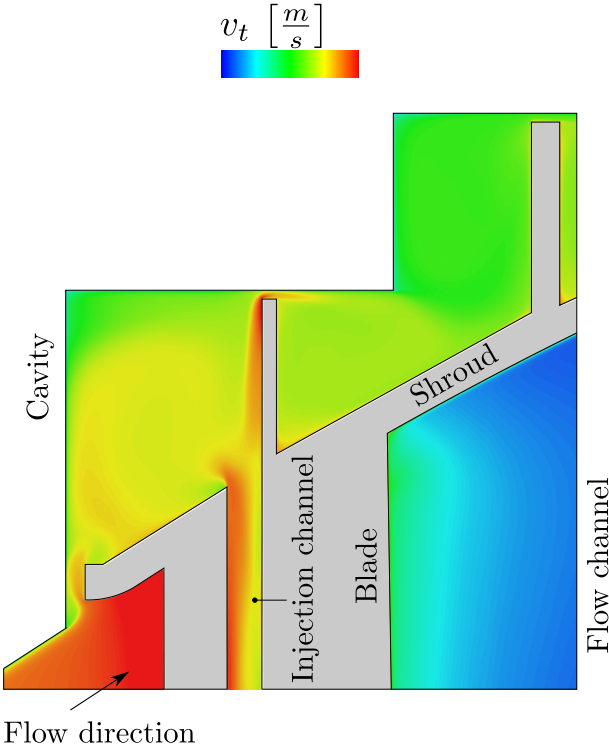


Figure 6.6.: Contour Plot of Absolute Circumferential Velocity of Leading Edge Injection in a Meridional Plane

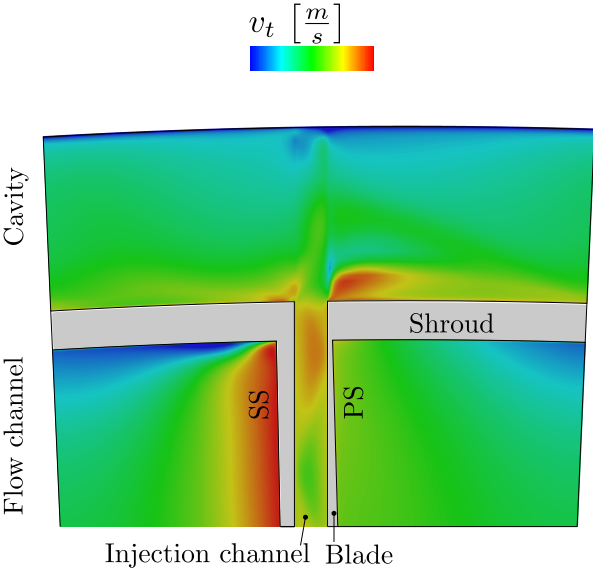


Figure 6.7.: Contour Plot of Absolute Circumferential Velocity of Leading Edge Injection in an Axial Plane

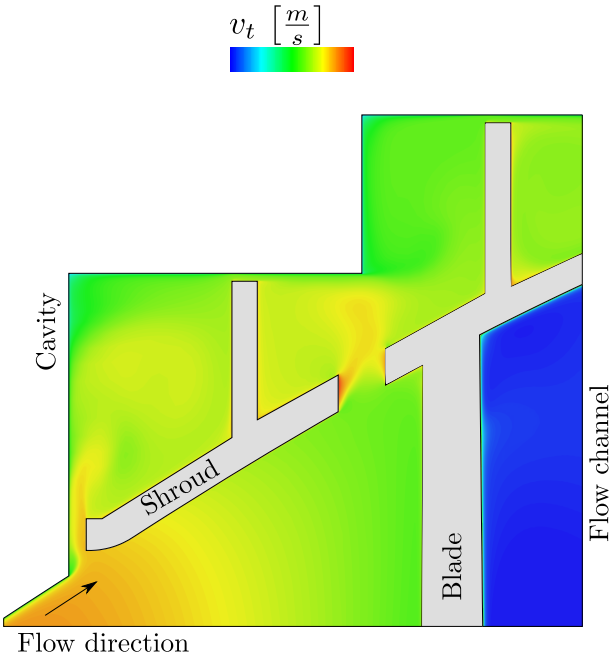


Figure 6.8.: Contour Plot of Absolute Circumferential Velocity of Through-Shroud Injection in a Meridional Plane

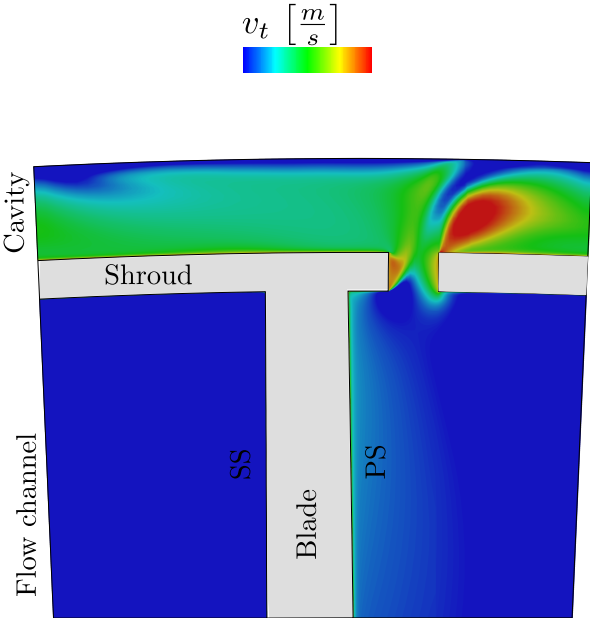


Figure 6.9.: Contour Plot of Absolute Circumferential Velocity of Through-Shroud Injection in an Axial Plane

6.6.1.3. Total Temperature

In Fig. 6.10 and 6.11 the contour plots of total temperature are depicted in the same planes as in the previous plots for the leading edge injection. Figures 6.12 and 6.13 present the total temperature contour plots for the case of through-shroud injection respectively.

One can clearly see that the injection flow features lower total temperature values in both cases. This behavior can be attributed to participation of the injection flow in specific stage work. This behavior can be attributed to participation of the injection flow in specific stage work. The mechanisms are, however, different. In the case of leading edge injection the injection flow contributes to specific stage work by its turning. In the case of through-shroud injection the injection flow is extracted after it has partially participated in stage work. Both mechanisms result in lower total temperature values.

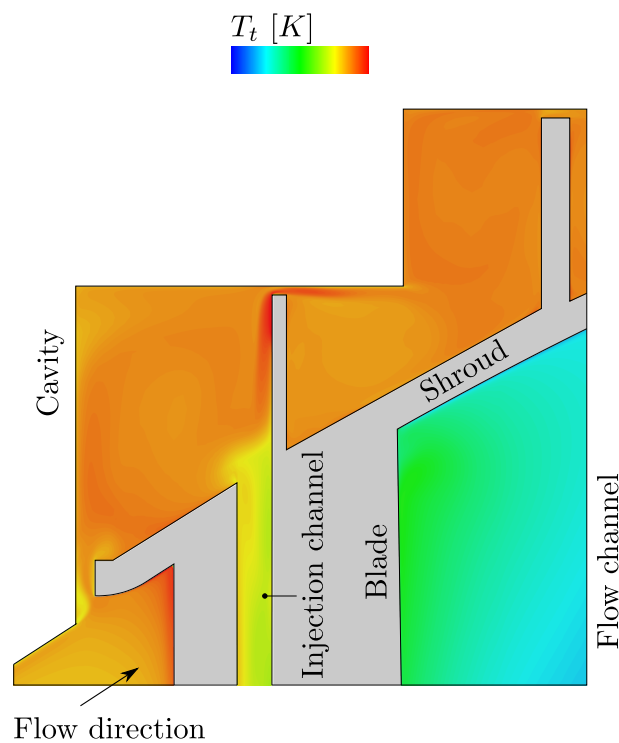


Figure 6.10.: Contour Plot of Total Temperature of Leading Edge Injection in a Meridional Plane

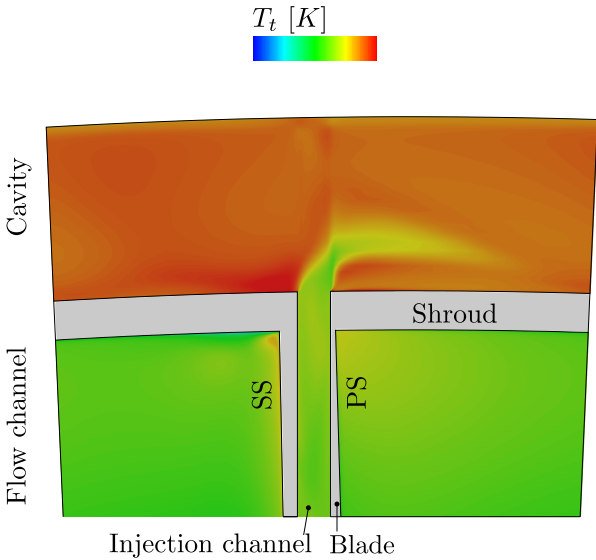


Figure 6.11.: Contour Plot of Total Temperature of Leading Edge Injection in an Axial Plane

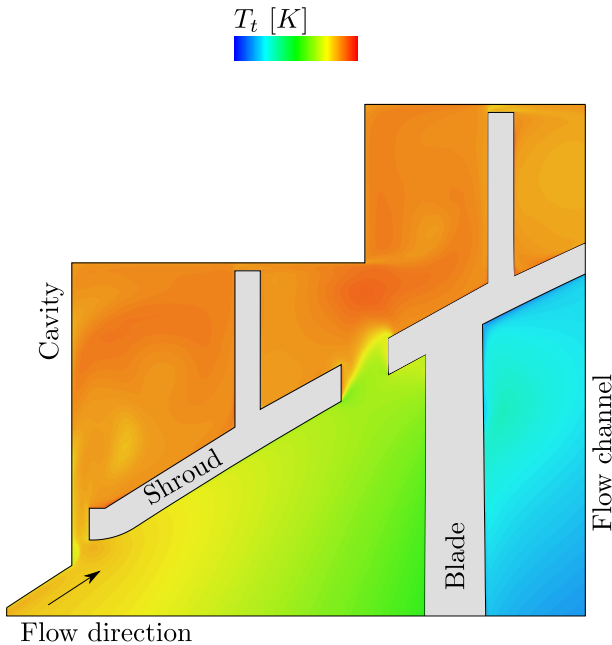


Figure 6.12.: Contour Plot of Total Temperature of Through-Shroud Injection in a Meridional Plane

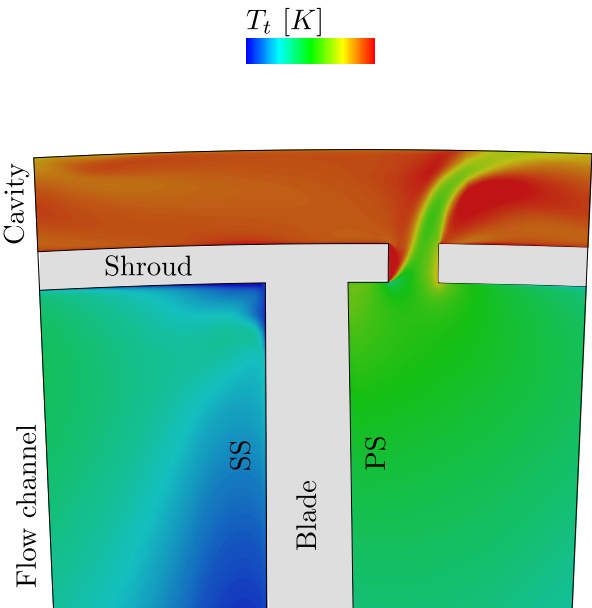


Figure 6.13.: Contour Plot of Total Temperature of Through-Shroud Injection in an Axial Plane

6.6.2. Streamlines

Finally the cavity streamlines taking into account relative velocity components are presented in Fig. 6.14 to 6.17 in the same planes as in the previous contour plots. The injection channel diameter of the leading edge injection is 2 mm.

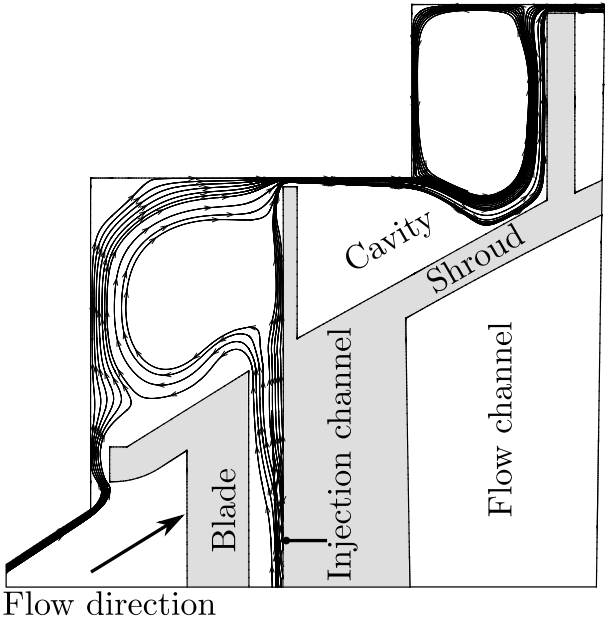


Figure 6.14.: Relative Streamlines of Leading Edge Injection in a Meridional Plane

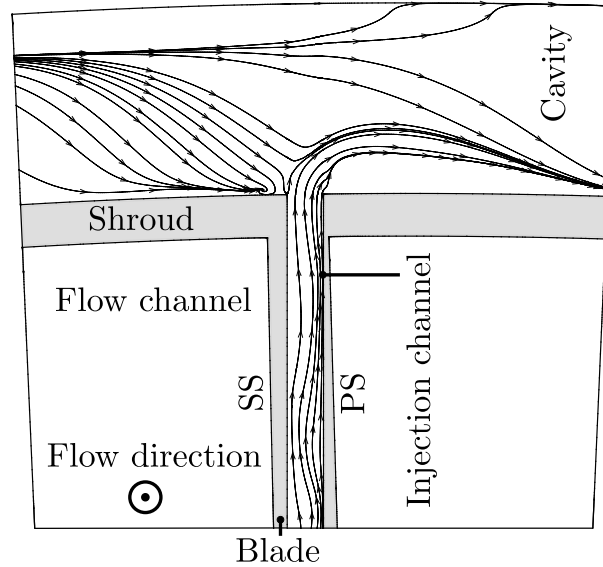


Figure 6.15.: Relative Streamlines of Leading Edge Injection in an Axial Plane

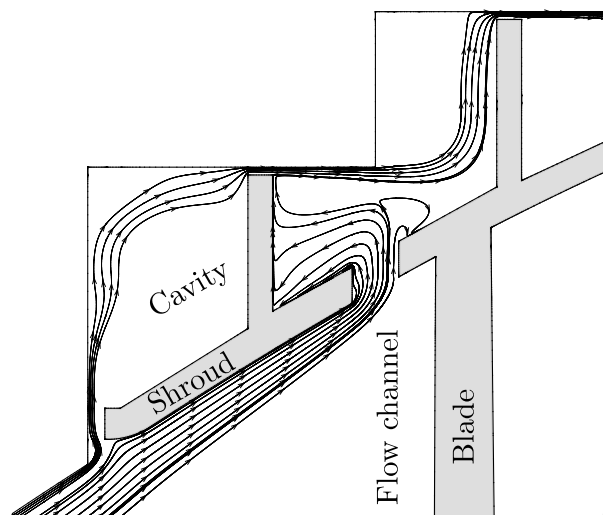


Figure 6.16.: Relative Streamlines of Through-Shroud Injection in a Meridional Plane

The inclination of the cavity streamlines opposite to the rotational direction is due to small cavity velocities resulting in circumferential velocity components opposite to the rotational direction in a relative frame of reference. It is further obvious that the cavity flow has a significant impact on the injected flow. The injection streamlines are inclined opposite to the rotational direction due to the cavity flow momentum. The streamline curvature of injection features a smaller radius in the case of leading edge injection because of a smaller channel diameter and hence lower mass flow rate and momentum in Fig. 6.15. The larger channel diameter of through-shroud injection results, however, in higher momentum of the injection flow and thus in a larger radius

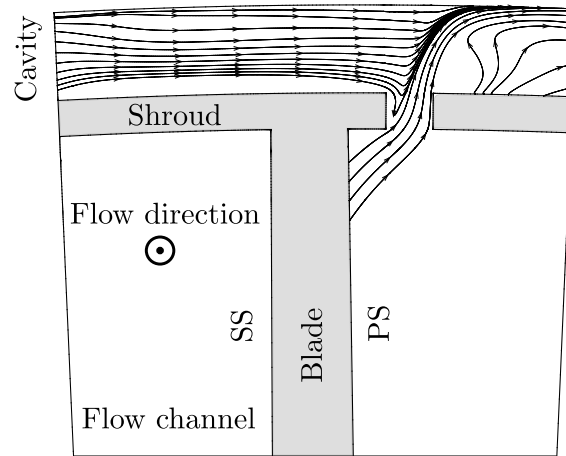


Figure 6.17.: Relative Streamlines of Through-Shroud Injection in an Axial Plane

of curvature in Fig. 6.17. In axial direction the injection flow merges with the leakage flow to the cavity outlet acting as a blockage (see Fig. 6.14 and Fig. 6.16).

6.6.3. Contour Plots of Measurement Data in Plane F

In this section the contour plots of the acquired measurement data in plane F are presented for both the shrouded geometry without injection and the case with passive through-shroud injection. In accordance with paper 4 the presented data comprise the flow angle and Mach number over the entire dimensionless channel height and over an angular range of 22.5° . In Fig. 6.18 and 6.19 the absolute exit flow angle measured from the negative circumferential direction is depicted.

As mentioned before the measurement data were phase averaged and subsequently time averaged. Comparing the exit flow angle contour plots of both cases one clearly recognizes that the region of higher flow angles in the vicinity of the casing is narrower in the case with through-shroud injection. Since the flow angle is calculated with respect to the negative circumferential direction, lower angles indicate lower circumferential velocity and higher specific stage work. This further signifies lower incidence of the following stage. Furthermore a migration of the entire flow field radially toward the hub is observable in the case without injection compared to the case with through-shroud injection. This migration can be attributed to the increased impact of the leakage flow on the downstream flow field, which is reduced in the case with through-shroud injection due to reduction in the low momentum leakage flow fraction. The migration of the casing fluid and the secondary flow toward the midspan is also addressed in [46] and [47].

In Fig. 6.20 and Fig. 6.21 the exit Mach number is depicted for both the shrouded geometry and the case with passive through-shroud injection. Lower Mach number values are apparent

6. Investigations on a Real Application

in the case with through-shroud injection in the vicinity of the casing. Furthermore they are closer to the mean flow Mach number, which can be attributed to lower leakage mass flow rate at the cavity outlet. Since Plane F is positioned downstream of the cavity, lower leakage mass flow rate results in lower deviation of the flow in the casing region from the passage main flow after mixing.

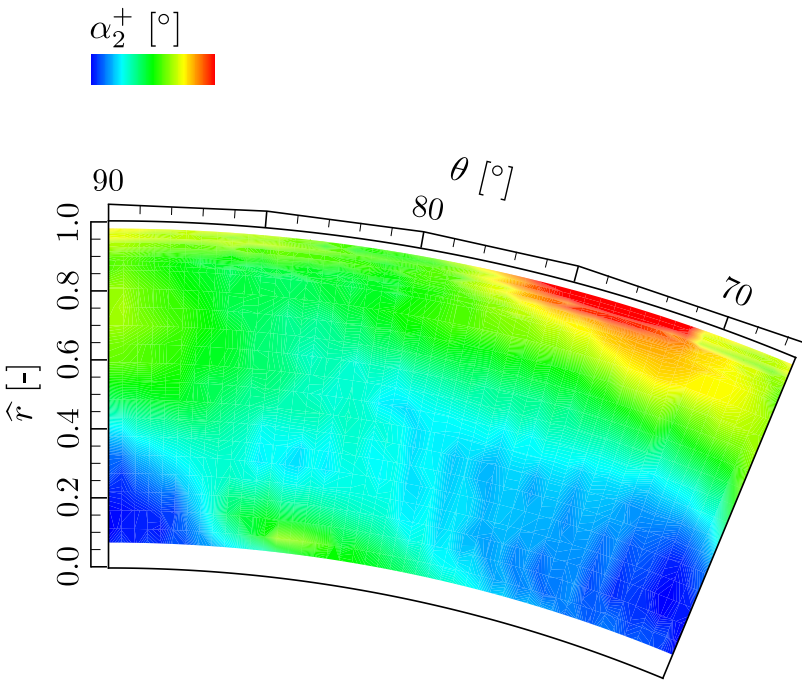


Figure 6.18.: Absolute Exit Flow Angle in Plane F for the Case without Injection

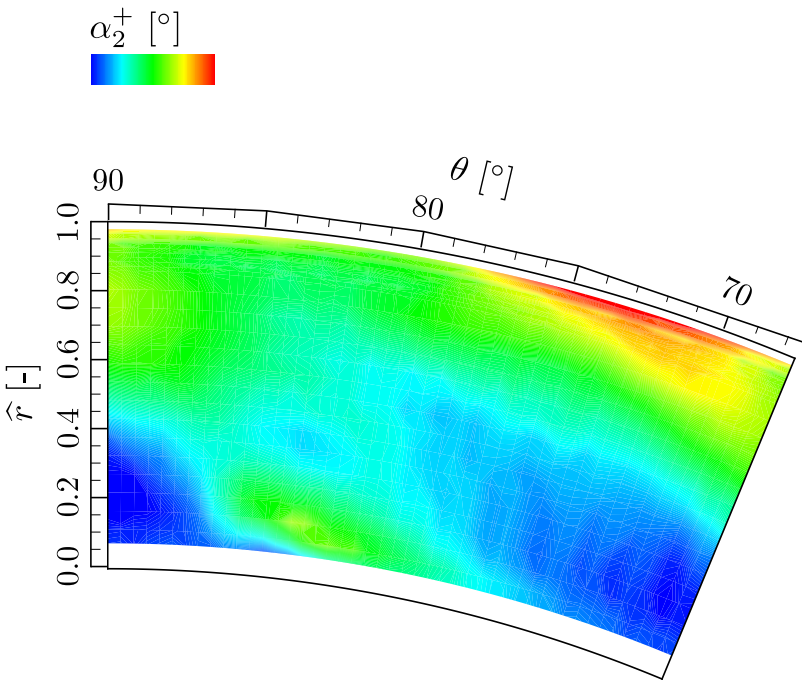


Figure 6.19.: Absolute Exit Flow Angle in Plane F for the Case with Through-Shroud Injection

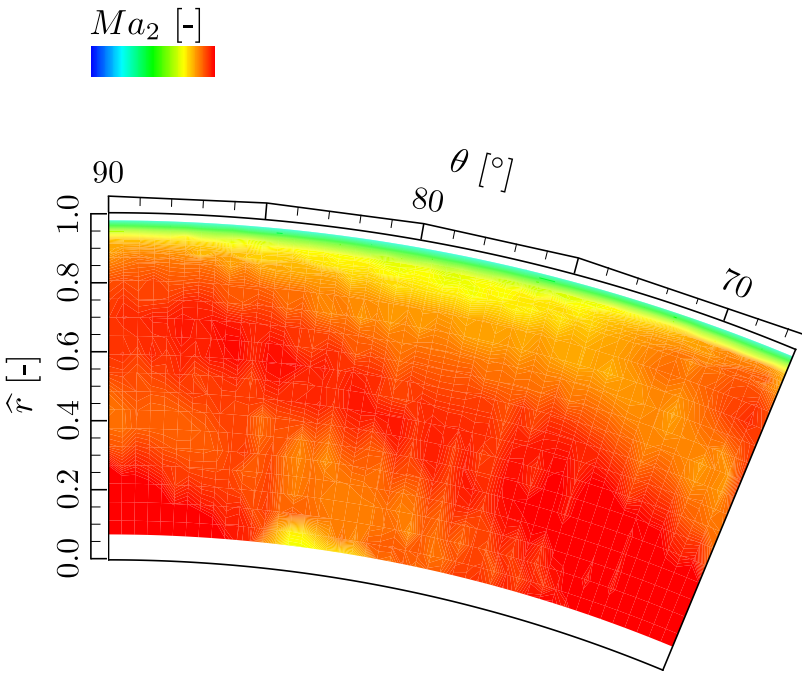


Figure 6.20.: Mach Number in Plane F for the Case without Injection

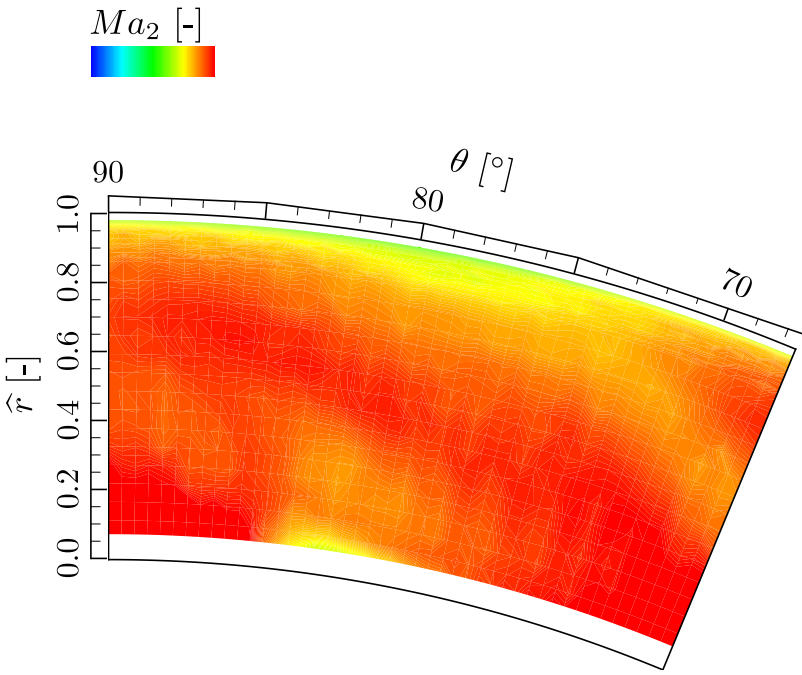


Figure 6.21.: Mach Number in Plane F for the Case with Through-Shroud Injection

7. Conclusion and Outlook

A lot of work has been dedicated to reduction of tip-leakage losses in turbomachinery in the past, since it accounts for a substantial part of overall losses. Modifications of the blade tip or applying shrouds to increase the aerodynamic resistance can be mentioned as examples. Disregarding the fact that the leakage flow, if at all, participates only partially in stage work, its ingress into the main flow causes mixing losses and impairs the inflow conditions of following blade rows. In this spirit the impact of additional components aiming at turning the leakage flow has been studied in the literature as well. Such arrangements, however, result in higher weight of the machine, which is rather a negative aspect concerning aircraft engines. As mentioned before in this thesis the technology of GTF makes advantages of higher rotational speed of the LPT. Due to the blade tip architecture of a high-spinning LPT rotor an appropriate sealing arrangement becomes significant. Furthermore using shrouded blades in uncooled LPT stages is necessary regarding structural aspects in addition to sealing function. Since, however, additional mass on an outer diameter of a high-speed rotor results in higher mechanical stress in the blade root a careful cut back of the blade shroud is conceivable. This arrangement is referred to as partial shrouds. The sealing function of such a shroud would deteriorate due to missing complete coverage of the blade tip region in peripheral direction.

In terms of these aspects additional sealing arrangements should be chosen with no weight increase and reasonable costs. In this regard fluidic jet barriers using fluid injection in the sealing area can offer a possibility. According as whether the injection flow is extracted out of an external source (compressor air) or the stage flow itself, it can be differentiated between active or passive methods. Injection of cooling air in HPTs can be mentioned as an example for active fluidic sealing. A variety of studies can be encountered in the literature regarding active fluidic barriers in combination with labyrinth seal arrangements. However, passive fluidic sealing has still not been investigated extensively.

The method of passive tip-injection in uncooled and unshrouded LPT rotors has already been studied at the department of Fluid-Flow Machinery of the Institute for Energy Systems and Thermodynamics at Technische Universität Wien by several works. Since, however, shrouds can not be disregarded in the last stages of a LPT, this thesis was dedicated to investigations regarding providing shrouds with passive tip-injection. The procedure was broken down into three stages with increasing complexity. This was necessary in order to conduct time-consuming CFD calculations and costly experiments systematically.

In the first stage the discharge behavior of a labyrinth seal application with two sealing fins was taken into consideration. For more insight into the flow physics and estimation of the impact of

various parameters on the overall leakage mass flow rate several analytical models in a meridional cross section were derived. In comparison to previous investigations related to unshrouded blades different overall discharge coefficients accounting for both the leakage mass flow rate and the injection mass flow rate were necessary with respect to different axial injection positions over the shroud surface. Furthermore the injection mass flow rate was modeled for each injection position and applied to the discharge model. It also has to be mentioned that the calculations were all carried out in a dimensionless manner and the injection flow was supposed to be extracted at the blade leading edge. In comparison to the previous discharge models various phenomena such as injection channel blockage and deviation of the injection direction from the channel direction were taken account of. This resulted in a variety of parameters, which were a priori not known for the evaluations. For this purpose 2D CFD calculations were carried out. It could be ascertained that the analytical models were capable of describing the flow physics in the tip section reflected in a satisfactory agreement between the discharge coefficients calculated by the analytical models and the CFD. In this regard it could be stated that only guided passive injection along the upstream surface of the first sealing fin can reduce the overall discharge coefficient. In the next stage the investigation complexity was extended to account for 3D cavity flow and its interaction with passive tip-injection. For this purpose linear cascade studies without rotation were conducted in order to view the cavity flow in isolation. Analytical considerations could, however, show that blade rotation has a secondary effect on the injection mass flow rate. Due to the restrictions the studies in this step were only based on CFD calculations with the advantage of shroud design flexibility allowing for considerations regarding partial shrouds. In this spirit one full shroud together with two partial shroud geometries were investigated. The volume reduction of the shroud was carried out in two ways. In one configuration the shroud volume was reduced mostly at the leading edge and in the other configuration mostly at the trailing edge. Based on the analysis findings before all shroud geometries were subsequently provided with guided passive tip-injection along the upstream surface of the first sealing fin in a single position over the shroud surface per blade spacing. In compliance with previous considerations the injection flow was extracted at the blade leading edge. The results showed that in the case of the full shroud guided passive tip-injection featured the highest cascade efficiency improvement. Furthermore the cascade efficiency of the partial shroud reduced mostly at the leading edge was impaired by guided tip-injection. This could be attributed to the fact that the blade profile was front-loaded and the guided injection was placed downstream of the position with the maximum pressure difference with missing sealing function and contributing to increased overall leakage mass flow rate. Due to shroud opening in the front region of the blade leakage flow from the pressure side to the suction side was present and the injection flow resulted in higher mixing losses. In this spirit unguided passive tip-injection at the place of the maximum profile pressure difference was additionally studied for this case. The cascade efficiency could be improved in comparison to the partial shroud only without injection. However, it could be stated that, in spite of improvements compared to the partial geometries, in none of the cases the passive tip-injection was capable of compensating the cascade efficiency penalty caused by

shroud volume reduction.

Based on the findings above the investigations were extended to studies on a real LPT rotor in the last stage of this work. In this spirit compressible flow in a rotational frame of reference was taken account of. Initially the method of guided passive tip-injection upstream of the first sealing fin with injection flow extracted at the blade leading edge was taken into consideration numerically. The results showed an enhancement of the downstream flow field reflected in lower exit flow angles and total temperatures in the vicinity of the casing. This is an indication for higher specific stage work. Since the injection occurs at a higher diameter as the extraction in this case, an analytical condition was derived regarding the specific work of the injection flow and its contribution to the stage work. It could be shown that under certain conditions the injection contributes positively to specific stage work. However, due to the thin blade leading edge of a LPT rotor in a turbofan the injection extraction slot would cause high stress peaks. Furthermore aerodynamic penalties could arise in the vicinity of the extraction slot at the blade leading edge. For this reason a further injection method with the injection channel manufactured radially through the shroud was studied numerically and experimentally. Additionally this method features higher feasibility and lower costs compared to the previous method requiring a groove in the first sealing fin as a guidance for the injection. A numerical approach was applied for determination of the final position of the injection channel. The experimental and numerical results indicated an enhancement of the downstream flow field. In addition an analytical model was derived accounting for the impact of geometrical parameters as well as inlet conditions on the specific stage work. The inclination of the injection opposite to the rotational direction of the rotor was also taken into consideration in this approach. For the injection mass flow rate the discharge model mentioned before was applied to the new model. In this regard off-design conditions could also be taken account of. It could be stated that for the given LPT rotor under design conditions passive tip-injection could improve the specific stage work. Nevertheless for other geometrical parameters and under off-design conditions the analytical model exhibited a reduction in specific stage work due to injection. The extent of the reduction, however, depends on the inclination of the injection opposite to the rotational direction.

The content of this thesis provides substantial knowledge related to functionality of passive tip-injection in uncooled and shrouded LPT rotors. Since weight reduction and thermal efficiency improvement are important issues designing aircraft engines, the passive tip-injection can be considered as a method reducing the tip-leakage losses without any additional weight. Furthermore linear cascade investigations showed that, even though the efficiency penalty due to shroud volume reduction can not be completely compensated, an efficiency improvement can be achieved by means of passive tip-injection in comparison to the partially shrouded configuration. This is in compliance with the requirement of shroud cut back for further weight reduction in high-speed LPTs of a GTF. In addition sophisticated analytical models were derived allowing for parameter studies with reasonable effort. In this regard not only the tip-leakage mass flow

rate and its reduction is considered in isolation but also its impact on the specific stage work under different load conditions. Finally the functionality of passive tip-injection was confirmed based on an experimental approach accounting for manufacturing feasibility as well.

In spite of the investigations in this thesis a lot of work can still be dedicated to application of passive tip-injection in a real configuration. The feasibility of this method and the choice of injection channel manufacturing depend highly on the blade geometry. As mentioned above lower blade leading edge thickness is a limitation regarding passive tip-injection with the injection flow extracted at the blade leading edge due to higher mechanical stress in the region of the injection inlet slot. In this spirit investigations on shrouded blade geometries with higher blade leading edge thickness and thus higher possible injection channel diameters can be an important issue for further studies.

The aerodynamic and fluid-mechanical aspects of passive tip-injection were addressed in the scope of the current thesis. It is, however, clear that the structural aspects can not be ignored modifying an available geometry in turbomachinery, which can also be an issue concerning further work in this area. In this regard the impact of passive tip-injection on the oscillation behavior as well as the acoustics can be considered.

Experimental study on various blade geometries as well as for different cavity geometries together with passive tip-injection could also be an important topic, in order to gain a wide spectrum of applicability of passive tip-injection. In this regard partially shrouded blades can also be taken into consideration. Furthermore inclined injection can also be studied experimentally. However, the manufacturing feasibility of inclined injection may be a limitation.

As it was mentioned before the functionality of passive tip-injection also depends on the operational conditions. In off-design operation the passive tip-injection can impair the specific stage work based on the shroud geometry and the inclination angle of the injection against the rotational direction. In this spirit additional measurements at different operational conditions can be carried out in order to gain a better understanding of the operational range of shrouded LPTs provided with passive tip-injection and support the analytical approach.

CFD is an inevitable instrument concerning evaluation of new methods prior to costly experimental studies. Furthermore the CFD codes including turbulence modeling develop very rapidly capturing the real flow structures more accurately. Nevertheless the turbulence modeling still stays a challenge for precise interpretation of the results and should hence be taken into consideration with caution. In this spirit more CFD calculations with different turbulence models can be the objective of possible future work. Additionally various velocity formulations together with different discretization methods, which are nowadays available at a large scale in each commercial CFD code, can be tested as well.

According to the findings in this thesis the injection position depends strongly on the volume reduction in case of partially shrouded blades. Prior to costly experiments CFD can be a suitable instrument in order to study various injection positions together with different partial shroud

geometries. This can also be undertaken in an optimization procedure.

Relating to the off-design behavior of passive tip-injection CFD calculations can be helpful for supporting the analytical considerations and the experiments. In this spirit modeling a full stage together with the downstream stage can help investigate also the impact of perturbations of the upstream blade row or the effects on the downstream blade row. Due to the transient behavior of such calculations unsteady CFD procedure is required in order to capture the real flow physics and account for the blade row interaction.

Bibliography

- [1] AIRBUS, GLOBAL MARKET FORECAST: Flying by Numbers. (2015)
- [2] ANKER J. E.; MAYER J. F.: Simulation of the Interaction of Labyrinth Seal Leakage Flow and Main Flow in an Axial Turbine, *ASME Paper GT2002-30348*. (2002)
- [3] ANSYS FLUENT 15.0: Theory Guide. (November 2013)
- [4] ANSYS FLUENT 15.0: User's Guide. (November 2013)
- [5] ARNOLD T.; EIFEL M.: Kalibrierbericht der pneumatischen Fünflochsonde mit Temperaturmessstelle. Institut für Strahlantriebe und Turboarbeitsmaschinen, RTWH Aachen. (2006)
- [6] ARTS T.: Turbine Blade Tip Design and Tip Clearance Treatment, *VKI Lecture Series 2004-02*. (2004)
- [7] AULD A.; HILFER M.; HOGG S.; INGRAM G.; MESSENGER A.: Application of an Air-Curtain Fluidic Jet Type Seal to Reduce Turbine Shroud Leakage, *ASME Paper GT2013-94198*. (June 2013)
- [8] AUYSER E. L.: Dynamic Sealing Arrangement for Turbomachines, *US Patent 2,685,429*. (January 1954)
- [9] BENONI A.: Einfluss von Geometrieparametern auf die Spaltverluste in einem axialen Turbinengitter mit passiver Einblasung. Technische Universität Wien, PhD thesis. (November 2013)
- [10] BINDON J. P.: Pressure Distribution in the Tip Clearance Region of an Unshrouded Axial Turbine as Affecting the Problem of Tip Burnout, *ASME Paper 87-GT-230*. (1987)
- [11] BOHN D.; KREWINKEL R.; TÜMMERS C.; SELL M.: Influence of the Radial and Axial Gap of the Shroud Cavities on the Flowfield in a 2-Stage Turbine, *ASME Paper GT2006-90857*. (May 2006)
- [12] BRÄUNLING W. J. G.: Flugzeugtriebwerke. Springer-Verlag, 3rd edition. (2009)
- [13] CELIK I. B.; GHIA U.; ROACHE P. J.; FREITAS C. J.; COLEMAN H.; RAAD P. E.: Procedure for Estimation and Reporting of Uncertainty Due to Discretization in CFD Applications, *ASME Journal of Fluids Engineering, Vol. 130, 078001-1 - 078001-4*. (July 2008)

- [14] CURTIS E. M.; DENTON J. D.; LONGLEY J. P.; ROSIC B.: Controlling Tip Leakage Flow over a Shrouded Turbine Rotor Using an Air-Curtain, *ASME Paper GT2009-59411*. (June 2009)
- [15] DENOS R.; PANIAGUA G.: Aero-Engine Design: From State of the Art Turbofans towards Innovative Architectures, *VKI Lecture Series 2008-03*. (2008)
- [16] DENTON J. D.: Some Limitations of Turbomachinery CFD, *ASME Paper GT2010-22540*. (June 2010)
- [17] DENTON J. D.: Loss Mechanisms in Turbomachines, *ASME Journal of Turbomachinery, Vol. 115, 621-656*. (October 1993)
- [18] DENTON J. D.; DAWES W. N.: Computational Fluid Dynamics for Turbomachinery Design, *Proc Instn Mech Engrs, Vol 213, Part C, 107-124*. (1999)
- [19] DEWANJI D.; RAO G. A.; BUIJTENEN J. v.: Feasibility Study of Some Novel Concepts for High Bypass Ratio Turbofan Engines, *ASME Paper GT2007-27786*. (June 2009)
- [20] DHAKAL T. P.; WALTERS D. K.: Curvature and Rotation Sensitive Variants of the K-Omega SST Turbulence Model, *ASME Paper FEDSM2009-78397*. (August 2009)
- [21] EL-DOSOKY M. F.; RONA A.; GOSTELOW J. P.: An Analytical Model for Over-Shroud Leakage Losses in a Shrouded Turbine Stage, *ASME Paper GT2007-27786*. (May 2007)
- [22] GAETANI P.: Report on Fast Response Aerodynamic Pressure Probe. Politecnico di Milano, Dipartimento di Energia. (2010)
- [23] GHAFFARI P.: Einfluss des Schaufelkantenradius sowie der Einblasung auf den Spaltmassenstrom in axialen Turbinenbeschaufelungen. Technische Universität Wien, master thesis. (October 2011)
- [24] GHAFFARI P.; WILLINGER R.: Preliminary Investigation of Passive Tip-Injection in a Linear Turbine Cascade with Shrouded Blades, *11th European Turbomachinery Conference ETC2015-205*, Madrid, Spain. (March 2015)
- [25] GHAFFARI P.; WILLINGER R.: Impact of Passive Tip-Injection on the Performance of Partially Shrouded Turbines: Basic Concept and Preliminary Results, *ASME Paper TBTS2013-2038*. (October 2013)
- [26] GHAFFARI P.; WILLINGER R.; BAUNGER S.; MARN A.: Impact of Passive Tip-Injection on Tip-Leakage Flow in Axial Low Pressure Turbine Stage, *ASME Paper GT2015-42226*. (June 2015)
- [27] GIBONI A.; WOLTER K.; MENTER J. R.; PFOST H.: Experimental and Numerical Investigation into the Unsteady Interaction of Labyrinth Seal Leakage Flow and Main Flow in a 1.5-Stage Axial Turbine, *ASME Paper GT2004-53024*. (2004)

- [28] HALBERTSCHLAGER C.: Festigkeitsberechnung für Laufschaufeln mit rudimentären Deckbändern in schnelllaufenden Niederdruckturbinen. Technische Universität Wien, master thesis. (January 2014)
- [29] HAMIK M.: Reduktion der Spaltverluste in einem axialen Turbinengitter durch passive Einblasung. Technische Universität Wien, PhD thesis. (April 2007)
- [30] HAMIK M.: Einfluss von Ausblasung auf die Strömung in einem radialen Schaufelspalt. Technische Universität Wien, master thesis. (October 2005)
- [31] HOGG S. I.; RUIZ I. G.: Fluidic Jet Barriers for Sealing Applications, *ASME Paper GT2011-45353*. (June 2011)
- [32] HUBINKA J.: Aufbau, Inbetriebnahme und Konstruktion eines Zweiwellenturbinenprüfstandes. Graz University of Technology, PhD thesis. (2012)
- [33] ICAO: Environmental Report. (2013)
- [34] KURZKE J.: Fundamental Differences between Conventional and Geared Turbofans, *ASME Paper GT2009-59754*. (June 2009)
- [35] LEEB K.: Experimentelle und numerische Untersuchungen zum Durchflußverhalten von Labyrinthdichtungen von Turbomaschinen unter dem Einfluß von Rotation, Wellendesaxierung und Drall der Zuströmung. Technische Universität Wien, PhD thesis. (November 1997)
- [36] MALZACHER F. J.; GIER J.; LIPPL F.: Aerodesign and Testing of an Aeromechanically Highly Loaded LP Turbine, *ASME Journal of Turbomachinery, Vol. 128, 643-649*. (October 2006)
- [37] MATTHIAS A.: Das Durchflussverhalten von Labyrinthdichtungen bei unterschiedlichen Betriebsbedingungen. Technische Universität Wien, PhD thesis. (October 2007)
- [38] PERSICO G.; GAETANI P.; GUARDONE A.: Design and Analysis of New Concept Fast-Response Pressure Probes, *Meas. Sci. Technol., Vol. 16, 1741-1750*. (2005)
- [39] PERSICO G.; GAETANI P.; GUARDONE A.: Dynamic Calibration of Fast-Response Probes in Low-Pressure Shock Tubes, *Meas. Sci. Technol., Vol. 16, 1751-1759*. (2005)
- [40] PFAU A.; KALFAS A. I.; ABHARI R. S.: Making Use of Labyrinth Interaction Flow, *ASME Paper GT2004-53797*. (June 2004)
- [41] PFAU A.; SCHLIENGER J.; RUSCH D.; KALFAS A. I.; ABHARI R. S.: Unsteady Flow Interaction within the Inlet Cavity of a Turbine Rotor Tip Labyrinth Seal, *ASME Paper GT2003-38271*. (June 2003)

- [42] PFAU A.; TREIBER M.; SELL M.; GYARMATHY G.: Flow Interaction From the Exit Cavity of an Axial Turbine Blade Row Labyrinth Seal, *ASME Journal of Turbomachinery*, Vol. 123, 342-352. (April 2001)
- [43] PRATT & WHITTNEY: PurePower Engine Family Specs Chart. (2012)
- [44] PRATT & WHITTNEY: PW1100G-JM Advantage. (2014)
- [45] RIEGLER C.; BICHLMAIER C.: The Geared Turbofan Technology-Opportunities, Challenges and Readiness Status, *1st CEAS European Air and Space Conference*, CEAS-2007-054. (2007)
- [46] ROSIC B.; DENTON J. D.: Control of Shroud Leakage Loss by Reducing Circumferential Mixing, *ASME Journal of Turbomachinery*, Vol. 130, 021010-1 - 021010-7. (April 2008)
- [47] ROSIC B.; DENTON J. D.; CURTIS E. M.: The Influence of Shroud and Cavity Geometry on Turbine Performance: An Experimental and Computational Study - Part I: Shroud Geometry, *ASME Journal of Turbomachinery*, Vol. 130, 041001-1 - 041001-10. (October 2008)
- [48] ROSIC B.; DENTON J. D.; CURTIS E. M.; PETERSON A. T.: The Influence of Shroud and Cavity Geometry on Turbine Performance: An Experimental and Computational Study - Part II: Exit Cavity Geometry, *ASME Journal of Turbomachinery*, Vol. 130, 041002-1 - 041002-10. (October 2008)
- [49] SANTNER C.: Experimental Investigation of Turning Mid Turbine Frame Designs. Graz University of Technology, PhD thesis. (2008)
- [50] SCHÄFER M.: Numerik im Maschinenbau. Springer-Verlag. (1999)
- [51] SCHREMPF M.: Kalibrierung von pneumatischen Dreilochsonden unter Nickwinkeleinfluss. Technische Universität Wien, master thesis. (May 2016)
- [52] SMIRNOV P. E.; MENTER F. R.: Sensitization of the SST Turbulence Model to Rotation and Curvature by Applying the Spalart-Shur Correction Term, *ASME Journal of Turbomachinery*, Vol. 131, 041010-1 - 041010-8. (October 2009)
- [53] SPATARO R.; GÖTTLICH E.; SANTNER C.; HEITMEIR F.: A Numerical Comparison on the Aerodynamic Performances of a Two-Stage Two-Spool Turbine Facility Predicted by Steady and Unsteady Simulations, *10th European Turbomachinery Conference ETC2013-039*, Lappeenranta, Finland. (April 2013)
- [54] SZYMANSKI A.; DYKAS S.; WROBLEWSKI W.: Flow Analysis of the Turbine Rotor Tip Seal on a Highly Rotary Test Rig, *11th European Turbomachinery Conference ETC2015-062*, Madrid, Spain. (March 2015)
- [55] TRAUPEL W.: Thermische Turbomaschinen, Band 1. Springer-Verlag. (1977)

- [56] TURNQUIST N. A.; BRUCE K. L.; CERRETELLI C.; TOURIGNY J. E.: Fluidic Sealing for Turbomachinery, *US Patent 2009/0297341 A1*. (December 2009)
- [57] WALLIS A. M.; DENTON J. D.; DEMARGNE A. A. J.: The Control of Shroud Leakage Flows to Reduce Aerodynamic Losses in a Low Aspect Ratio, Shrouded Axial Flow Turbine, *ASME Paper 200-GT-475*. (May 2000)
- [58] WALTERS D. K.; LEYLEK J. H.: Impact of Film-Cooling Jets on Turbine Aerodynamic Losses, *ASME Journal of Turbomachinery, Vol. 122, 537-545*. (July 2000)
- [59] WILCOX D. C.: Turbulence modeling for CFD. DCW Industries, Inc. (1994)
- [60] WILLINGER R.; HASELBACHER H.: On the Modeling of Tip Leakage Flow in Axial Turbine Blade Rows, *ASME Paper 2000-GT-633*. (May 2000)
- [61] WITTIG S.; SCHELLING U.; KIM S.; JACOBSEN K.: Numerical Predictions and Measurements of Discharge Coefficients in Labyrinth Seals, *ASME Paper 87-GT-188*. (1987)
- [62] YOON S.: The Effect of the Degree of Reaction on the Leakage Loss in Steam Turbines, *Journal of Engineering for Gas Turbines and Power, Vol. 135, 1-9*. (February 2013)
- [63] YOON S.; CURTIS E.; DENTON J.; LONGLEY J.: The Effect of Clearance on Shrouded and Unshrouded Turbines at two Levels of Reaction, *ASME Paper GT2010-22541*. (June 2010)

A. Appendix

A.1. CFD Results of the LPT Rotor Calculated with the SST k/ω -model

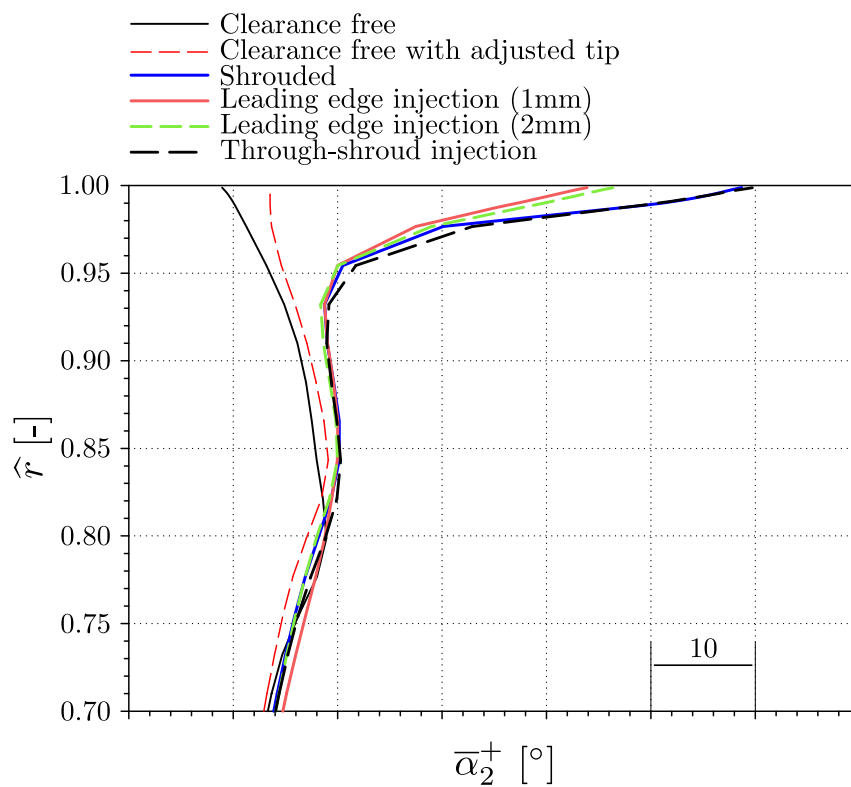


Figure A.1.: Circumferentially Averaged Exit Flow Angle Calculated with Respect to the Negative Circumferential Direction in Plane F

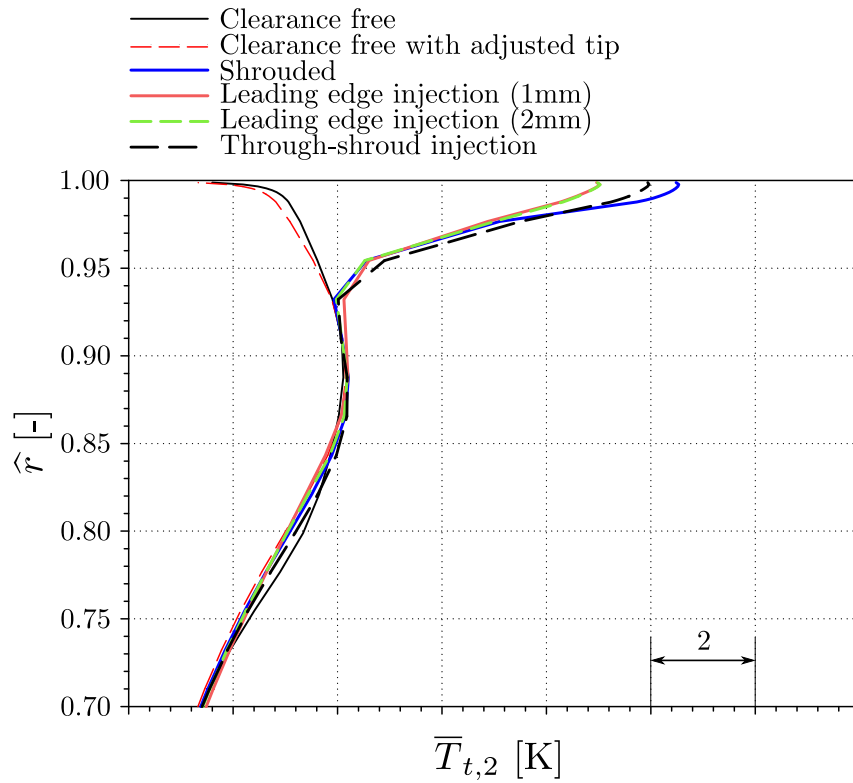


Figure A.2.: Circumferentially Averaged Total Temperature in Plane F

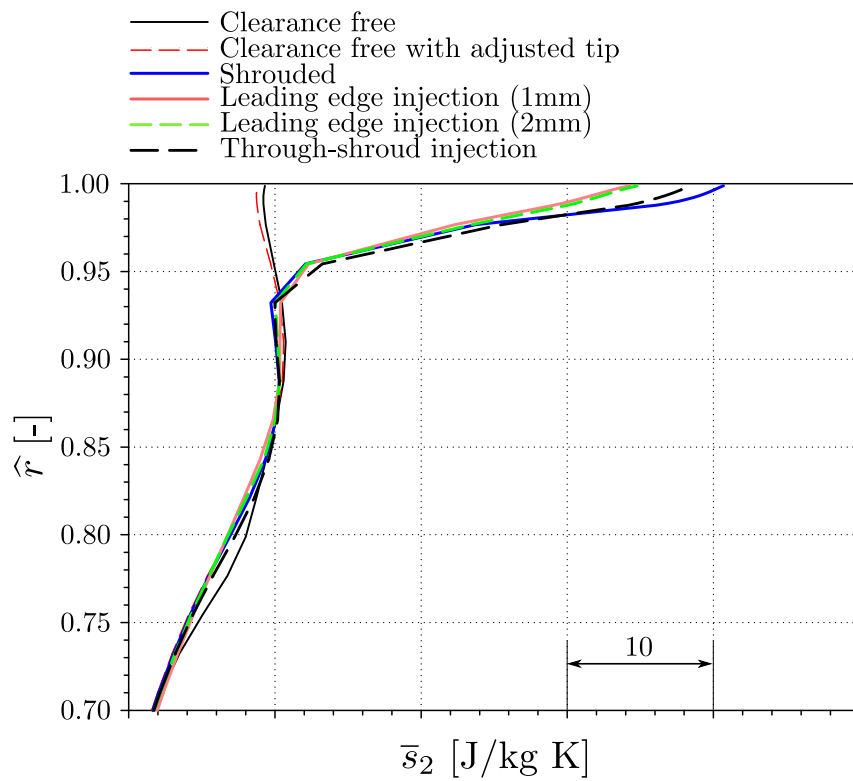


Figure A.3.: Circumferentially Averaged Specific Entropy in Plane F

Curriculum Vitae

Personal Data	Born in Tehran/Iran 22 September 1987	
Experience	University assistant , Technische Universität Wien, Institute for Energy Systems and Thermodynamics, department of Fluid-Flow Machinery <ul style="list-style-type: none">• Master lectures of thermal turbomachinery• Supervising bachelor and master theses• Research	since 2013
	Project assistant , Technische Universität Wien, Institute for Energy Systems and Thermodynamics, department of Fluid-Flow Machinery <ul style="list-style-type: none">• Flow simulations and experiments• Laboratory activities• Supervising bachelor and master theses	2012-2013
	Tutor , Technische Universität Wien <ul style="list-style-type: none">• Mechanics and mechatronics• Thermodynamics	2009-2011
Education	Master of Science, MSc in mechanical engineering, thermal turbomachinery (Diplom-Ingenieur), graduation with excellency at Technische Universität Wien	2011
	Bachelor of Science, BSc in mechanical engineering, Technische Universität Wien	2009

Matura (general qualification for university entrance) in Vienna, graduated in natural sciences	2006
Upper school in Vienna	2004-2006
Matura (general qualification for university entrance) in Tehran (Iran), graduated with excellency in mathematics and physics	2004
Second upper school in Tehran (Iran), with specialization in mathematics and physics	2001-2004
First upper school in Tehran (Iran)	1998-2001
Elementary school in Tehran (Iran)	1993-1998

Skills

Languages:

- **Persian:** native language
- **German:** fluently
- **English:** fluently
- **Spanish:** fluently
- **Arabic:** high school level
- **French:** high school level

Certified in the "High Potential Program" at Technische Universität Wien (TUtheTOP): 2011-2012

- High potential programs assisted by diverse companies
- In-depth seminars and workshops concerning moderation, presentation and communication assisted by "Corporate Consult" (certified)

Member of the committee for postdoctoral lecture qualification, Technische Universität Wien, Faculty of Mechanical and Industrial Engineering 2011

Publications **Ghaffari P.**, Willinger R.: Impact of Passive Tip-Injection on the Performance of Partially Shrouded Turbines: Basic Concept and Preliminary Results, ASME Turbine Blade Tip Symposium 2013, Hamburg, Germany, Paper number: TBTS2013-2038

Ghaffari P., Willinger R.: Preliminary Investigation of Passive Tip-Injection in a Linear Turbine Cascade with Shrouded Blades, 11th European Turbomachinery Conference 2015, Madrid, Spain

Ghaffari P., Willinger R., Bauinger S., Marn A.: Impact of Passive Tip-Injection on Tip-Leakage Flow in Axial Low Pressure Turbine Stage, ASME Turbo Expo conference 2015, Montreal, Canada, Paper number: GT2015-42226

Ghaffari P., Willinger R.: On the Impact of Passive Tip-Injection on the Downstream Flow Field of a Shrouded LP-Turbine: CFD and Experimental Results, ASME Turbo Expo conference 2016, Seoul, South Korea, Paper number: GT2016-56196